TEAR DYNAMICS

By

HENG ZHU

A DISSERTATION PRESENTED TO THE GRADUATE SCHOOL
OF THE UNIVERSITY OF FLORIDA IN PARTIAL FULFILLMENT
OF THE REQUIREMENTS FOR THE DEGREE OF
DOCTOR OF PHILOSOPHY

UNIVERSITY OF FLORIDA

2007

To my parents, Quanshou Zhu and Yimei Zhang, and my wife, Jia Cai

ACKNOWLEDGMENTS

First I thank my advisor, Professor Anuj Chauhan, for his guidance, inspiration and patience. His guidance on my research and on other aspects of life has been essential to the completion of my degree and will benefit me throughout my life. From the beginning through the end of my PhD study, he has also offered generous help on preparing me for my future career. I thank my committee members, Professors Ranga Narayanan, Richard Dickinson and Roger Tran-Son-Tay, for their valuable discussion and advice on my research. Especially I thank Dr. Subir Bhatia for his time and generous help on canaliculus anatomy and basic eye physiology. I also thank my group colleagues, Derya Gulsen, Marissa Fallon, Zhi Chen, Chi-Chung Li, Yash Kapoor, Jinah Kim, Brett Howell and Chhavi Gupta, as well as all the undergrad students in my group, for their enjoyable company and help. I also thank other faculties and the staff in Chemical Engineering Department for their advice and help.

Finally, I thank my parents for their unconditional love, encouragement and support through all these years. I also give my gratitude to my wife, who made great sacrifice for my study abroad and stands behind me through difficulties. Last but not the least I am thankful to my other family members for their support and help.

TABLE OF CONTENTS

LIST OF TABLES

LIST OF FIGURES

Abstract of Dissertation Presented to the Graduate School
of the University of Florida in Partial Fulfillment of the
Requirements for the Degree of Doctor of Philosophy

TEAR DYNAMICS

By

Heng Zhu

August 2007

Chair: Anuj Chauhan
Major: Chemical Engineering

The quantity and quality of tear fluid in an eye under normal circumstances is an important factor in maintenance of comfort and health of ocular tissue. It is thus important to assess the effect of various physiological parameters on the tear volume and composition, and to determine the factors that can increase them. We developed mathematical models for various aspects of tear dynamics such as canalicular drainage, conjunctival absorption/secretion, and the tear mixing under lower eyelids.

We performed a tear mass balance on an eye. The mass balance requires mathematical models for the flows from or into the tear film such as canalicular drainage, evaporation and transport across cornea and conjunctiva. The tear drainage model developed is based on the lacrimal pump mechanism, according to which the muscle action during a blink drives the tear drainage. We also developed a mathematical model for the transport of ions and water through the conjunctival epithelium. The drainage and conjunctiva transport models were incorporated into a tear mass balance, which can predict the steady state tear film thickness and the residence time of fluids and drugs after drop instillation. The tear balance is based on the assumption that tears on the ocular surface is well mixed, which is supported by our mathematical model of tear mixing under lower lids based on Taylor dispersion mechanism. In addition, models are

developed for the drainage of both high viscosity Newtonian and non-Newtonian fluids through canaliculi, and these models are used to study the effect of fluid viscosity on its drainage rate and ocular residence time.

We found that the mechanical properties of the lacrimal canaliculi, which are responsible for tear drainage, are essential to determining the tear drainage rates. The mechanical properties of porcine canaliculus were measured in compression mode while submerged in isotonic fluid by using a dynamic mechanical analyzer (DMA). Both storage modulus (E') and loss modulus (E") were measured at physiologically relevant frequencies. When subjected to repeated loading-recovery cycles to simulate the blink cycles, the canalicular tissue relaxes at the same time scale as the pressure relaxes in a human canaliculi suggesting that the drainage of tears through the canaliculi is controlled by the mechanical properties of the canaliculi.

The model predictions agree with various physiological experiments. The model also helps resolve the differences between various tear drainage experiments and can be used to design more effective dry eye treatments and also more efficacious ophthalmic drug delivery vehicles.

CHAPTER 1
INTRODUCTION

Tear Physiology and Tear Balance

A number of eye-related issues such as dry eye syndrome, ocular drug kinetics and contact lens fitting are related to the composition and the quantity of tears in the precorneal tear film. The preocular tear film that lies on the surface of the cornea is very important to ocular health. Its smooth surface is necessary for vision and it provides lubrication between eyelids and ocular surface and also helps in immunization of the corneal tissue.[1] The preocular tears can be divided into three compartments: the precorneal tear film, the conjunctival sac and the tear menisci containing a majority of the tears.[2] In each blink, the tears in the three compartments are mixed and re-distributed.[3] The tear film is composed of three layers (Figure 1-1). Contacting the corneal epithelium is a hydrophilic mucus layer approximately 0.02 to 0.05 μm in thickness.[4] As the underlying cornea itself is extremely hydrophobic, this layer is believed to provide a wetting substrate for the aqueous layer above it, which is about 6 to 9 μm thick.[4, 5, 6, 7] Outside the aqueous layer is a 0.1 to 0.2 μm thick lipid layer that reduces tear evaporation.[4, 8] In my study I focus mainly on the aqueous layer of the tear film, which consists most of the tear film volume.

Tears function cooperatively with the ocular surface epithelium to maintain the health of ocular surface and the abnormal quantity or quality of tears may result in ocular disease.[9] Additionally, the thickness of the tear film is a key indicator of ocular problems like the dry eyes. Thus, it is important to understand and quantify the effect of various physiological and anatomical features on tear volume and tear film thickness. It is clear that the balance between the production and elimination of tears determines the quantity of preocular tears, and an increase in the production or a reduction in elimination will increase tear volume and tear film thickness. It is also well known that an increase in tear elimination rates can result in a reduction

in tear volume. For example, it is known that a reduction in tear production or an increase in evaporation due to destruction of the lipid layer covering the tear film results in thinner tear films.[1] However, there is no mathematical model in literature that relates the tear volume and tears film thickness to tear production and elimination rates. Quantitative assessment of the factors that control the tear film thickness has not received much attention in the literature. To investigate such issues, we analyzed the main contributors to the production and elimination of aqueous tears, which are the lacrimal glands, lacrimal canaliculi, the ocular surface epithelia and evaporation.

Tears are produced mainly by the secretion of various glands and are eliminated by evaporation from mainly the precorneal tear film, the drainage through the canaliculi and possibly by absorption through the epithelia of the conjunctiva (Figure 1-2).[10, 11] Each of these routes of tear elimination has been extensively studied experimentally. Lacrimal glands secrete about 1-4 μL/min and account for most of the tear production, [12,13] active drainage through the lacrimal canaliculi is responsible for about 60% of the tear elimination,[10] and evaporation rate is about 0.10 μL/min.[14] The ocular surface epithelium, most of which is conjunctival epithelium, can actively transport solutes and water from and into the preocular tears. The secretion rate of fluid through rabbit conjunctiva is measured to be comparable with the tear turnover rate of rabbits,[15] and therefore epithelium secretion might also be important for the tear dynamics. However, the mechanisms that relate the tear production and elimination to the total tear volume have not been addressed at a quantitative level. A mathematical tear balance model requires quantitative models for tear production and tear elimination (drainage, evaporation and absorption), which requires the detailed understanding of the physiology of these processes. It is believed that the tear evaporation is a passive process, while the production, absorption and

drainage are active processes. Due to the relatively simple mechanism, the theory for tear evaporation is relatively well established[16] while the quantitative theoretical approaches for other routes of tear circulation remain limited. The production of tears is regulated by hormonal and neural control, and the mechanisms of the regulation processes are not yet completely understood, thus a mathematical description of the tear production is difficult.[17] Tear absorption is an active process involving the active transport of sodium, chloride and potassium ions as well as water, glucose etc, and these mechanisms are also not fully understood.[18] The mechanism of tear drainage is still not completely clear in spite of hundreds of years of study.[19]

In addition to experimental studies, there have also been theoretical studies on certain aspects of the tear dynamics. Wong et al.[20] showed that the tear film thickness can be related to the radius of curvature of the meniscus. This result only shows that a relationship exists between the meniscus curvature and the tear film thickness and Wong's model cannot predict either one of them. Based on previous experimental and theoretical work, Levin et al. developed an ocular surface transport model in which they treated the conjunctival epithelium and the corneal epithelium as a single layer of uniformly distributed cells. The predictions of this model agreed well with the experimental data for the transepithelial potential difference.[21]

The theoretical work cited above cannot be used to predict the effect of various physiological parameters on tear volume and composition because these studies only modeled individual processes relevant to tear dynamics, such as evaporation, and the corneal and conjunctival epiehtlium transport. Therefore, we hope to develop a comprehensive model that can relate various physiological parameters to the key variables of the tear film such as the tear volume and tear thickness. The proposed model is a dynamic tear balance in the eye, which states that the rate of accumulation of tears in the eyes is the difference between the rates of

inflow (lacrimal gland secretion) and the outflow (evaporation and drainage through the canaliculi). For the lacrimal drainage through the canaliculi, (Figure 1-2) we first developed a mathematical model[22] that was based on the active drainage mechanism suggested by Doane,[23] which is described below. Then we developed a mathematical model for the ion and water transport through ocular epithelia, which includes corneal and conjunctival epithelia. The mechanisms of transport across corneal and conjunctival epithelia involve both active and passive transport of solutes. Due to the large surface area of the conjunctiva, the ion and water transport through the conjunctiva is expected to play a more important role in the tear dynamics.[15, 24] Even though transport across corneal epithelium has been studied and modeled[25], it was decided to neglect the corneal epithelium in this part of the study partly because of the small area and permeabilities of cornea, and partly to avoid making the model too complex. It should be pointed out that the corneal transport of solutes and water may have considerable effects on the pre-corneal tear film, as during the interblink, the thinned tear film near the tear meniscus regions (black lines) may impede the exchange of solutes and water between the pre-corneal tear film and other regions of tear film. This issue is neglected in the current model, but can be explored later. Because the lacrimal gland secretion mechanism is relatively complicated, in my study we assume that the secretion rate of the lacrimal gland is constant. A mathematical model of the ion and water secretion by the lacrimal gland can be developed in the future work, and it can be easily incorporated into the tear dynamics model. The tear evaporation rate is assumed to be constant in this study, and the effect of its variation on the tear film is explored. Based on the drainage mechanism described above, we also developed a mathematical model of the drainage of Newtonian fluids with viscosity higher than tear viscosity as well as non-Newtonian fluids

through canaliculi. In addition, we also developed a mathematical model of the mixing of tears under the lower eye lid based on Taylor dispersion mechanism.

Tear Drainage

Tear Drainage Mechanism

It is estimated that tear drainage contributes to more than 50% of the normal tear elimination,[10] and thus investigation of tear drainage mechanism is valuable for understanding the factors that may lead to tear depletion in the eyes. There have been a number of experimental studies on tear drainage but no theoretical model has been developed for the process of tear drainage through the canaliculi. We first develop a mathematical model to predict the tear drainage rates from the canaliculi. The model can serve to validate the mechanisms proposed in the literature and can also be used to estimate the effect of various parameters on tear drainage rates.

It is widely accepted that the tear drainage through the canaliculi is an active process, in which blinking plays an important role. Based on anatomical studies, Jones proposed that during a blink the canaliculi are shortened and compressed by pretarsal muscles, and the lacrimal sac expands, leading to tear flow from the canaliculi to the sac. The cyclic actions of the canaliculi and the lacrimal sac together result in tear drainage.[26] Rosengren inserted catheters into the canaliculi to measure the pressure during the blink and the interblink[27] and Maurice and Wright[10] used dark particles as visual tracers to observe the flow of tears in the eyes. Based on the direct visualization, they concluded that most of the tears in the meniscus flow along the lower meniscus, and go into the lower punctum. This observation was later supported by the studies by Nagashima et al.[28] In addition, Rosengren concluded that there must be a valve mechanism between the canaliculi and the lacrimal sac during the interblink, which was later confirmed by studies that used radioactive tracers.[29] Both Maurice and Rosengren also concluded that the

canaliculi are compressed during a blink and that the tears are squeezed from the canaliculi into the lacrimal sac,[10, 27] which agrees with the high-speed photography observation of Doane.[23] However the physiological studies of Rosengren[27] also show that the pressure in the lacrimal sac increases during blinking, which contradicts the finding of Jones.[30] The main difference between the conclusions of the studies listed above concerns the role of the lacrimal sac in drainage. Because it was reported that tear drainage was not greatly affected even with a disabled lacrimal sac,[27] it is reasonable to assume the lacrimal sac does not play any important role in the tear drainage. Our mathematical model is based on the drainage mechanisms proposed by Doane, which are described in detail below.

At the beginning of the lid-closing period, the canaliculi are filled with tears and the lids begin to move towards each other. Because the puncta are at the medial end of the lids, they meet tightly and are closed when the lids are 1/3 to 1/2 closed. During the rest of the lid-closing period, the canaliculi are compressed by the muscles, and with closed puncta, the tears are squeezed out of the canaliculi and into the lacrimal sac. At the beginning of the lid-opening period, during which the lids are moving apart from each other, the canaliculi are no longer compressed. The puncta continue to be firmly attached until the lids are about half-open, and during this time the pressure inside the canaliculi drops as the force on the canaliculi is removed and the elastic canaliculus wall tends to expand. Then the puncta burst open and the tears in the tear menisci are drawn into the puncta by the pressure difference between the canaliculi and the menisci. This blink-interblink cycle acts as a pump, which drives the drainage of tears (Figure 1-3 and 1-4).[23]

While there are minor discrepancies in the proposed mechanism of tear drainage, it is accepted that canaliculi play a key role in the process of active tear drainage. Therefore,

understanding the anatomy of the canaliculi is essential to the assessment of the tear drainage rate. According to anatomical studies, each canaliculus has a vertical part that is about 2 mm long and a horizontal part that is about 10 mm long.[23] The diameter of the vertical and the horizontal parts are about 0.3 mm and 0.5 mm, respectively. The joint between these two parts is called the ampulla and its diameter can be up to 2 to 3 mm.[30] Before the superior and the inferior canaliculi open into the lacrimal sac, they merge and form the common canaliculus, which has an inner radius smaller than each of the other canaliculi. The walls of the canaliculi are made of tissue that consists of elastic fibers which allows the canaliculi to stretch and shrink during each blink cycle, which is essential for tear drainage.[31] Anatomic studies show that the Horner's muscle applies contraction force on both the vertical and the horizontal parts of the canaliculi. The force is largest for the vertical part and it decreases along the horizontal part towards the lacrimal sac.[32]

It is noted that while the mechanism detailed above is commonly accepted, several questions related to the tear drainage remain unanswered. For instance, it is unclear how tears drain during sleep. Also the composition of the lacrimal part of the orbicularis oculi muscle is unknown and in particular it is not clear whether the lacrimal part of the orbicularis oculi muscle have specialized muscle spindles like the outer eye muscles[33, 34]. The exact structure of the muscles will effect the distribution of the applied force on the canaliculi and thus impact the drainage.

Mechanical Properties of Lacrimal Canaliculi

According to the mechanisms proposed by Doane, the blink-interblink cycle leads to repeated compression and expansion of the canaliculi that pushes tears from the tear film to the lacrimal sac.[23] According to this mechanism, the mechanical properties of the canaliculi are expected to be a key factor to the drainage rate of tears. Our preliminary studies showed that both

the rate and the time scale of tear drainage depend on the modulus of the canaliculus. However, there had been no reports in literature regarding the mechanical properties of the lacrimal canalicuil. In our preliminary studies, the modulus of the canaliculus is estimated by matching the inflow and outflow of tears under physiological conditions. However by using this fitted value of the modulus, the model predicted a much smaller time scale for pressure relaxation in the canaliculi compared to the experiments, especially for the interblink period. The errors in the model prediction likely arose from the assumption that the canaliculus is a linearly elastic material. The structure of the lacrimal canaliculi is complex and thus it is expected to be viscoelastic, and so its mechanical properties can be described using the storage modulus (E'), which represents the elastic property, and the loss modulus (E"), which represents the damping ability of the tissues. The goal of this part of the study is to measure the viscoelastic behavior of the canaliculi and compare it with the estimated values obtained by matching the tear inflow with tear outflow. Specifically, we measured the dependence of dynamic mechanical properties of porcine canaliculi on frequency and age by using a Dynamic Mechanical Analyzer (DMA). Typically, in DMA a sinusoidal stress is applied and the resulting strain is measured, and the storage modulus and the loss modulus are calculated from the in-phase and out-of-phase portions of the strain, respectively. Also, the canaliculi were subjected to repeated loading-recovery cycles to simulate blinking, and the results were compared with reported measurements on pressure relaxation in the canaliculi and also with prediction of our tear drainage model.

Conjunctiva Epithelium Transport of Solutes and Ions

Other than the tear drainage through cancliculi, the transport of water and ions through conjunctival epithelium is also believed to play an important role in tear dynamics. The conjunctival epithelium consists of three to six layers of epithelial cells, which transport ion and water, and goblet cells, which secrete the mucus layer of the tear film.[35] In this study we focus on

the aqueous portion of tears, and therefore on the transport of ions and water by normal epithelial cells. The cell membrane of the epithelial cells contains ion channels, water channels, cotransporters and pumps that transport solutes and water. Solutes and water are also transported through paracellular pathways. Since the movement of electric charges is involved, transport processes depend both on concentration and potential difference across the membranes. For the conjunctival epithelium, the apical side contacts tears and the basolateral side contacts blood through the fenestrated capillaries.

Before developing a model for conjunctiva transport it is essential to understand the transport mechanisms of ions and water from the in vitro and in vivo studies reported in literatures. In the in vitro studies on conjunctival epithelium, typically the excised rabbit conjunctival epithelia are mounted between Ussing-chambers, where tissues are mounted between two chambers with controllable media compositions, and the short-circuit current (I_{SC}) or the open-circuit potential difference (PD) is measured. By controlling the solute concentrations in the Ussing chambers and by using specific pathway inhibitors Kompella et al.[36] and Shi and Candia[37] showed that the conjunctival epithelium transport mainly occurs through Cl channels and Na-Glucose cotransporters at the apical side, and Na-K pump, Na-K-Cl cotransporters and K channels at the basolateral side. To simplify the notation, the sign and magnitude of the electrical charge associated with each ion is not explicitly included in this study. The studies cited above also suggested that the conjunctival epithelium could either secrete or absorb water, depending on the solute concentrations on the apical and basolateral sides. These experiments also quantified the contribution of Na and Cl transports to I_{SC}. The basic mechanisms proposed by Kompella et. al. and Shi and Candia were supported by other experiments in Ussing-chambers[38,39,40,41,42,43,44] and also by immulocalization techniques.[45,46]

Other studies focused on the changes in water transport as a result of addition of chemicals or changes in osmolarities.[15,24] In addition to the in vitro studies listed above, Levin and Verkman[47,48, 21] measured the water permeabilities of the conjunctival tissue and the cell membrane in living mice, and also studied the effects of modulation or deletion of CFTR (Cystic Fibrosis Transmembrane conductance Regulator) and the Na transport pathways on the potential difference between the apical and basolateral sides.

Effect of Viscosity on Tear Drainage and Ocular Residence Time

Eye drops are commonly instilled to treat a variety of ocular problems such as dry eyes, glaucoma, infections, allergies, etc. The fluid instillation results in an increase in tear volume, and it slowly returns to its steady value due to tear drainage through the canaliculi, and also fluid loss through other means such as evaporation or transport across the ocular epithelia. In fact, if the instilled fluid has a viscosity similar to that of tears, which is about 1.5 cp, the instilled fluids or solutes are eliminated from the tears in a few minutes. As a result, the fluids or solutes have a short contact time with the eye surface, which results in reduced effects for artificial tears or low bioavailability for ophthalmic drugs. To increase the duration of comfort after drop instillation and to increase the bioavailability of the drugs delivered via eye drops, it is desirable to prolong the residence time for the instilled fluid. It has been suggested and also shown in a number of clinical and animal studies that increasing the viscosity of the instilled fluid leads to an increase in the retention time. Zaki et al.[49] showed that increasing the viscosity of instilled fluid leads to a minor effect on the residence time unless the viscosity of instilled solution increases above 10.2×10^{-3}Pa·s. The study by Wilson[50] also supports the notion that the viscosity needs to be above a certain value in order to slow down the fluid clearance significantly, and that critical value is larger than 8×10^{-3}Pa·s. However little was known about the reason for the existence of such critical viscosity. Additionally, although increasing fluid viscosity increases the residence

time, it may also cause discomfort and damage to ocular epithelia due to an increase in the shear stresses during blinking. Shear thinning fluids such as sodium hyaluronate (NaHA) solutions can be used to obtain the beneficial effect of an increase in retention and yet avoid excessive stresses during blinking. The likely reason is that the shear rates during blinking are very high and at such high shear rates these shear-thinning fluids exhibit low viscosity but during the interblink which is the period during which tear drainage occurs, these fluids act as high viscosity fluids leading to reduced drainage rates and a concurrent increase in residence time.

While the mechanisms of the impact of viscosity on residence time are qualitatively understood for both Newtonian and non-Newtonian fluids, no quantitative model has been yet proposed that can explain the detailed physics and predict the effect of viscosity on drainage rates and on retention time of eye drops. Such a model is likely to lead to an improved quantitative understanding of the effect of viscosity on tear dynamics, and also aid as a tool in development of better dry eye treatments and drug delivery vehicles. The goal of this part of the study is to develop a mathematical model to predict the effect of viscosity on drainage rates and the residence time for both Newtonian and non-Newtonian fluids. This part of the study is based on the tear drainage mechanism proposed by Doane,[23] and it is an extension of our tear drainage model that focused on modeling drainage of tears, which were considered to be Newtonian fluids with a viscosity of 1.5 cp. In this study, the drainage model will be modified to calculate the drainage rate of instilled fluids with viscosities that are larger than the critical viscosity, and so the system does not reach steady state in the blink phase. Additionally, the drainage rates will be calculated for power-law fluid, which is a typical type of non-Newtonian fluid used for ocular instillation. Finally, the modified tear drainage model will be incorporated into a tear balance model to predict the effect of viscosity on residence time of eye drops.

Tear Mixing Under the Lower Eyelid

In order to develop a tear dynamics model, it is important to understand whether the preocular tears are well-mixed, since if they are indeed well-mixed it will greatly simplify the tear dynamics model. The preocular tears can be divided into three compartments: the precorneal tear film, the conjunctival sac and the tear menisci.[2] The fluid in these compartments gets mixed due to the convection generated in the eyes by the blink. However it is not completely known whether these compartments are perfectly well-mixed or whether there are concentration differences between these compartments. This issue is of fundamental importance to the understanding of tear dynamics and it is also relevant to applications such as ophthalmic drug delivery. For instance it has been suggested that the residence time of ophthalmic drugs could be increased if these are injected into the lower conjunctival sac because of limited mixing between the sac and the tear film.

During blinking the upper lids move downwards about 10 mm,[51, 52, 53, 54] covering the area of the exposed tear film, and the lower lids move upwards but the amplitude is only about 1 mm or less.[55, 56] It is thus expected that the tears in the upper conjunctiva sac and the exposed tear film are better mixed than those in the lower conjunctiva sac. To understand the mixing of the whole tear film, it is essential to first understand the mixing of the tears in the lower conjunctiva sac.

It has been shown that after instilling a dye solution into the lower conjunctiva sac, it takes about a few minutes for the dye to emerge on the lower lid edge, which is shorter than the time expected for purely diffusion-driven mixing.[55] To elucidate the mixing mechanism under the lower lids, Macdonald and Maurice instilled fluorescein into the lower conjunctiva sac and studied the time of fluorescein appearance on the lid edge with the subjects blinking normally. The time of fluorescein appearance was observed to be much shorter that the estimated time for

the mixing driven only by diffusion. It had also been shown in earlier research that the rate of the fluorescein loss through the conjunctiva is slow compared to the tear mixing.[57] Thus it was suggested that the mixing might be caused by the periodic tear flow generated during the blink cycle. [55, 58] The mechanism that was suggested by Macdonald and Maurice is commonly called "Taylor dispersion", and this mechanism is illustrated in Figure 1-5. To illustrate this mechanism, let us consider a case in which a fluid is contained in between two flat plates, and the top plate oscillates with a periodic velocity. This situation is analogous to the lower conjunctival sac. Let us now consider that a pulse of solute that is uniform in the y direction is introduced at some axial location at t = 0. The goal of Taylor dispersion modeling is to quantify the spread of this pulse. The periodic movements of the eyelids create a velocity field of tears and the solutes move in the x direction driven by convection. The time scale for the diffusion of the solutes in the y direction is comparable to that for the periodic motion, and so as axial velocity stretches the initial rectangular pulse to a trapezoidal shape, lateral diffusion reestablishes the rectangular shape with a larger than original width. Due to the combination of temporal (y direction) diffusion and axial (x direction) convection, the pulse will be spread and the solutes will be transported in the along the lower lids from the fornix to the edge of the lower lids. Although the experiments by Macdonald and Maurice provided data that supports such mechanism,[55] the quantitative relationship between lid/globe motion and the solute transport was not available. While the above researchers' discussion is only based on the movement of the lower lid, the same mechanism similarly applies for the mixing related to the movement of the globe.

If the tear mixing in the lower conjunctiva sac is indeed driven by Taylor dispersion, the mixing time is expected to depend on the relative motion between the lower lid and the globe.

During a blink the lower lid moves horizontally towards the nose by about 3 mm[57,59] and also moves up but with much smaller amplitude. It has been shown that the globe rotates horizontally towards the nose and downwards vertically by about 1~5˚ each and then returns to the original position within the first 0.05 s of a blink.[56] In addition to the vertical and horizontal shearing described above, during blinking the lids also press against the globe and the globe retreats in the posterior direction for about 1-2 mm,[51, 59, 60] which suggests that the tear film may also be squeezed during the blinking. Because the time course for the globe retreat is in sync with the eyelid motion,[56] if the squeezing of the tear film exists, the squeezing motion would be finished within the first 0.2 s of a blink cycle.

The purpose of this part of the study is to develop a mathematical model to relate the mixing in tears to the cyclic movement of the globe and the lower eyelid during blinking. Based on the experimental studies listed above, we develop models for two different velocity profiles: (1) shear flow generated by vertical (inferior-superior) motion of either the globe or the lower eyelid, (2) squeeze flow generated by the motion of the globe perpendicular to the eyelid. In reality both of these motions occur together but since there is insufficient data regarding the exact kinematics of the globe and eyelid movement and the two kinds of motion are not in sync, we construct mathematical models for each of the two cases separately. In addition, although it is likely that the horizontal lower-eyelid motion in the nasal-temporal direction also contributes to the mixing of tears, it is not included into the model due to the relative complex mixing mechanism for this scenario. However this case will qualitatively discussed.

In this part of the study, we first mathematically analyze the mixing in the lower lid, and develop a model which can predict the concentration of tracers both under the lower eyelid and in the exposed tear film after administration of tracers in the tears below the lower eyelid. We

compare the predictions with experimental data to validate the model. In addition to elucidating the mechanism of tear mixing, the study can also be helpful in the interpretation of various experimental studies in which tracer concentrations are monitored in various parts of eyes after fluid instillation.

Application of the Tear Dynamics Model

Since the tear dynamics model is physiology-based, it intrinsically contains many of the parameters that are relevant to understanding and alleviating problems related to tears. The mathematical model can be solved to either predict the time course of the parameters such as tear volume and tear film thickness, or predict the steady state of such parameters. The model is expected to predict the tear osmolarity, and other issues related to the effect of salt concentration on tear volume, conjunctival secretion, and the transport of ions across the conjunctiva. The model is also able to predict the dependence of the tear film thickness on various parameters such as tear viscosity, surface tension, tear evaporation rates, canaliculi elasticity, etc. Additionally the model is able to predict the rates of changes in tear volumes after instillation of a specific volume of tear fluid and the residence time of tracers and drugs in the tear film, and thus it can be incorporated into an ocular pharmacokinetic model. Such a model can effectively be used to develop an improved understanding of the tear dynamics and also help in evaluating and designing treatments for tear-related alignments such as dry eye syndrome, a common but poorly understood disease.

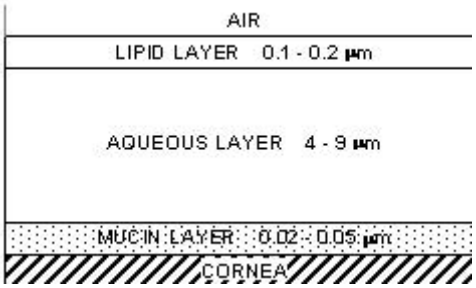

Figure 1-1 The structure of the tear film

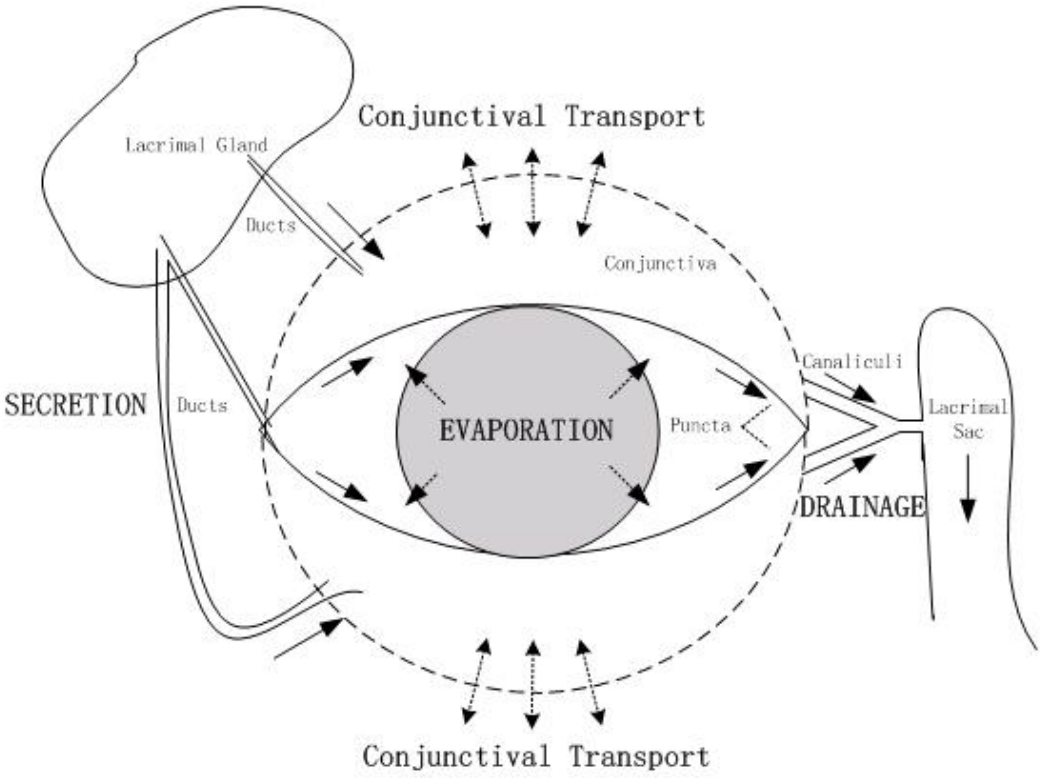

Figure 1-2 Tear production and elimination pathways

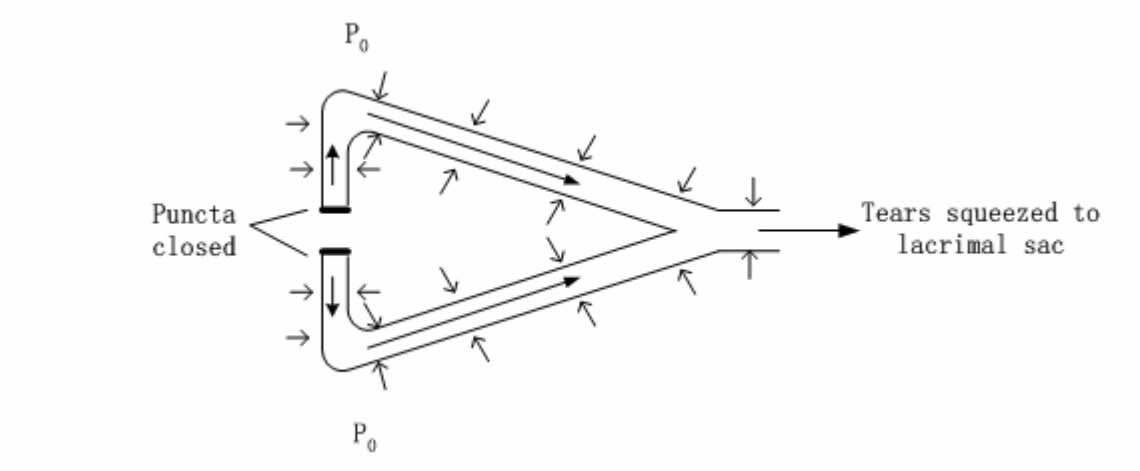

Figure 1-3 The lacrimal canaliculus during the blink phase

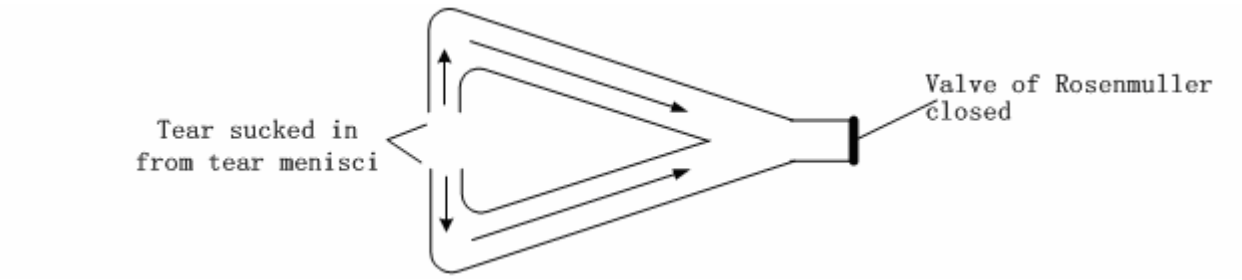

Figure 1-4 The lacrimal canaliculus during the interblink phase

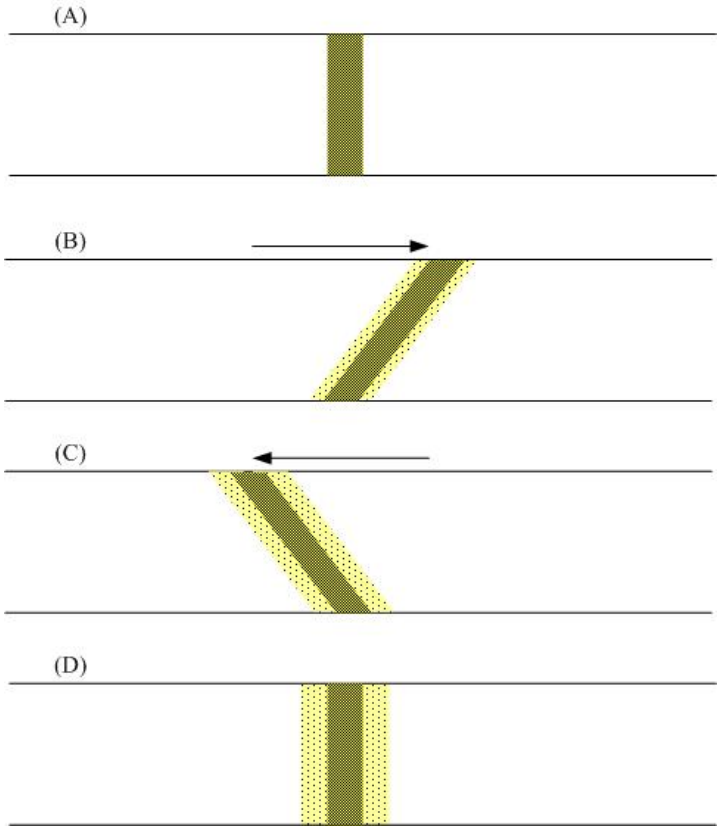

Figure 1-5 Taylor dispersion due to shearing. A) A pulse of solute is introduced at t=0. B) The solutes are transported laterally due to convection. C) Meanwhile the solutes diffuse transversely. D) The pulse widens due to the combination of convection and transverse diffusion.

CHAPTER 2
MATERIALS AND METHODS

In this part of the study, first the mathematical models for tear drainage and conjunctiva transport were developed, and then they were incorporated into a tear dynamics model. Due to the lack of information about the mechanical properties of the lacrimal canaliculi, which are responsible for the tear drainage, dynamic mechanical analysis (DMA) was conducted during the development of the tear drainage model. Then the drainage model was extended to describe the drainage of Newtonian fluids with high viscosity as well as non-Newtonian fluids. At last, a mathematical model was developed for the tear mixing under the lower eyelids.

Tear Drainage Model

Model Development

Based on the tear drainage mechanisms described in the introduction, we develop a mathematical model for tear drainage in the canaliculi. According to the mechanism described by Doane,[23] the blink-interblink cycle can be divided into four periods, which are detailed in Figure 3 of the reference cited above. The first period begins with the downward motion of the upper eyelids and ends when the puncta are occluded due to the contact of the lid margins. In the second period, the upper eyelid continues to move down, the puncta stay occluded, and the lid closure acts to squeeze the canaliculi to drain the fluid. The third period begins with the lid opening and ends when the punctual papillae "pop" apart to open the canaliculi to the meniscus. In this period the compressive force on the canaliculi is removed leading to creation of suction. In the fourth period, the lids open up completely and then remain stationary till the next blink. During this period, the vacuum created in the canaliculi draws fluid from the menisci. In our model, periods 1 and 3 do not lead to drainage and thus are neglected. In the following sections, period 2 is called the "blink phase", period 4 is called the "interblink phase", and a cycle of one

blink and one interblink is referred to as a "blink cycle". To summarize the mechanism, during the blink phase, the puncta are occluded and the canaliculi are compressed, and this causes a flow towards the sac. This flow stops when the pressure in the canaliculi equals that in the sac, where the pressure is assumed to always be atmospheric. During the interblink phase the pressure in the canaliculi is reduced due to the removal of the muscle force, and the valve at the sac end of the canaliculi closes. Since the meniscus is at a higher pressure than the canaliculi at this time, tears flow into the canaliculi till the pressure equalizes. The mechanism described above is illustrated in Figures 1-4 and 1-5 and also by Doane.[23] A recent study has suggested that the valve at the sac end of the canaliculi is not a real valve but is caused by the swelling of the cavernous body of the lacrimal passage.[61] It is noted that whether the valve at the sac end is real or is based on different swelling states does not affect our proposed model.

In our mathematical model, the canaliculus is simplified as a straight pipe of length L with an undeformed radius R_0 and wall thickness b. The stress-strain relationship is complicated for soft tissues like the lacrimal canaliculi, but due to lack of data and to simplify the model, it is assumed that the canalicular wall is linearly elastic with a modulus E. The canaliculus is considered to be a thin shell, i.e., its thickness is negligible in comparison to the radius, and thus, axial deformation is neglected and the length of the canaliculi L is assumed to be constant.

During the blink phase, the muscles around the canaliculus apply a pressure p_0, which is assumed to be constant and uniform, to compress the canaliculus, and this pressure is balanced by the hoop stress. Additionally, axial pressure gradients drive fluid flow inside the canaliculus. The fluid flow equations are combined with the solid deformation model to yield a single partial differential equation that can be solved to predict the radius of the canaliculus as a function of

the axial position and time. The details of the derivation are in Appendix A. The linearized form of the partial differential equation is

$$\frac{bER_0}{16\mu_{tear}}\frac{\partial^2 R}{\partial x^2} = \frac{\partial R}{\partial t} \tag{1}$$

where E and b are the elastic modulus and the thickness of the canaliculus wall, respectively, μ_{tear} is the viscosity of tears or fluids instilled on the ocular surface, R is the canaliculus radius, x is the axial coordinate originating at the puncta and t denotes time. Equation (1) describes the variation of canalicular radius as a function of time and axial position during the blink cycle and from the radius variation the drainage rate and pressure can be predicted.

In order to solve the above partial differential equation, boundary conditions and initial conditions are needed. Based on the photography observation of Doane,[23] the following assumptions are made. During the blink phase, the canaliculus is occluded at the punctal side and it opens into the sac on the other side. Thus, the flow rate is assumed to be zero at x = 0, and the pressure at $x = L_{canaliculi}$ is assumed to stay constant at the sac pressure, where $L_{canaliculi}$ is the length of canaliculi. Since it is assumed that the sac pressure stays zero (i.e., atmospheric), the pressure at x=L remains zero during the blink phase. During the interblink phase, the canaliculus is occluded at the sac side and is open at the punctal side, so there is no flow at $x = L_{canaliculi}$. We further assume that the pressure at the punctal end i.e., at x = 0 equals the pressure in the tear menisci. Due to the cyclic nature of the blink-interblink process, the initial conditions for the blink phase are the same as the conditions at the end of the interblink. Similarly, the conditions at the end of the blink are used as the initial conditions for the interblink phase.

Thus, the boundary conditions and initial conditions for the blink phase (from t = 0 to $t = t_b$) are

$$
\begin{aligned}
&q(x = 0,\ t) = 0 \\
&p(x = L_{canaliculi},\ t) = 0 \\
&R(x,\ t = 0) = R_{ib}
\end{aligned}
\tag{2}
$$

where q is the tear flow rate, p is the internal pressure, R_{ib} is the radius of the canaliculus at the end of the interblink phase and t_b is the duration of the blink phase.

The boundary conditions and initial conditions for the interblink phase (from $t = t_b$ to $t = t_c$) are

$$
\begin{aligned}
&p(x = 0, t) = -\frac{\sigma}{R_m} \\
&q(x = L_{canaliculi}, t) = 0 \\
&R(x, t = t_b) = R_b
\end{aligned}
\tag{3}
$$

where σ is the surface tension of tears, R_m is the radius of curvature of the meniscus, R_b is the radius of the canaliculus at the end of the blink phase, and t_c is the duration of the blink-interblink cycle. It is noted that even though the menisci pressure is negative due to the tear-menisci curvature, tears flow into the canaliculi during the interblink because the pressure in the canaliculi is even more negative. Furthermore due to the presence of the valve at the sac end, the pressure in the canaliculi at x = L is no longer forced to be equal to the zero pressure in the sac.

The steady state radii, i.e., the radii obtained by the method described in the Appendix are:

$$
R_b = \frac{R_0}{1 + \dfrac{(p_0 - p_{sac})R_0}{bE}} \tag{4}
$$

$$
R_{ib} = \frac{R_0}{1 + \dfrac{\dfrac{\sigma}{R_m}R_0}{bE}} \tag{5}
$$

where p_0 is the pressure outside the canaliculus, p_{sac} is the pressure in the lacrimal sac, and R_b and R_{ib} are the steady state radii at the end of the blink and the interblink phases, respectively.

The details of the derivation of R_b and R_{ib} are also given in Appendix a. Based on equations (4) and (5) and the fact that the radius of the canaliculus reaches steady states during the blink and the interblink phase for normal tear fluid, the average tear drainage rate can be written as

$$q_{drainage} = \left(\frac{\pi L_{canaliculi}}{t_c}\right)\left[\left(\frac{R_0}{1+\frac{\frac{\sigma}{R_m}R_0}{bE}}\right)^2 - \left(\frac{R_0}{1+\frac{p_0 R_0}{bE}}\right)^2\right] \quad (6)$$

Mechanical Properties of Lacrimal Canaliculi

Tissue Samples

Porcine eyes with eyelids were purchased from Animal Technologies Inc (Tyler, TX). Eyes from pigs belonging to two age groups (6 to 9 months old, n=25 and over 2 years old, n=23) were used for the measurement of E' and E". The loading-recovery tests were done on a separate batch of eyes from 6 to 9 months old pigs (n=8). The tissues were kept at 5 °C until the extraction of the canaliculi. The porcine eyes have only a single canaliculus and it was extracted using surgical blades and a lacrimal probe within 38 hours postmortem. The mechanical properties of the tissue that surrounds the canaliculus are significantly different from that of the canaliculus. Accordingly, the presence of even a very small amount of surrounding tissue in the samples is manifested in significant deviations in the measured mechanical properties. Therefore extreme care was taken to ensure adequate removal of surrounding tissues and the reproducibility in the measurements suggest that the samples utilized in the study reported here did not contain any tissue other than the canaliculus. Each canaliculus sample was cut along the length to obtain a flat sheet. The samples were kept in the isotonic Dulbecco's phosphate buffered saline (Sigma, St. Louis, MO) under room temperature until the measurements. The

samples were numbered and were photographed with a digital camera (Coolpix 5600, Nikon, Japan). The sample areas, which are required as input parameters for DMA, were measured from the digital photos using ImageJ image analysis software available on the NIH website. [62]

Dynamic mechanical analyzer (DMA) setup

The rheological measurements were conducted on a Dynamic Mechanical Analyzer (DMA Q 800, TA Instruments, New Castle, DE) in compression mode while submerged in Dulbecco's phosphate buffered saline at ambient temperature (24.0±0.3°C). Briefly, the flat-sheet samples were mounted between the moving upper clamp and the fixed chamber, which contained saline, and the strains in the samples under programmed stress were recorded (Figure 2-1). All the measurements were conducted within 40 hours postmortem.

Frequency dependent rheological response

The rheological response was measured in a compression mode with a periodic force. At the beginning of each run, a static preload force of 0.01 N was applied to ensure adequate contact between the clamps and the sample, and then the sample thickness was measured automatically by DMA. During these measurements, the DMA applies a periodic compressive strain and measures the force required to achieve the desired strain. The magnitude of strain needs be sufficiently small so that the response is in the linear range, which implies that the viscoelastic properties do not depend on the strain magnitude. Pilot experiments were conducted with the frequency fixed at 1, 10 or 25 Hz and the oscillation amplitude changing between 5 μm to 100 μm to determine the linear range of viscoelasticity. A plateau region of 5 to 50 μm for both the storage modulus and the loss modulus was observed, within which the variation of the moduli is less than 15% and beyond which the moduli rose to over 900% of the plateau values. The oscillation amplitude of 40 μm, which is in the linear range was eventually chosen to ensure that

the corresponding stress was comparable to the physiological stress in a canaliculus during blinking, which is about 400 Pa. A "Force Track" of 115% was used in these experiments, which means that an additional time independent compressive force that equals to 15% of the amplitude of the dynamic force was imposed to ensure adequate contact between the samples and the clamps. Physiologically, the duration of the canaliculi compression is about 0.04 s (blink), and the duration of the canaliculi expansion is several seconds (interblink).[23] Therefore, the frequency range of interest should be between 1 Hz and 25 Hz. Accordingly, the storage modulus (E') and loss modulus (E") were obtained under three different frequencies, 1 Hz, 10 Hz and 25 Hz.

Simulation of blink-interblink cycles

To simulate the blink-interblink cycles, the canaliculus sample was exposed to repeated cycles that comprised of a loading phase during which a constant stress of 400 Pa was applied (blink) and a recovery phase during which the static force was removed (interblink). Ideally, to simulate a real blinking cycle, the durations of blink and interblink should be about 0.04 s and 6 s, respectively. However, it was found that due to equipment limitation, the shortest duration of the loading period is 0.01 min. Due to this limitation, the duration of the loading (blink) period was set to be 0.01 min (0.6 s). Experiments were conducted with a recovery (interblink) phase duration of 5.4 s so that the duration of one blink-interblink cycle is equal to the physiological value of 6 s. Similar to the frequency sweep protocol, the sample thickness was measured at the beginning of each test with a preload force of 0.01 N. In these experiments, this static force of 0.01 N was applied at all times to ensure sample-clamp contact. Application of this static force is equivalent to using "Force Track", which was used in the frequency dependent rheological measurements, except that if a "Force Track" is applied, the magnitude of the static force is determined by the equipment. The experiments comprised of measuring the dynamic stress and

strain as the samples were subjected to the repeated blink-interblink cycles. It is noted that each sample was first subjected to 21 cycles with 6 s recovery duration and then 11 cycles of 57.6 s recovery duration.

Statistical methods

Unless otherwise stated, the results are expressed as mean±S.D.. A two-way Analysis of Variance (ANOVA) was used to analyze the dependence of the moduli on frequency and age, and the significant level was chosen to be 0.01.

Conjunctiva Epithelium Transport Model

The epithelium typically consists of about 3~6 cell layers, but there is little quantitative data on transport of solutes and water between adjacent cell layers. It has been suggested that the layer of cells in contact with the tears offers a majority of the resistance to transport, and so subsequent cell layers can be neglected.[21] Therefore, in this model the epithelium is assumed to consist of a single cell layer, with a uniform distribution of homogeneous cells. With these simplifications, the system consists of three compartments: the apical compartment, the cellular compartment and the basolateral compartment. In this part of the study, we include the transport of Na, K, Cl ions, and glucose and water molecules, both across the cellular compartment boundaries (transcellular) and through the space in between adjacent cells (paracellular). The main transport mechanisms included in the model are the Na-Glucose cotransport, the Cl channel and water transport at the apical membrane, the Na-K pump, Na-K-2Cl cotransport and the K channel and water transport at the basolateral membrane,[36,37] as well as the paracellular transport of Na, K, Cl, Glucose and water. The flux of water is assumed to be the sum of the osmotic flow through the transcellular and paracellular pathways and the electro-osmotic flow through the paracellular pathway, for which the water flow is proportional to the paracellular electric current.

The simplified scheme of the epithelium structure, along with the transport mechanisms is shown in Figure 2-2.

It is possible that some unknown transport pathways are not included in the model. In fact, there is experimental evidence that one kind of apical Na-amino acid cotransport exists in rabbit conjunctiva epithelium.[63,64] This pathway is not included in the model due to lack of adequate information for this cotransport mechanism. Furthermore, the role of acid-base transport in tear dynamics is not clear. It is also speculated that there may be more than one kinds of Cl channel on the apical surface of the epithelium. We hope to include these mechanisms into the tear dynamics model as adequate information about these mechanisms is developed from experimental studies.

Incorporation of the Tear Drainage Model and the Conjunctiva Transport Model into the Tear Balance

General Tear Balance Model

Below we perform mass balances for ions, glucose and water in the apical, cellular and basolateral compartments, and use the electroneutrality condition in each compartment. In the model developed below, we consider each compartment to be ideally mixed, which is reasonable in view of the small sizes of the cells and the large convection during the blink in the tear film. Since the basolateral compartment is in contact with blood through fenestrated capillary vessels[35] the solute concentrations in this compartment are assumed to be known constants. Solutes other then Na, K, Cl and glucose are lumped together into a single concentration variable (C_{Others}) and it is assumed that these 'other' solutes are not transported across the conjunctiva. Based on Figure 1 and the above assumptions, the model contains 12 unknowns, including 8 concentrations, which are the concentrations of Na, K, Cl and glucose in the apical ($C_{Na,a}$,$C_{K,a}$,$C_{Cl,a}$ and $C_{Glu,a}$)and the cellular ($C_{Na,c}$,$C_{K,c}$,$C_{Cl,c}$ and $C_{Glu,c}$)compartments, 2 volumes,

which are the volumes of the apical and the cellular compartments (V_a and V_c), and 2 electric potential differences, which are the potential differences across the apical and the basolateral membranes. To obtain these 12 unknowns, 12 equations can be written using the mass balance and electroneutrality conditions and these are listed below. The mass balances of Na, K, Cl, glucose and water in the apical compartment (tear side) yield equations (7)-(11):

$$\frac{d\left(C_{Na,a}V_a\right)}{dt} = q_{secretion}C^0_{Na,tear} - q_{drainage}C_{Na,a} - \left(2J_{Na-Glu} + J_{Na,paracellular}\right)S_{conj} \tag{7}$$

$$\frac{d\left(C_{K,a}V_a\right)}{dt} = q_{secretion}C^0_{K,tear} - q_{drainage}C_{K,a} - J_{K,paracellular}S_{conj} \tag{8}$$

$$\frac{d\left(C_{Cl,a}V_a\right)}{dt} = q_{secretion}C^0_{Cl,tear} - q_{drainage}C_{Cl,a} - \left(J_{Cl,channel} + J_{Cl,paracellular}\right)S_{conj} \tag{9}$$

$$\frac{d\left(C_{Glu,a}V_a\right)}{dt} = q_{secretion}C^0_{Glu,tear} - q_{drainage}C_{Glu,a} - \left(J_{Na-Glu} + J_{Glu,paracellular}\right)S_{conj} \tag{10}$$

$$\frac{dV_a}{dt} = q_{secretion} - q_{drainage} - q_{evaporation} - \left(J_{w,paracellular} + J_{w,transcellular,a}\right)S_{conj} \tag{11}$$

Equations (12)-(16) are the mass balance equations of Na, K, Cl, glucose and water in the cells, respectively.

$$\frac{d\left(C_{Na,c}V_c\right)}{dt} = \left(2J_{Na-Glu} - 3J_{pump} + J_{Na-K-Cl}\right)S_{conj} \tag{12}$$

$$\frac{d\left(C_{K,c}V_c\right)}{dt} = \left(2J_{pump} + J_{Na-K-Cl} - J_{K,channel}\right)S_{conj} \tag{13}$$

$$\frac{d\left(C_{Cl,c}V_c\right)}{dt} = \left(2J_{Na-K-Cl} + J_{Cl,channel}\right)S_{conj} \tag{14}$$

$$\frac{d\left(C_{Glu,c}V_c\right)}{dt} = \left(J_{Na-Glu} - r_{Glu}\left(C_{Glu,c}\right)\right)S_{conj} \tag{15}$$

$$\frac{dV_c}{dt} = \left(J_{w,transcellular,a} - J_{w,transcellular,b}\right)S_{conj} \tag{16}$$

Equations (17) and (18) are the electroneutrality conditions for the total fluxes entering the apical and cellular compartments, respectively.

$$-J_{Cl,channel} + 2J_{Na-Glu} + J_{Na,paracellular} + J_{K,paracellular} - J_{Cl,paracellular} = 0 \quad (17)$$

$$2J_{Na-Glu} - J_{Cl,channel} - J_{pump} - J_{K,channel} = 0 \quad (18)$$

In the above equations, the J's represent the flow rates of solutes, which are functions of the 12 unknowns and are normalized by the surface area of conjunctiva, S_{conj}. J_{pump}, $J_{Na\text{-}K\text{-}Cl}$ and $J_{Na,Gluare}$ the turnover rates of the Na-K pump, the Na-K-Cl cotransport and the Na-Glucose cotransport, respectively. $J_{Na,paracellular}$, $J_{K,paracellular}$, $J_{Cl,paracellular}$, $J_{Glu,paracellular}$ and $J_{w,paracellular}$ are the paracellular flow rates of Na, K, Cl, Glucose and water, respectively. $J_{Cl,channel}$ and $J_{K,channel}$ are the flow rates of Cl and K through their respective channels. $J_{w,transcellular,a}$ and $J_{w,transcellular,b}$ are the rates of water transport through the apical and the basolateral cell membranes, respectively. $C_{Na,tear}^{0}$, $C_{K,tear}^{0}$, $C_{Cl,tear}^{0}$ and $C_{Glu,tear}^{0}$ are the concentration of Na, K, Cl and Glu in the lacrimal gland secretion. r_{Glu} is the rate of glucose consumption in the cell. We note that fluxes in the direction of apical to basolateral are defined to be positive, and the turnover rates are always positive numbers. The fluxes of ion, glucose and water through channels, transporters or the paracellular route are functions of concentrations and membrane potentials, and the expressions for these fluxes are detailed in the appendix. In the above equations, $q_{secretion}$ and $q_{evaporation}$ are the flow rates of lacrimal tear secretion and evaporation, respectively, and these are assumed to be constants. Furthermore, $q_{drainage}$ is the flow rate of tear drainage through canaliculi, which is given by equation (6)

In the above equations, the value of $C_{Glu,tear}^{0}$ is assumed to be zero, and thus the tear glucose is contributed solely by transport from the blood through the conjunctival epithelium. This assumption is consistent with the fact that the tear glucose level is correlated with the blood

glucose level, which has been exploited as a method to monitor the blood glucose concentration.[65] In the above equations, the glucose consumption rate in the cell is normalized by the surface area of conjunctiva (S_{conj}). We note that in equation (15), the function $r_{Glu}(C_{Glu,c})$ represents the glucose consumption rate inside the cell, and it is assumed to be linearly dependent on the cellular glucose concentration, i.e.,

$$r_{Glu}\left(C_{Glu,c}\right) = r_{Glu}^{0}\,\frac{C_{Glu,c}}{C_{Glu,c}^{0}} \tag{19}$$

where r_{Glu}^{0} is a fitting constant whose value was obtained by matching the model prediction with experiments for the time scale of the changes in the I_{SC} after Na-K-Cl cotransporter blockade[36] In the above expression $C_{Glu,c}^{0}$ is arbitrary, and for convenience, it can be set equal to the normal glucose concentration in cells, which is typically 0.5 mM. [66] Results of model simulations indicate that the time scales for changes in ion transport rates are very sensitive to the glucose consumption rate. The fitted value of r_{Glu}^{0} is close to the glucose consumption rate measured for corneal epithelium cells,[67] which suggests that this value is perhaps reliable. However, it is likely that the expression for glucose consumption is more complex than the assumed linear kinetics. The metabolism of glucose in cells is expected to involve actively-controlled processes, and the activities of enzymes will definitely affect the glucose consumption. If additional information about cellular glucose consumption is available, it can be incorporated into the model to yield more reliable predictions.

Modified Model for an Ussing Chamber

The above equations couple all the routes of inflow and outflow of solutes and water into an eye, and thus represent a comprehensive model for tear dynamics. To validate the model, the set of equations given above can be modified to simulate in vitro experiments in Ussing-

chamber. Below we modify the equation set developed above to simulate Ussing-chamber experiments, and compare the model predictions with experiments.

In the Ussing-chamber experiments, the chamber volumes are sufficiently large so that only negligible changes in concentration can occur during the experiment. Accordingly, the concentrations in both the apical and the basolateral chambers can be treated as fixed constants. For the cellular compartment, equations (12) to (16) account for the mass balances and equation (18) accounts for electroneutrality. For the short-circuit experiments, the 6 unknowns (cellular concentrations of Na, Cl, K, glucose, cell volume and the potential across the cell membrane on either the apical or the basolateral sides) can be obtained by solving equations (12) to (16) and equation (18). For the open-circuit case there are 7 unknowns because the potential differences across the apical and the basolateral sides are different, and these 7 unknowns can be obtained by solving equation (12) to (16), which account for cellular mass balances, and equations (17), (18), which account for electroneutrality.

In Ussing-chamber experiments, typically the I_{SC} or the transepithelial potential difference is measured for a variety of different compositions in the apical and the basolateral compartments. In some cases, ions that are transported through specific pathways are replaced by other solutes, and in some other cases, chemicals are added to block some specific transport pathway. To simulate the ion channel blockade conditions in our model, the corresponding channel permeability or maximal flux was changed to 1/1000 of the normal value. Similarly, to simulate the stimulation of Cl channel by certain chemicals, the Cl channel permeability was increased to 10 times of the normal value. The factor of 10 was chosen so that simulations conducted with the increased permeability correctly predicted the increase in I_{SC} in the Ussing-chamber experiments. [15] To simulate the Cl free condition on the apical side, Cl concentration in

apical compartment was set to zero, and the change in osmolarity was compensated by increasing the concentration of the inert ions in the same compartment. Other ion substitution cases were simulated similarly.

Algorithm

A procedure similar to that used by Fischbarg and Diecke[25] and Novotny and Jakobsson[68] was used to solve the equations. Briefly, in each time step, the concentrations and membrane potentials from the previous time step were used in equations (A8) to (A12) to compute the ion and glucose fluxes. Next, the computed fluxes and the volumes from the previous time step were utilized in equations (7)-(10) and (12)-(15) to obtain the concentrations at the new time step. The computed concentrations were then used to compute the fluxes of water, and then the volumes were computed by using equations (11) and (16). Finally, the concentrations were updated again by using the computed volumes, and the potentials were then calculated using the electroneutrality conditions, i.e., equations (17-18). The time scales of the solute and water transport suggested that the time steps in the simulations should be on the order of 0.1 s. However, calculations showed that changing the time step from 0.1 s to 1 s led to undetectable differences in the results, and thus a time step of 1 s was used in all the calculations.

Model Parameters and Initial Conditions

A number of parameters are required in the tear dynamics model. Some of these are available in literature (Table 2-1[36, 69, 70, 71,66,72,66, 26 ,30 ,69 ,70 ,73,74,75,47,76, 22, 2, 10, 16]), and some were estimated based on reported studies (Table 2-2). We note that the surface tension value used in the current study is the static surface tension of the air-liquid (tear) interface.[69] In Table 2-1, $C_{Na,b}$, $C_{K,b}$, $C_{Cl,b}$ and $C_{Glu,b}$ are the basolateral concentrations of the respective solutes; $C_{Others,a}$, $C_{Others,b}$, and $C_{Others,tear}^{0}$ are the concentrations of the inert ions in the apical and basolateral compartments and the lacrimal gland secretion; $P_{Cl,paracellular}$, $P_{K,paracellular}$, $P_{Na,paracellular}$ and

$P_{Glu,paracellular}$ are the paracellular permeabilities of the respective solutes; and $P_{w,paracellular}$ and $P_{w,transcellular}$ are the paracellular and transcellular water permeabilities. The remaining parameters (Table 2-2) were obtained by following the procedure described in Appendix C. In this study, kinetic parameters were based on findings from pigmented rabbit conjunctiva. These parameters could be substituted with more accurate measurements from humans as these become available, e.g. Na-Glucose cotransport varies across species and so the rates obtained from rabbits may be inaccurate.[77]

Application of the Tear Dynamics Model

The tear dynamics model can provide quantitative information for the steady state and the transient state of the tear film. Below some of the examples of the model application will be presented, and additional examples will be presented in the discussion chapter.

Tear Film at Steady State

At steady state, i.e., under normal conditions, the tear volume is relatively constant and thus the left hand side of equation (11) can be equated to zero. The right hand side of equation (11) includes the drainge rate, which depends on R_m and various physiological parameters L, t_c, R_0, σ, bE, p_0 and p_{sac}. These parameters are either known or have been estimated, and the values of them are listed in Table 2-1. Thus, equation (11) can be used to determine R_m at steady states by setting the left hand side of equation (11) to be zero. The precorneal tear film thickness is related with the radius of curvature by equation (20),[20]

$$h = 2.12R_m\left(\frac{\mu_{tear}U}{\sigma}\right)^{\frac{2}{3}} \qquad (20)$$

where h denotes the tear film thickness; μ_{tear} is the tear viscosity; U is the velocity of the upper lid; and σ is the tear surface tension. By using equation (11) one can determine the steady state meniscus radius of curvature and then equation (20) can be used to determine the tear film

thickness. By following this procedure, the dependence of the steady state tear film thickness on various physiological parameters such as $L_{canaliculi}$, t_c, R_0, σ, bE, p_0, p_{sac} and the tear evaporation and production rates can be determined.

Tear Film at Transient States

Balance of tear fluid

Now let us consider the case when a volume of fluid is instilled into an eye and as a result the tear volume suddenly deviates from the steady value. In this case the left hand side of equation (11) is no longer zero. Therefore it is necessary to develop a relationship between R_m and the tear volume (V_{total}) so that equation (11) can be solved to determine the dynamic changes of R_m and the total ocular fluid volume V_{total}. By anatomical considerations, Mishima et al [2] approximated the preocular tear volume as the sum of the tear volume in the precorneal tear film, the tear menisci and the conjunctival sac, and calculated the tear volume of three parts separately. Using a similar approach, the relationship between the total ocular fluid volume and the meniscus curvature can be written as

$$V_{total}(R_m) = 2.12R_m\left(\frac{\mu U}{\sigma}\right)^{\frac{2}{3}}\left(\frac{1}{2}\times 4\pi R_{globe}^2\right) + (1-\frac{1}{4}\pi)R_m{}^2 L_{lid} \qquad (21)$$

where L_{lid} is the perimeter of the lid margin and R_{globe} is the radius of the globe, which has been assumed to be spherical in shape. The details of the derivation of equation (21) are given in Appendix B. The instillation of extra fluid will increase the tear volume and also the tear radius of curvature. For the normal drainage, tears are mainly drained through the lower canaliculus,[78] however, when the ocular fluid volume is significantly larger than normal, as for instillation, the upper canaliculus also contributes to drainage.[79] Therefore, for the case of extra fluid instillation, the term corresponding to the drainage rate through the canaliculi in equation (11) should be multiplied by a factor, the value of which is between 1 and 2, depending on the fluid volume

remaining on the ocular surface. In the results described below for the dynamic tear volumes after instillation, a factor of 2 has been used. The relationship between tear volume and tear meniscus radius depends on geometric factors and is not expected to change significantly after fluid instillation. Thus, if no spillage occurs after instillation, substitution of equation (6) into the modified equation (11) gives the following differential equation

$$\frac{dV_{total}(R_m)}{dt} = q_{secretion} - q_{evaporation} - \left(J_{w,paracellular} + J_{w,transcellular,a}\right)S_{conj}$$
$$-2\times\left(\frac{\pi L_{canaliculi}}{t_c}\right)\left[\left(\frac{R_0}{1+\frac{\frac{\sigma}{R_m(t)}R_0}{bE}}\right)^2 - \left(\frac{R_0}{1+\frac{(p_0-p_{sac})R_0}{bE}}\right)^2\right] \quad (22)$$

where the total volume V_{total} now is the sum of the tears and the instilled fluids. This equation can be integrated to yield the dynamic radius of curvature. After the dynamic radius of curvature is obtained, the dynamic tear volume can be determined from equation (21). In all the following calculations and discussions for the drainage of tears or fluids with viscosities close to tear viscosity, the density, viscosity and surface tension of the ocular fluid after the instillation are assumed to be the same as those of tears. The effect of viscosity for Newtonian fluids with high viscosity or non-Newtonian fluids will be studied later in this study.

Balance of solutes

Now let us consider the balance of the solute that is present in the instilled fluid. This solute could either be a tracer that does not penetrate the cornea, sclera and the conjunctiva and has been added only to measure the drainage rate, or it could be a drug that can pass through the epithelium to enter the ocular tissues and the blood stream. Assuming that that the solute is always uniformly mixed in the tear fluid, below we utilize the tear model shown above to

develop solute balances for each of these two cases: non-penetrating solutes and penetrating solutes.

In the first case it is assumed that the tracers are not absorbed by cornea, sclera or conjunctiva and are eliminated only by canalicular drainage. If the instilled fluid is mixed ideally with tears, the concentration of the solute is uniform in the tears and the decrease in the total mass of solute in the tears is equal to the solute that flows out with the drained tears, i.e.,

$$\frac{d\left(cV_{total}\right)}{dt} = -cq_{drainage} \tag{23}$$

where c is the concentration of the tracer or drug in the bulk tears. After combining equations (23) and (10) and integrating, we get the following expression for the tracer concentration in the tears:

$$\frac{c(t)}{c_0} = \exp\left(\int_{t_0}^{t} -\frac{q_{secretion} - q_{evaporation} - \left(J_{w,paracellular} + J_{w,transcellular,a}\right)S_{conj}}{V_{total}(t)}\,dt\right) \tag{24}$$

where c(t) is the concentration of tracers in the bulk tears at time t after instillation, c_0 is the tracer concentration in the bulk tears just after instillation, and $V_{total}(t)$ is the total volume of tears and the instilled fluid at time t. Since $V_{total}(t)$ can be calculated with equation. (21) and c(t) can be found from equation. (24), the total amount of tracer left in the tear fluid can be calculated as cV_{total}. In this part of the study, the secretion and evaporation rates are assumed to remain unchanged after the instillation of fluid. This is perhaps an inaccurate assumption because the instillation may change the salt concentrations in the tears and thus the transport of tears through the conjunctiva may be altered. Furthermore, the instillation of the extra fluid impairs the integrity of the lipid layer, therefore the rate of evaporation will also change. However, due to lack of data for these effects, and also to keep the model simple, the secretion and evaporation rates are treated as fixed.

In the second case, the solute can be absorbed by the cornea and the conjunctiva. If the instilled drops contain a drug, a fraction of the drug is absorbed into the cornea and conjunctiva, and some drug is drained through the lacrimal ducts into the nasal cavity, where it is absorbed systemically through the nasal pathway. Also some drug may be lost due to spillage. Below we develop a model that can be used to predict the ocular bioavailability, which is defined as fraction of the drug that is absorbed by the cornea.

In this study I assume that the drug that is drained through the canaliculi and that is absorbed by conjunctiva enter the blood stream and do not contribute to the ocular bioavailability. Also the sclera absorption is neglected since it is not a major elimination pathway for a number of topically applied drops.[80] In addition, we neglect any drug loss by spillage. The transport mechanism of drug molecules through epithelia is complicated, but in this study we assume the drug transport through the ocular tissues to be passive, and calculate the transport rate using the permeability coefficient given in literatures.[81] It is further assumed that the concentration of the drug is uniform in the ocular fluid, and that the concentration at the inner side of the cornea and conjunctiva is zero. Therefore, the decrease in the amount of the drug in the tears is the sum of the drug amounts that is contained in the drained tears and also the amount that is absorbed by the cornea and the conjunctiva, i.e.,

$$\frac{d\left(cV_{total}\right)}{dt} = -c\left(K_{conjunctiva}S_{conjunctiva} + K_{cornea}S_{cornea}\right) - cq_{drainage} \tag{25}$$

where K's and S's are the permeabilities and surface areas, respectively of the subscripted ocular tissues. The value of them are liste in Table 2-1. After combining equations (25) and (10) and integrating, we obtain the following expression for the tracer concentration in the tears

$$\frac{c}{c_0} = \exp\left(-\int_{t_0}^{t} \frac{\left(K_{conjunctiva} S_{conjunctiva} + K_{cornea} S_{cornea}\right) + q_{secretion} - q_{evaporation}}{V_{total}} dt \right) \quad (26)$$

The ocular bioavailability (β) can be expressed as:

$$\beta = \frac{K_{cornea} S_{cornea}}{\left(V_{tear} + V_{drop}\right)} \int_0^{\infty} \frac{c}{c_0} dt \quad (27)$$

where V_{drop} is the drop volume and V_{tear} is the total tear volume before the application of eye drops. Note that c_0 is the concentration in the bulk tears immediately after instillation and not the solute concentration in the drop.

Effect of Viscosity on Tear Drainage and Ocular Residence Time

Drainage of a Newtonian Fluid

It can be shown by the tear drainage model that for tears with a viscosity of 1.5 cp, the canaliculus radius will reach steady states during both the blink and the interblink phase. The canaliculus reaches a steady state in the blink phase when the stresses generated by the deformation of the canaliculi balance the pressure applied by the muscles. The steady state is reached in the interblink when the canaliculi has relaxed to an extent at which the pressure in the canaliculi equals that in the tear film. Achieving steady state both in the blink and the interblink implies that if the duration of the interblink and the blink are further increased, there will be no changes in total tear drainage per blink. However, the drainage rates will decrease due to the reduction in the number of blinks per unit time. The canaliculus radius was shown to reach a steady state in a time $\tau = \frac{16 \mu_{tear} L_{canaliculi}^2}{\pi^2 b E R_0}$, where $L_{canaliculi}$, b and R_0 are the length, thickness and the undeformed radius of the canaliculi, E is the elastic modulus of canaliculi, and μ_{tear} is the viscosity of the instilled Newtonian fluid. As the viscosity of the fluid increases, the time to achieve steady state increases, but as long as the canaliculus reaches a steady state in both the

blink and the blink, there is no change in the total amount of fluid drained in a blink, and so there is also no change in the drainage rates. This explains the observation of Zaki that below a critical viscosity, increasing viscosity does not lead to enhanced retention.[49] However, as the viscosity increases to a critical value at which the time to achieve steady state becomes larger than the duration of the blink phase, the canaliculus does not deform to the fullest extend possible, and so the amount of tears that drain into the nose during the interblink decreases. In this case the equations (1) to (3) are still valid, and the only difference is that the canaliculus radius cannot reach steady state during the blink phase. The radius of the canaliculus can be solved analytically as a function of axial position and time from equations (1). The volume of fluid contained in the canaliculus at any instant in time can be computed by using the following equation:

$$V_{canaliculi} = \int_0^L \pi R^2(x)dx \tag{28}$$

The volume of fluid drained in one blink-interblink cycle can then be computed as the difference between the volume at the end of an interblink ($V_{interblink}$) and that at the end of the blink (V_{blink}), and then the drainage rate through the canaliculus can be computed as

$$q_{drainage}(t) = \frac{V_{interblink}(t) - V_{blink}(t)}{t_c} \tag{29}$$

The above procedure can be used to calculate the effect of viscosity on the drainage of Newtonian fluids. In order to determine the effect of fluid viscosity on the residence time of eye drops, the tear drainage rates are incorporated in a tear mass balance.

Incorporation of Tear Drainage into Tear Balance

To simplify the model, in this part of the study the conjunctival transport is assumed to have a constant rate and thus a mass balance for the fluids on the ocular surface yields

$$\frac{dV_{total}}{dt} = q_{production} - q_{evaporation} - q_{drainage} \tag{30}$$

where V_{total} is the total volume of the fluids on the ocular surface, including tears and the instilled fluids, $q_{production}$ is the combined tear production rate from the lacrimal gland and conjunctiva secretion.

Combining equation (30) and (23) yield the following equation for the total quantity of solutes

$$\frac{I}{I_0} = \frac{V_{total}}{V_0} \exp\int\left(-\frac{q_{production} - q_{evaporation}}{V_{total}}\right)dt \tag{31}$$

where I (= cV_{total}) is the total quantity of solutes, and I_0 and V_0 are the values of I and V immediately after instillation. It is noted that the drainage rate calculations are coupled to the tear balance because the radius of curvature of the meniscus depends on the total tear volume, and the drainage rate is affected by the curvature through boundary condition **Error! Reference source not found.**. The tear volume can be related to the meniscus curvature by the following equation modified from equation (21):

$$V_{total}(R_m) = V_{film} + (1 - \frac{1}{4}\pi)R_m{}^2 L_{lid} \tag{32}$$

where V_{film} is the combined volume of fluid in the exposed and the unexposed tear film and L_{lid} is the perimeter of the lid margin. Equation (21) shows that V_{film} can be written as a function of R_m for fluids with a viscosity close to that of tears. But when the fluid viscosity is high, as is the case in the current study, it can be shown that the function $V_{film}(R_m)$ used in our previous study yields unrealistic tear film thickness and therefore is not likely to be applicable for high viscosity. Therefore in this part of the study V_{film} is assumed to be a constant, and the instillation of any extra fluid only contribute to the volume of tear menisci. The value of V_{film} is assumed to

be the combined volume of the exposed and the unexposed tear film before any instillation, which can be calculated to be 9.9 μL.

By solving equations (1), (29), (30) and (31) simultaneously using finite difference method, the transient quantity of the solutes in the ocular fluids can be obtained as a function of time.

For ocular drugs delivered via drop the mass balance needs to be modified to include drug transport through the ocular tissue. The bioavailability of such drugs can be obtained as the following using the same derivation process for equation (27)

$$\beta = \frac{K_{cornea} A_{cornea}}{V_0} \int_0^{\infty} \exp\left[- \int_{t_0}^{t} \frac{\left(K_{conj} A_{conj} + K_{cornea} A_{cornea}\right) + \left(q_{production} - q_{evaporation}\right)}{V_{total}} dt \right] dt \qquad (33)$$

Non-Newtonian Fluid

Using similar methods to the above, we can calculate the residence time of non-Newtonian fluids that are instilled onto the ocular surface, with only equation **Error! Reference source not found.** modified. Unlike Newtonian fluids, which have a linear relationship between the shear stress and the shear rate, non-Newtonian fluids have more complicated relation between the shear stress and the shear rate. One of the most common non-Newtonian fluids for dry eye treatment is sodium hyaluronate solution. Rheological measurements have shown that at the concentration used for ocular instillation it can be approximated as power-law (shear-thinning) fluid, i.e. the relation between the shear stress τ and the shear rate γ can be written as

$$\tau = \mu_0 \gamma^n \qquad (34)$$

where μ_0 is a constant with the unit of viscosity and n is a constant ($0<n<1$), and both of the constants can be obtained from by best curve fitting from the rheological measurements in

literatures. Using equation (34) the equation for the deformation of canaliculi as a result of blinking can be derived as

$$\frac{\partial R}{\partial t} = a\left(-\frac{\partial R}{\partial x}\right)^{\left(\frac{1}{n}-1\right)} \frac{\partial^2 R}{\partial x^2} \tag{35}$$

where a is a constant that is defined as

$$a \equiv \frac{1}{2}\left(\frac{bE}{2\mu_0 R_0^2}\right)^{\frac{1}{n}} \frac{R_0^{\frac{2n+1}{n}}}{3n+1}$$

The derivation of equation (35) is described in detail in Appendix A. It is noted that Newtonian fluid is a special case of a power-law fluid with n = 1, and equation (35) correctly reduces to equation (1) for this case. By solving equations (35), (29), (30) and (31) simultaneously using finite difference method, the transient quantity of the solutes in the ocular fluids can be obtained as a function of time. Similar to the Newtonian fluid case, the bioavailability can be also calculated using equation (34) after obtaining the volume transient from equations (35), (29) and (30). The rheological data for non-Newtonian fluids used in the calculations in this study are obtained from literature and fitted using equation (34) and the fitting results, which are listed in Table 2-3.

Tear Mixing Under the Lower Eyelid

Physical Description of the System

The geometry of the system and the motions considered in the tear mixing model are shown in Figure 2-3. In this study we simplify the geometry of the tear film under the lower eyelid as a thin film of thickness h sandwiched between the eyeball (y = 0) and the lower eyelid (y = h), both of which are treated as flat plates. This assumption is valid because the tear film thickness, which is several microns, is much smaller than the radius of the eyeball, which is

about 12 mm. The positions x = 0 and L (= 10mm for this study) correspond to the lower fornix and the position at which the lower sac meets the exposed tear film, respectively.

As described in the previous section, only the vertical shearing between the globe and the lid (motion (a) along x direction in Figure 2-3) and the squeezing of the globe against the lid (motion (b) along y direction in Figure 2-3) are modeled in this study, and they are considered separately. In the vertical shearing motion, the globe rotates inferiorly at the beginning of a blink, then it quickly returns to its original position, at which it remains still until the beginning of the next blink. In this case the tear film is considered to have a constant thickness of about 7 μm. In the squeezing motion, the lid moves interiorly against the globe at the beginning of a blink, then it quickly returns to its original position, at which it remains still until the beginning of the next blink. In this case, the thickness of the tear film changes as a result of the squeezing.

Mathematical Modeling

According to Figure 2-3, the characteristic lengths in x and y directions are L and h, respectively, and thus dimensionless lengths are defined as $\eta \equiv \frac{x}{L}$ and $\xi \equiv \frac{y}{h}$. It can be shown that the problem contains a short time scale corresponding to blinking and the diffusion along the y direction (τ_s), and a long time scale corresponding to the diffusion along the x direction (τ_l). Therefore the nondimensionalization of time variables is given in the appendix in the context of detailed derivations instead of in the method section for clarity. The current study is based on a mass balance of the solutes instilled into the tear film in the lower conjunctiva sac. Since the mixing of the solutes is depends on the lid/globe motion, the velocity functions of the lid/globe and the velocity profiles in the tear film are first given below.

Velocity profiles

Vertical shearing. The periodic displacement in x direction of the lid with respect to the globe (Δ) for vertical shearing can be described by the following equation:

$$\Delta = \Delta_0 f(\omega t) \tag{36}$$

where Δ_0 is the amplitude of the shearing motion, and $f(\omega t)$ is a periodic function with an agular velocity ω corresponding to blinking. According to the above physical description of the shearing motion, the function $f(\omega t)$ is assumed to have the following form:

$$f(\omega t) = -\frac{1}{2}\cos\left(\frac{2\pi}{T_{shearing}} t\right) \quad (0<t<T_{shearing})$$

$$f(\omega t) = -\frac{1}{2} \quad (T_{shearing}<t<T_c) \tag{37}$$

where $T_{shearing}$ is the duration of the shearing motion and is 0.05 s[56], and T_c is the total time for a blink-interblink cycle and is 6 s. Equation (37) states that during one blink cycle ($0<t<T_c$), from $t=0$ to $t=T_{shearing}$ the lid moves upwards with respect to the globe and then back to its original position, and from $t=T_{shearing}$ to the end of the blink cycle the lid is stationary, i.e. the displacement is a constant. The constant -1/2 is chosen so that the absolute value of the maximal displacement during one cycle is Δ_0 and the lid velocity is positive at the beginning of each blink. The velocity of the lid with respect to the globe is simply the derivative of the displacement, and the velocity profile in the tear film can be written as the following according to the lid velocity for Couette flow

$$u(t,\xi) = \Delta_0 \omega \dot{f}(\omega t)\xi$$

$$v(t,\xi) = 0 \tag{38}$$

where u is the velocity in x, v is the velocity in y direction, which is zero at all times, and $\dot{f}(\omega t)$ is the derivative of $f(\omega t)$. It can be seen that $\omega=2\pi/T_c$.

Squeezing. The periodic displacement in y direction of the lid with respect to the globe (Δ') for vertical shearing can be described by the following equation:

$$\Delta' = \Delta_0' g(\omega t) \tag{39}$$

where Δ_0' is the amplitude of the squeezing motion, and g(ωt) is a periodic function with an agular velocity ω corresponding to blinking. Similar to the shearing motion, the function g(ωt) is assumed to have the following form:

$$g(\omega t) = -\frac{1}{2}\cos\left(\frac{2\pi}{T_{squeezing}} t\right) \quad (0<t<T_{squeezing})$$

$$g(\omega t) = -\frac{1}{2} \quad (T_{squeezing}<t<T_c) \tag{40}$$

where $T_{squeezing}$ is the duration of the squeezing motion and is 0.2 s. Similar to the case for shearing flow, the Couette-flow velocity profile in the tear film can be written as the following

$$u(t,\xi) = 6\eta\frac{L}{h}\Delta_0'\omega\dot{g}(\omega t)(\xi - \xi^2)$$

$$v(t,\xi) = \Delta_0'\omega\dot{g}(\omega t)(2\xi^3 - 3\xi^2) \tag{41}$$

where $\dot{g}(\omega t)$ is the derivative of $g(\omega t)$.

Mass balance of the tear film

Since only the vertical shearing and the squeezing motions are modeled, the transport in the horizontal direction is neglected to simplify the model, rendering the problem two dimensional. The dimensional 2D mass balance of the instilled solutes under the lower lid yields

$$\frac{\partial c_{sac}}{\partial t} + u\frac{\partial c_{sac}}{\partial x} + v\frac{\partial c_{sac}}{\partial y} = D\left(\frac{\partial^2 c_{sac}}{\partial x^2} + \frac{\partial^2 c_{sac}}{\partial y^2}\right) \tag{42}$$

in which c_{sac} is the concentration of the solute in the lower conjunctival sac (under the lower eyelid), u and v are the fluid velocity components in the x and the y directions, respectively, D is the diffusivity of the solute in the fluid, and t, x, y are time and position coordinates. For Taylor dispersion, it can be shown that the solute concentration in the above equation can be approximated as a function of τ_l and η, and it can be obtained by solving the equation

$$\frac{\partial c_{sac}}{\partial \tau_l} = D^* \frac{\partial^2 c_{sac}}{\partial \eta^2} \tag{43}$$

in which D^* is the Taylor dispersion coefficient. In this model, it is assumed that the instilled solute does not penetrate into the epithelium because of the short duration of the nixing time in comparison to the conjunctival uptake times,[57] and therefore there is no flux of solutes at the fornix, or at the y = 0 (eyeball) and y = h (palpebral conjunctiva) surfaces. It is also assumed that the solution drops are instilled to the bottom of fornix at the beginning. It is also assumed that there is no mass transfer barrier at the edge of the lower eyelid and so the concentration at x = L equals the concentration in the tear film. Based on the above assumptions, the boundary conditions and initial conditions can be expressed as

$$c_{sac} = c_{tear} \text{ at } \eta = 1$$

$$\frac{\partial c_{sac}}{\partial \eta} = 0 \text{ at } \eta = 0$$

$$c_{sac} = c^* \text{ from } \eta = 0 \text{ to } \eta = \eta^* \text{ at } t = 0$$

where η^* is the dimensionless width of the initially instilled solute plug and c^* is the concentration in the plug. These two parameters are related through the equation

$c^* L\eta^* Wh = c_{drop}V_{drop}$, where c_{drop} and V_{drop} are the concentration and volume of the instilled drop, h is the distance between the lower lid and the eyeball, and W is the width of the lower eyelid from the medial canthus to the lateral canthus, which is approximated as πR_{globe}. Equation (43) can be solved for the solute concentration under the lower lid if D^* and c_{tear} are known.

The dispersion coefficient D^* is related to the fluid velocity u and therefore depends on the lid/globe kinematics, it needs to be derived for the two possible scenarios separately. It is shown in the appendix that for the vertical shearing case, the ratio between the Taylor dispersion coefficient D^* and the molecular diffusion coefficient D can be expressed by

$$\frac{D^*}{D} = 1 + \sum_{n=1}^{\infty} \frac{4d_n d_{-n}}{n^2} \frac{\Delta_0^{\,2} N^2}{2h^2} \left[1 - \frac{(\sinh\kappa_n + \sin\kappa_n)}{\kappa_n(\cosh\kappa_n + \cos\kappa_n)} \right] \tag{44}$$

where N is defined as $T_c/T_{shearing}$, d_n an d_{-n} are the Fourier series coefficients for the function $\dot{f}(\omega t)$ and $\kappa_n \equiv \sqrt{\frac{n\omega h^2}{2D}}$. The Fourier series coefficients can be obtained for arbitrary periodic function F(t) with a period T by

$$d_n = \frac{1}{T}\int_t^{t+T} F(t) e^{-i\omega\omega n} dt \tag{45}$$

Similarly, the dispersion coefficient D^* for the squeezing case can be given by the following expression

$$\frac{D^*}{D} = 1 + \sum_{n=1}^{\infty} \frac{4d_n' d_{-n}'}{n^2} \frac{6\Delta_0'^{\,2} N^2}{h^2} \left(\frac{x}{h}\right)^2 \left[1 - \frac{3(\sinh\kappa_n - \sin\kappa_n)}{\kappa_n(\cosh\kappa_n - \cos\kappa_n)} \right] \tag{46}$$

where d_n' and d_{-n}' are the Fourier series coefficients for the function $\dot{g}(\omega t)$. It is noted that although in this study the velocity function is approximated with the simplified forms, the method presented in this study can be used for arbitrary periodic velocity functions to derive D^*.

The concentration profile in the tears under the lower lid is coupled to the concentration transients in the exposed tear film (c_{tear}) through the boundary condition of equation (43). Thus in order to solve the problem, one also needs to solve the mass balance equation for the exposed tear film. It is assumed that the fluorescence does not penetrate into the ocular surface, and therefore the fluorescence is eliminated from the ocular surface only by the tear drainage into the lacrimal canaliculi. It is also assumed that the instillation of fluorescence does not cause significant reflex tearing, and thus the tear secretion rate is a constant. Because the instilled volume is small compared to the total tear volume, it is assumed that the tear volume remains in a steady state, i.e. the tear production and elimination rates are equal and they remain constant. In addition, the much velocity of the upper lid during blinking is much larger than that of the lower lid. Thus it can be shown that the time scale for tear mixing in the upper conjunctiva sac and the exposed tear film is much smaller than the tear mixing under the lower lid. Therefore the tears in the upper conjunctiva sac and the exposed tear film are assumed to be well-mixed. Based on these assumptions, a mass balance of the fluorescence on the ocular surface yields

$$\frac{d\left(c_{tear} V_{tear}\right)}{dt} = j_{dye} - c_{tear} q_{drainage} \tag{47}$$

The initial condition of equation (47) is

$$c_{tear} = 0 \text{ at } t = 0$$

In equation (47) V_{tear} is the volume of the tears in the exposed tear film and under the upper lid, and j_{dye} is the total flow rate of the fluorescence from the lower conjunctiva sac to the tear film, which is given by the following expression,

$$j_{dye} = -D^* \frac{dc_{sac}}{dx} A \tag{48}$$

where A (=Wh) is the total area of contact between the lower lid and the exposed tear film.

The concentrations $c_{sac}(x,t)$ and $c_{tear}(t)$ can now be obtained by numerically solving equations (43) and (47) using the expression for D^* given in equations (44) and (46). To compare with the experiments by Macdonald and Maurice[55], it is useful to extract from the simulated profiles for c_{tear} the time for appearance of fluorescence in the tears (T_{app}) and the time for the fluorescence to reach maximal concentration in the exposed tear film (T_{max}). Since it can be seen from equations (47) and (43) that c_{tear} and c_{sac} are linearly related to c^* and so below the results for concentrations are normalized by c^*.

Table 2-1 Model parameters based on literature

Parameter name	Parameter Value
$C_{Na,a}$ (=$C_{Na,b}$) (mM) *	141 [36]
$C_{K,a}$ (=$C_{K,b}$) (mM) *	5 [36]
$C_{Cl,a}$ (=$C_{Cl,b}$) (mM) *	118.5 [36]
$C_{Glu,a}$ (=$C_{Glu,b}$) (mM) *	5 [36]
$C_{Others,a}$ (=$C_{Others,b}$) (mM) *	30.5 [36]
$C_{Na,b}$ (mM) **	139.9 [69]
$C_{K,b}$ (mM) **	3.92 [69]
$C_{Cl,b}$ (mM) **	107.1 [69]
$C_{Glu,b}$ (mM) **	5 [66]
$C_{Others,b}$ (mM) **	44.08
$C_{Na,tear}^{0}$ (mM)	135 [72]
$C_{K,tear}^{0}$ (mM)	46 [72]
$C_{Cl,tear}^{0}$ (mM)	123 [72]
$C_{Others,tear}^{0}$	58
$C_{Glu,tear}^{0}$ (mM)	0
$q_{evaporation}$ (μL/min)	0.8
$q_{production}$ (μL/min)	2
$q_{secretion}$ (μL/min)	0.6
bE (Pa • s)	2.57 [22]
$L_{canaliculi}$ (m)	1.2×10^{-2} [26]
L_{lid} (m)	5.7×10^{-2} [2]
μ (Pa·s)	1.5×10^{-3} [69]
t_c (s)	6 [22]
R_0 (m)	2.5×10^{-4} [30]
σ (N/m)	43×10^{-3} [69]
p_0 (Pa)	400 [70]
p_{sac} (Pa)	0 (atmospheric)
$P_{Cl,paracellular}$ (m/s)	9.5×10^{-9} [73] (rabbit)
$P_{K,paracellular}$ (m/s)	9×10^{-9} (rabbit)
$P_{Na,paracellular}$ (m/s)	8.6×10^{-9} [73] (rabbit)
$P_{Glu,paracellular}$ (m/s)	5×10^{-8} (rabbit)
K_{cornea} (m/s)	1.5×10^{-7} [81]
K_{conj} (m/s)	5.2×10^{-7} [81]
$K_{Na,pump}$ (mM)	8.3 [74]
$K_{K,pump}$ (mM)	0.92 [74]
$K_{Na,Na\text{-}K\text{-}Cl}$ (mM)	105 [75]
$K_{K,Na\text{-}K\text{-}Cl}$ (mM)	1.22 [75]
$K_{Cl,1,Na\text{-}K\text{-}Cl}$ (mM)	103 [75]
$K_{Cl,2,Na\text{-}K\text{-}Cl}$ (mM)	23.9 [75]
$P_{w,transcellular}$ (m/s)	2.5×10^{-4} [47] (mouse)
$P_{w,paracellular}$ (m/s)	1.1×10^{-5} [47] (mouse)
R_{globe} (m)	1.2×10^{-2} [2]
$R_{m,0}$	3.65×10^{-4} [101]
S_{cornea} (m^2)	1.04×10^{-4} [76]
S_{conj} (m^2)	17.65×10^{-4} [76]

U	5×10^{-2} m/s	[16]

* Parameters for the Ussing-chamber experiments. ** Parameters for the tear dynamics model.
The value of $C_{Others,b}$ is determined by assuming that the blood osmolarity is 300 mM. The range of reported values for tear secretion is 1-4 μL/min[12,13] but these measurements represent the total input of tears into the eyes, and thus include the lacrimal and the conjunctival secretions. Thus we choose $q_{secretion}$, which is the contribution from lacrimal secretions, to be 0.6 μL/min. For the tear evaporation rate, we adopt the value from our previous study[89], so that the portion of the tear drainage in the total tear elimination is still 60%, in accordance with a previous report[10]. The value of $C_{Others,tear}^{0}$ is set by using the reported concentrations for all ions and then using the electroneutrality condition.

Table 2-2 Model parameters obtained by fitting data from experiments on rabbits

File name	This file contains
$P_{Cl,channel}$ (m/s)	1.68×10^{-8}
$P_{K,channel}$ (m/s)	3.15×10^{-8}
$J_{pump,max}$ (mol·s^{-1}·m^{-2})	1.56×10^{-6}
$J_{Na\text{-}K\text{-}Cl,max}$ (mol·s^{-1}·m^{-2})	2.65×10^{-6}
C_T (mol of Na-Glucose transporter.m^{-2})	7.22×10^{-8}
r_{Glu}^0 (mol·s^{-1}·m^{-2})	2.2×10^{-7}

Table 2-3 Parameters obtained from fitting the rheological data in literature using the power-law equation $\tau=\mu_0\gamma^n$

Solution	μ_0 (cp)	n	R^2
0.2 % NaHA	323.3	-0.329	0.973
0.3 % NaHA	884.2	-0.3913	0.9788
CMC (low MW)	194.8	-0.09201	0.9285
CMC (high MW)	194.4	-0.2943	0.933
Human tears	5.578	-0.264	0.9963

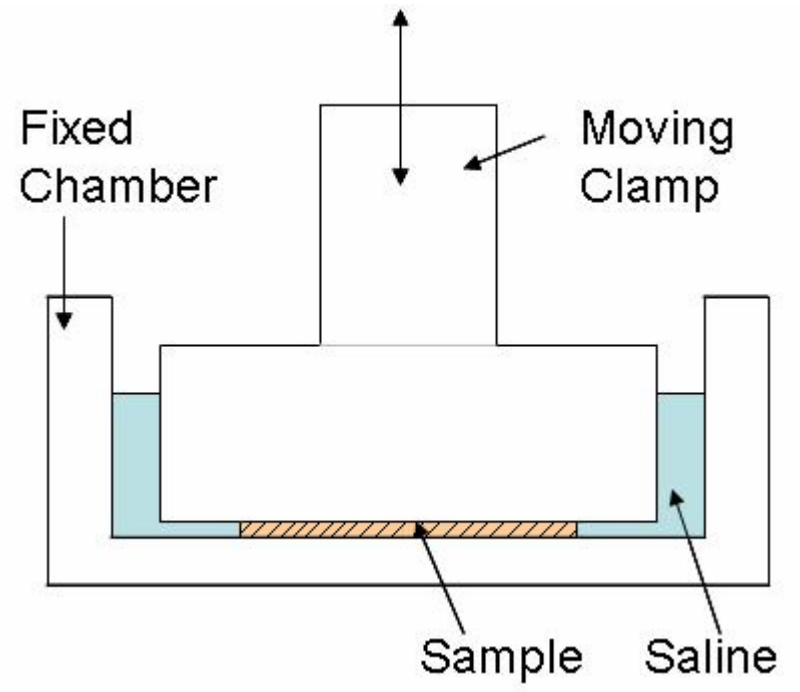

Figure 2-1 DMA clamp setup.

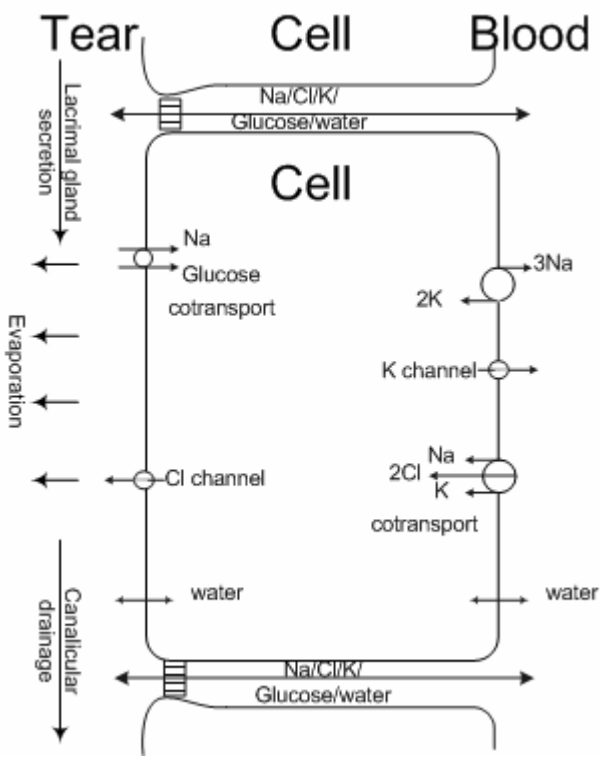

Figure 2-2 Simplified epithelium structure and transport mechanisms

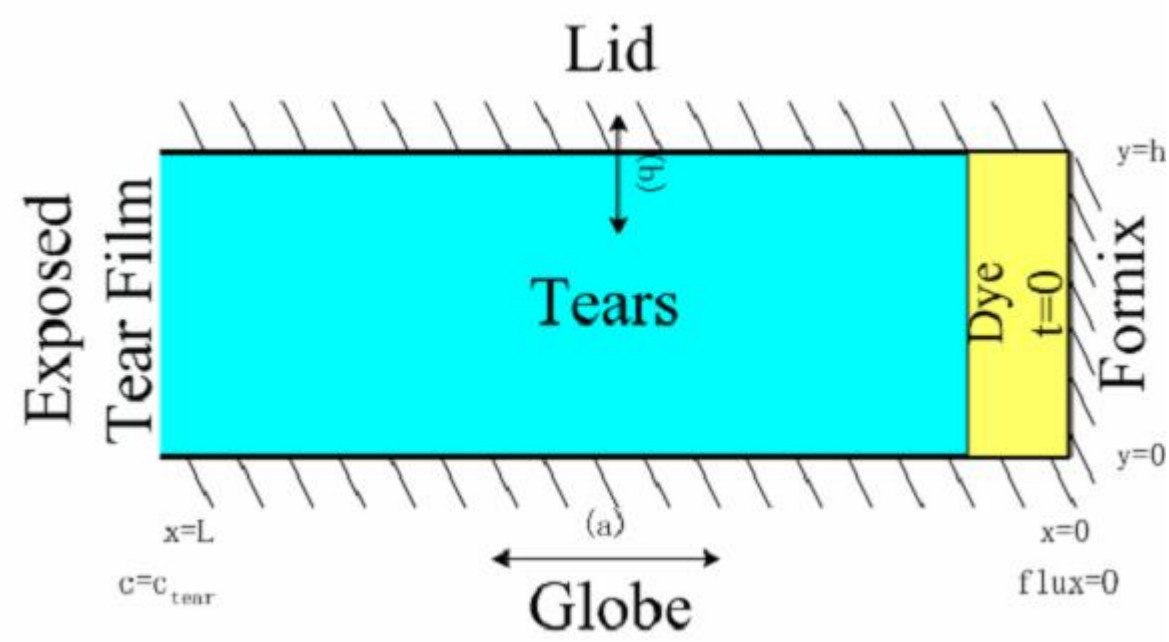

Figure 2-3 Spreading of instilled dye due to shearing and squeezing motion of the lid and the globe

CHAPTER 3
RESULTS

Below, first the results of the tear drainage model and the conjunctiva transport model for Ussing-chamber experiments under short-circuit and open-circuit conditions are presented. The comparison between the predicted results and those observed in chamber experiments helps justify the choices of parameters. Then the results of integrating both the tear drainage model and the conjunctiva model into tear dynamics are presented. The effect of viscosity on tear drainage and residence time and the tear mixing under the lower eyelids are presented at the end of the section.

Tear Drainage through Canaliculi

Mechanical Properties of the Lacrimal Canaliculi

Frequency dependent rheological response

The frequency dependent storage moduli (E') and the loss moduli (E") are listed in Table 1 for both age groups. An unbalanced two factor ANOVA shows that E' and E" depends significantly on frequency ($p \sim 0$ and $p \sim 0$, respectively), but not significantly on age ($p = 0.0379$, $p = 0.2056$, respectively). The product of the storage modulus and the tissue thickness, which is corresponding to the parameter "bE" in the tear drainage model, varies from 4.33 to 7.51 Pa·m, which agrees reasonably well with the value (2.57 Pa·m) estimated earlier by balancing the tear inflow and outflow. In view of the possibility of the variation of bE across species and subjects, throughout the whole study we still used the bE value of 2.57 Pa·m, and studied the dependence of tear film variables on bE by varying bE around the normal value. Additionally, although the DMA study showed that the canaliculi are viscoelastic rather than elastic, for the current study the linear elasticity assumption can still provide a good approximation for tear drainage rate, and the reason will be discussed in the following chapter.

Simulation of blink-interblink cycles

Figure 3-1 shows typical stress and strain transients during the loading-recovery cycles. Individual data points are separated by time of 0.1 s. The data shows that stress and strain reach periodic steady states in about 2 cycles.

To quantify the recovery of the canaliculus, we fitted the strain transient during the recovery period with exponential functions. It was found that the strain recovery occurred on two different time scales (τ_1 and τ_2), i.e., a double-exponential function ($\varepsilon = ae^{-t/\tau_1} + be^{-t/\tau_2}$) fits the data much better than a single exponential function. A sample recovery curve along with the best fit curve is plotted in Figure 3-2. The values of a, b, τ_1 and τ_2 are listed in Table 3-2 for each sample, along with the R^2 value for the fits. It is noted that data for all the periods after the first two were used in the fit.

Canaliculus Radius and Pressure Transients

Equation (1) is solved analytically with the boundary conditions and initial conditions given in (2) and (3) and the results are given below.

For the blink, the radius change is expressed as

$$\frac{R(x,t)-R_b}{R_{ib}-R_b} = \sum_{n=0}^{\infty} \frac{2(-1)^n}{\left(\frac{1}{2}+n\right)\pi} \cos\left[\left(\frac{1}{2}+n\right)\pi \frac{x}{L_{canaliculi}}\right] e^{-\left(\frac{1}{2}+n\right)^2 \frac{t}{\tau}} \tag{49}$$

and for the interblink, the radius change is expressed as

$$\frac{R(x,t)-R_b}{R_{ib}-R_b} = 1 - \sum_{n=0}^{\infty} \frac{2}{\left(\frac{1}{2}+n\right)\pi} \sin\left[\left(\frac{1}{2}+n\right)\pi \frac{x}{L_{canaliculi}}\right] e^{-\left(\frac{1}{2}+n\right)^2 \frac{t}{\tau}} \tag{50}$$

Figures 3-3 and 3-4 show the radius profiles at different times for the blink and the interblink phases, respectively. In these figures the dimensionless radius is plotted as a function of

$x/L_{canaliculi}$ for four different values of the dimensionless time t/τ, where $\tau=16\mu_{tear}L^2_{canaliculi}/(\pi^2 bER_0)$.

By using the solid mechanics equation (A1), which relates the radius with the pressure, the pressure transients can be determined for the blink phase and the interblink phase. The pressure transients at $x = L_{canaliculi}/4$, $L_{canaliculi}/2$ and $3\ L_{canaliculi}/4$ are plotted in Figures 3-5 and 3-6 for the blink and the interblink, respectively. In these figures the pressure is plotted as a function of dimensionless time t/τ. In the figures described above, time t = 0 denotes the beginning of the blink phase in Figure 3-3 and 3-5, and it denotes the beginning of the interblink phase in Figure 3-4 and 3-6. As the figures show, at the beginning of the blink phase, the internal pressure suddenly increase to 233 Pa, and then quickly drops to a steady state value of zero, i.e. atmospheric, pressure. The pressure drops to -400 Pa immediately at the beginning of the interblink, and increases to a steady state value of about -167 Pa, which is $-\sigma/R_m$. The time to get to the steady states for blink and interblink phase is about $41\mu L^2/(bER_0)$. For bE is in the range of 0.649 to 34.022 Pa·m, the time to reach steady state is expected to be between 0.0546 to 0.0010 second.

Conjunctiva Transport Model for the Simulation of a Ussing-chamber

In order to validate the conjunctiva transport model, the computed values of cellular concentrations, fluxes, cellular volume and potential differences under both short-circuit and open-circuit conditions are compared with experiments.

Cellular Concentrations and Cell Size

In the Ussing-chamber experiments, the cellular concentrations were not measured, and so we can not directly compare the model predictions with experiments. However cellular compositions have been measured for the cornea endothelial cells, which may be comparable to

the cellular concentrations in conjunctiva and so in Table 3-3[25,66,82] we compare the predicted cellular concentrations with corneal concentrations. In Table 3-3, $C_{Na,c}^{0}$, $C_{K,c}^{0}$, $C_{Cl,c}^{0}$ and $C_{Others,c}^{0}$ are the reference cellular concentrations of Na, K, Cl and the inert ions, and V_c^0 is the reference volume of the cellular compartment.

Short-circuit Current I_{SC}

The short-circuit current (I_{SC}) can be computed by solving equations (12) to (16) and (18), and then imposing electroneutrality on the apical and the basolateral compartments. This gives the following equation for I_{SC}:

$$I_{sc} = F\left(2J_{Na-Glu} - J_{Cl,channel}\right) \tag{51}$$

The I_{SC} obtained this way is the current normalized by the surface area of conjunctiva. In addition to measuring I_{SC} under physiologically relevant conditions, experimentalists typically vary ion concentrations and add drugs to construct situations that correspond to apical Cl free, both sides Cl free, apical Na free, pump inhibition, Cl channel inhibition, K channel inhibition, and Na-K-Cl cotransporter inhibition. In these experiments, the time course of changes in I_{SC} is measured after performing one of the maneuvers described above. The simulated time courses of I_{SC} after various maneuvers are plotted in Figure 3-7 below. We note that the curves for "both sides Cl free" and "Na-K-Cl inhibition" almost overlap. The control represents the current under normal conditions, and other curves correspond to different maneuvers that are indicated on each curve.

The comparison between the calculated values and those measured in experiments is shown in Table 3-4 [36,37] for I_{SC} and in Table 3-5 [36] for $t_{1/2}$, i.e., the time required for I_{SC} to achieve 50% of the total change.

Sodium (Na) and Chloride Cl Fluxes

The net fluxes of Na and Cl have been measured experimentally by isotope method in Ussing-chamber experiments under both short-circuit and open-circuit conditions, and these can also be computed by the model. For the apical and basolateral compositions listed in Table 2-1, the comparison of calculated and measured Na and Cl net fluxes is shown in Table 3-6. [44,42,39]

Transepithelial Potential Difference (PD)

To check whether the values of paracellular permeabilities of ions are reasonable, we compare the predicted PD under open-circuit condition with experimental values. The PD reported in experiments on rabbit conjunctiva with Ussing-chambers is 17.7±0.8 mV[36] or 14.6±1.5 mV [37], compared to the model prediction of 15.7 mV.

Fluid Secretion under Open-circuit Condition

To further compare model predictions with experiments, the effects of Na-K pump inhibition and the apical addition of 20 mM glucose on fluid secretion were simulated. Addition of 20 mM glucose to the apical compartment increases the fluid secretion from basolateral to apical compartment by about 2.7 times, mainly due to changes in osmotic flow. This is contradictory to the observation that adding 20 mM glucose apically decreased the water secretion.[24] The reason for this discrepancy will be discussed later. In addition, when Na-K pump maximal flux is decreased to 0.001 of the normal value, the model predicts undetectable fluid secretion, which agrees with experimental observation.[24]

While the predictions for the conjunctiva model are not in perfect agreement with the experiments, there is sufficient qualitative and quantitative agreement to suggest that the values of model parameters are reasonable, and that the model developed above has captured the essential mechanisms, and thus it can be included into the comprehensive tear dynamics model.

Therefore, the conjunctiva model is integrated into the tear dynamics model and the results for the tear dynamics are presented below.

Incorporation of the Tear Drainage Model and the Conjunctiva Transport Model into the Tear Balance

Model Prediction of Steady-State Tear Variables

Normal tear parameters

The tear dynamics model can be solved to predict the tear volume and composition, drainage rate, and transport rates of water and various ions across the conjunctiva. The steady state tear composition and volume obtained by the simulations are compared with experimentally measured values in Table 3-7. [83,84]

The model predicts a value of 1.10 μL/min for the water secretion rate from the conjunctiva, which is within the range of the tear turnover rate of about 1~4 μL/min. The potential difference between the apical and basolateral sides has been measured in vivo to be about -15mV on rabbits[85] and about -23 mV on mice,[21] with the basolateral side as the reference. This compares well with the predicted value of -15.1mV. The model predicts values of 7.1 μL and 297.6 mM for the tear volume and osmolarity, respectively. In addition to the steady state values under the normal conditions reported above, the model can be used to compute both steady and transient compositions, volumes, and potentials of tears and the conjunctival cells, and also the canalicular drainage rate, and the fluxes of water and ions and solutes across the conjunctiva. Some of these model predictions are discussed below and these predictions are compared to experimental data, if they are available.

Steady-state tear film thickness as a function of tear evaporation rate

It has been reported that when the lipid layer in the tear film is impaired, the evaporation rate may increase to up to 17 times the normal value[86] and therefore the parameter α, which is

defined as the ratio of the evaporation rate to the secretion rate, can easily reach 1.0. In Figure 3-8 the parameter α is varied from the normal value 0.4 to 1.0, which is a possible range based on the experimental results.

As shown by Figure 3-8, when α varies from 0.4~1.0, the steady state tear film thickness varies from 11.2 μm to 3.3 μm.

Steady-state tear film thickness as a function of mechanical properties of canaliculi

The parameter bE is estimated to be about 2.57 Pa·m under normal conditions[22]. Due to the possibility of cross-subject variation of bE mentioned above, in this part of the study we vary bE between 0.1 Pa·m and 3 Pa·m. Figure 3-9 shows the steady state tear film thickness for different values of bE. When bE is varied between 0.1 Pa·m and 3 Pa·m, the steady state tear film thickness changes from 4.0 μm to 17.4 μm.

Steady-state tear film thickness as a function of tear surface tension

Figure 3-10 shows the steady state tear film thickness for different values of surface tension. As shown in the figure, as σ is varied from 20×10^{-3} N/m to 60×10^{-3} N/m, the steady state tear film thickness changes from 8.7 μm to 12.5 μm. We note that this behavior is contradictory to the commonly accepted observation that lower surface tension is desirable for a more stable tear film, and this issue will be discussed in the next chapter.

Model Prediction of Dynamic Tear Variables

The effect of ion channel modulation on tear film

When the Cl channel permeability ($P_{Cl,channel}$) is increased, the secretion of water through the conjunctival epithelium is expected to increase due to the coupling between water and ion transport. As shown in Figure 3-11, when $P_{Cl,channel}$ is increased to 10 times its original value, the predicted tear volume increases to a maximum of 8.1 μL, and then decreases to a steady state of about 7.3 μL in about 50 min. The prediction for the conjunctival fluid secretion increases from

1.10 μL/min to 1.83 μL/min, and then reaches a steady state of 1.12 μL/min. Additionally, when the Cl channel permeability is increased, the model predicts hyperpolarization and there is an immediate change in PD from -15.1 mV to -20.1 mV and then a gradual change to a stabilized value of -15.5 mV, which agrees qualitatively with experimental observation.[21] Furthermore, since it is suggested that the permeabilities of Cl channel and the K channel ($P_{Cl,channel}$ and $P_{K,channel}$) can both be increased by cAMP,[41] calculations were also conducted for this situation. As shown in Figure 3-11, when $P_{Cl,channel}$ and $P_{K,channel}$ are both increased to 10 times the original values, the steady state tear volume increases to a maximum of 10.0 μL, and then decreases to a steady state of about 7.3 μL in about 43 minutes. In this case, the conjunctival fluid secretion increases from 1.10 μL/min to a maximum of 5.44 μL/min and then reaches a steady state value of 1.12 μL/min. Thus, as expected, increasing the permeability of both K and Cl channels leads to a larger increase in the conjunctival fluid secretion and tear volume compared to increasing the permeability of only Cl channels.

The effect of evaporation rates on tear film

It is commonly believed that dry eye symptoms are alleviated or reduced if the subjects are exposed to controlled humidity conditions, possibly due to an increase in the tear volume. To understand the potential benefits of reduction in evaporation on dry eye symptoms, we used our model to simulate the effect of changes in evaporation rates on the quantity and composition of the tear film. These results are shown in Figure 3-12.

The effect of osmolarity in dry eye medications on dry eye

A typical dry eye treatment comprises of instilling about 25-30 μl of solution into the eyes. One may expect that hypoosmolar tear solutions may be more efficient at relieving dry eye symptoms but there are contradictory claims in literature.[87] To explore this issue, we simulated

the dynamic changes in tear volumes and osmolarities after instilling 25 μl drops of varying osmolarities. The results for the dynamic tear volumes, tear osmolarities and the conjunctival secretion are shown in Figures 3-13.

The effect of punctum occlusion and moisture chambers on dry eye

Punctum occlusion can be simulated by setting the canalicular drainage rate to be zero. The model predicts that the tear osmolarity and conjunctival secretion reach a new steady state after punctum occlusion, but the tear volume increases continually, and thus tears are expected to roll off the eyes. While there are some reports of tear overflow (epiphora) caused by punctum occlusion, punctum plugs do not always lead to overflow, and this discrepancy will be discussed later. To further investigate the change in tear dynamics by punctum occlusion, the fluorescence clearance after the occlusion of both puncta was simulated. In accordance with the experiments, the fluorescence in the eyes was computed for 15 minutes after instillation of 5 μL of fluid with 2% fluorophore concentration.[88] In these calculations, it was assumed that the fluorophore does not penetrate into the ocular surface. It was also assumed that tear spillage does not occur, which is a reasonable assumption due to the small instillation volume and the short duration of the experiment (15 min). In Figure 3-14, the predicted fluorophore concentration is plotted as a function of time.

Besides punctum occlusion, moisture chambers, which can decrease the tear evaporation rate, have also been explored as potential treatments for dry eyes. As shown above, if evaporation rate is increased, the tear film volume decreases and osmolarity increases, and these symptoms are similar to those experienced by dry eye sufferers. To determine the impact of moisture chambers on dry eye sufferers, we conducted simulations in which the initial condition corresponded to the steady state results with four times the normal evaporation rate, and

accordingly a thin, hyperosmolar tear film, and then we reduced the evaporation rate to the normal level. The model predicts that the tear volume and the tear osmolarity go back to their respective baseline values in about 13 minutes, and thus it is expected that moisture chambers should bring a rapid relief to dry eye sufferers.

The effect of drop volume on clearance time

The effect of drop volume on clearance time was studied with our preliminary study of a tear dynamics model, which did not include the active transport through conjunctival epithelium.[89] In this part of the study, the time course of ocular fluid after instillation was recalculated after incorporation of the conjunctiva model. As shown in Figure 3-15, the new tear dynamics model predicts that after instilling 15 μL and 25 μL of isosmolar fluid, the ocular fluid volume returns to its baseline in about 18 minutes and 24 minutes, respectively. As in the previous study, the baseline was defined as the value within 1% of the eventual steady state.

Bioavailability of drugs delivered by drops with low viscosity

The bioavailability of ocular drugs that are applied through drops that have viscosities close to that of tears was computed in our preliminary study, [89] and we recalculated the bioavailability with the current tear dynamics model. In these simulations, an isosmolar drop of timolol was instilled, and it was assumed that the drug diffuses only passively. The current model predicted a bioavailability of 1.27. These predictions agree with the reports that only about 1% of the instilled drug is absorbed by the cornea.[80]

Effect of Viscosity on Tear Drainage and Ocular Residence Time

Effect of Viscosity on Tear Drainage

The effect of viscosity on tear drainage rate $q_{drainage}$ immediately after instilling 25 μL of fluids is shown in Figure 3-16 for a Newtonian fluid. The drainage rates for shear-thinning fluids depend on μ_0 and n, and the results for shear thinning fluids are shown in Figure 3-17. We

note that since the drainage rate increases when the volume of ocular fluids increases, the drainage rates in Figures 3-16 and 3-17 are generally larger than the tear drainage rate without instilling extra fluids.

Effect of Viscosity on Residence Time of Instilled Fluids

The effect of viscosity on residence time in eyes is typically measured by instilling the high viscosity fluid laden with tracers such as radioactive or fluorescent compounds, and then following the total amount of tracer present in the tear volume by measuring the radioactivity of fluorescence. The transients of the total tracer mass in the tear volume solute quantity, I(t), which is a measure of the total signal from the tracer, are plotted in Figure 3-18 for Newtonian fluids for a range of viscosities. It is noted that for fluids with viscosities lower than 4.4 cp, the transients of I overlap. In these and all other calculations reported below, the volume of all the instilled drops is set to be 25 μL. Additionally, the viscosity of the tear fluid draining through the canaliculi is assumed to be changing linearly from the viscosities of the instilled fluids to the viscosity of tears (1.5 cp) to account for the dilution due to tear refreshing.

For non-Newtonian fluids, the transients of I are calculated for sodium hyaluronate acid of 0.2% and 0.3% w/v concentrations, which are commonly used for ocular instillation. The initial values of μ_0 and n for these and all other shear-thinning fluids that are discussed in this study are listed in Table 2-3. To account for the dilution due to tear refreshing, μ_0 is assumed to change linearly from the initial values of μ_0 to the viscosity of tears, and the values of n is assumed to be unchanged. The solute quantity transients I(t) are plotted in Figure 3-17 for these two fluids.

Bioavailability of Instilled Drugs in High Viscosity and Non-Newtonian Vehicles

The bioavailability of instilled drugs is calculated for both Newtonian and non-Newtonian fluids and is listed in Table 3-8.

Tear Mixing Under the Lower Eyelid

Concentration Transients and Mixing Time

Below we present the predicted concentration of fluorescence in the tear film for the shearing and squeezing cases, respectively. The amplitude varies for different gaze positions[56] and additionally, for the squeezing motion the exact value of the amplitude is not clear. Therefore, we will explore the effect of the amplitude and frequency of the lid/globe movement on the tear mixing. According to the data reported by Riggs et al., the shearing amplitude is calculated by assuming that the eyeball rotation varies from 1 to 5 degrees depending on different gaze positions.[56] The amplitude of motion is simply the product of the eyeball radius and the angular rotation in radians. For the squeezing case, the amplitude has not been reported in literatures, but it should not exceed the tear film thickness of about 7 μm. Accordingly, in this part of the study, the squeezing amplitude is varied from 1 μm to 5 μm. It is noted that throughout this study, the appearance time of the solute in the exposed tear film is defined as the time when the concentration reaches 1% of the maximal concentration. In all the results discussed below, unless specified the value of η^* is fixed at 0.04. The effect of variations in this parameter is discussed later.

Figures 3-20 and 3-21 show the concentration transients in the exposed tear film for the cases of shearing and squeezing, respectively for $T_{squeezing} = 0.2$ s, $T_{shearing} = 0.05$ s and $T_c = 6$s. In Figure 3-20, the amplitudes of shearing varies from 1 to 5 degree, and Figure 3-21, the amplitude for squeezing varies form 1 to 5 μm. The values of T_{app} and T_{max} can be obtained from each curve in Figures 3-20 and 3-21, and these are listed in Table 3-9 for shearing and Table 3-10 for squeezing.

To investigate the effect of blinking frequency on tear mixing, the period for a blink-interblink cycle (T_c) is varied from 1 s to 8 s while the amplitudes of the shearing and squeezing are fixed at 1 degree and 3 μm, respectively. In these calculations, T_c is varied but the actual time period for lid/globe movement, i.e. $T_{shearing}$ or $T_{squeezing}$, are kept fixed at 0.05 and 0.2s, respectively. The T_{app} and T_{max} are plotted as a function of T_c in Figures 3-22 and 3-23 for shearing and squeezing, respectively.

Effect of Instillation Volume on Tear Mixing Time

In the experiment the instilled drop volume could vary between 0.05 to 0.2 μl, while in the model it is fixed at 0.1 μl. The change in the instilled volume will affect the width of the fluorescent band in the initial condition of the model, and both T_{app} and T_{max} will decrease if the band width increases, and vise versa. Since the 2D problem in this study essentially assumes the concentration is uniform in the third (nasal-temporal) direction, the initial condition used in this study does not accurately describe the actual situation when a drop of dye is instilled into the fornix. To validate the above assumption, the effect of η^* on T_{app} and T_{max} is calculated**.** If the instilled volume is changed from 0.1 μl to 0.2 μl in the model, the predicted T_{app} and T_{max} for the shearing amplitude of 1˚ will decrease to 51.1 min and 279.0 min, respectively. If the instilled volume is changed from 0.1 μl to 0.05 μl in the model, the predicted T_{app} and T_{max} will increase to 52.6 min and 280.6 min, respectively. For the squeezing mode with the amplitude of 3 μm, if the instilled volume is changed from 0.1 μl to 0.2 μl, the predicted T_{app} and T_{max} for the shearing amplitude of 1˚ will decrease to 0.8 min and 9.2 min, respectively. If the instilled volume is changed from 0.1 μl to 0.05 μl, the predicted T_{app} and T_{max} will increase to 1.3 min and 10.0 min, respectively.

Table 3-1 The storage moduli and loss moduli of porcine lacrimal canaliculi.

Variable	1Hz	10 Hz	25 Hz
E' young* (kPa)	3.07±0.94	3.36±1.17	4.96±1.54
E" young (kPa)	0.82±0.28	2.08±0.65	4.54±1.14
E' old** (kPa)	2.70±1.08	2.84±1.45	4.31±2.23
E" old (kPa)	0.68±0.23	1.84±0.85	4.39±1.21

* 6~9 months old (n=25) ** >2 years old (n=23)

Table 3-2 Parameter values obtained by fitting the strain recovery to a double exponential.

Sample #	a (%)	b (%)	τ_1 (s)	τ_2 (s)	R^2
1	13.4	2.15	0.115	1.28	0.998
2	12.6	2.82	0.0921	2.02	0.987
4	15.1	2.10	0.0542	1.37	0.998
5	7.83	1.29	0.163	1.92	0.998
6	14.0	2.13	0.106	2.01	0.987
8	13.5	1.19	0.192	4.95	0.987
9	13.4	1.07	0.194	2.97	0.993
10	9.39	1.49	0.179	2.64	0.984

Table 3-3 Comparison of cellular concentrations for Ussing-chamber simulation.

	Measured Values	Model Predictions
$C_{Na,c}^0$ (mM)	13 [25]	12.56
$C_{K,c}^0$ (mM)	132 [25]	132.69
$C_{Cl,c}^0$ (mM)	40 [25]	47.90
$C_{Glu,c}^0$ (mM)	0.5 [66] (pig)	0.68
$C_{Others,c}^0$ (mM)	114.50	106.32
V_c^0/S_{conj} (m^3/m^2)	11.9×10^{-6} [82]	12.84×10^{-6}

In Table 3-4, $C_{Others,c}^0$ represents the concentration of inert solutes, and its value is set so that the initial cellular osmolarity is 300mM. Accurate measurements of conjunctival epithelium cell height are not reported, but the cell height and the dimension of cell surface are expected to be comparable. So, in Table 3-4, the calculated value for V_c^0/S_{conj}, which in fact represents the dimension of the cell at the apical side, is compared with the cell height reported in the literature. It is also confirmed by our calculation that changing the value of V_c^0/S_{conj} to a value of 10 μm, which is a typical value for cell height, does not make significant differences in the predictions.

Table 3-4 Comparison of steady state I_{SC} after different maneuvers.

Condition	Experimental data (rabbit)	Model prediction
Control	0.144A/m^2 [37]	0.151A/m^2
Apical Na free	20%~50% decrease [37]	34.3% decrease
Apical Cl free	10% [37] or 180% [36] increase	2.6% increase
Apical and basolateral Cl free	75% decrease [36]	51.6% decrease
K channel blockade	80% decrease [36]	87.5% decrease
Cl channel blockade	80% decrease [36]	49.8% decrease
Na-K pump blockade	100% decrease [36,37]	98.9% decrease
Na-K-Cl cotransporter blockade	42% [36] or 44% [37] decrease	51.5% decrease

Table 3-5 Comparison of $t_{1/2}$ of I_{SC} after different maneuvers.

Manuvers	Experimental data[36] (rabbit)	Model prediction
Na-K pump inhibition	41.5±6.06 min	18.57 min
Na-K-Cl cotransporter inhibition	8.33±0.98 min	8.86 min
Cl channel blockade	0.92± 0.14min	~0 min
K channel blockade	5.5± 0.8 min	~0 min

Table 3-6 Comparison of net Na and Cl fluxes.

Net flux (basolateral to apical being positive)	Experimental Data (rabbit)	Model Predictions
Cl ($mol \cdot m^{-2} \cdot s$)	$(6.94 \pm 1.67) \times 10^{-7}$ (short-circuit)[44] $(4.17 \pm 1.39) \times 10^{-7}$ (open-circuit)[42]	9.69×10^{-7} (short-circuit) 1.73×10^{-7} (open-circuit)
Na ($mol \cdot m^{-2} \cdot s$)	-4.17×10^{-7} (short-circuit)[39] $-(3.89 \pm 1.39) \times 10^{-7}$ (short-circuit)[44]	-5.99×10^{-7} (short-circuit)

Table 3-7 Comparison of the apical composition and volume.

	Experimental Data	Model Predictions
$C_{Na,a}$ (mM)	133.2 [83]	128.3
$C_{K,a}$ (mM)	24.0 [83]	20.2
$C_{Cl,a}$ (mM)	127.2 (estimated)	109.9
$C_{Glu,a}$ (mM)	0.56 [84]	0.63
$C_{Others,a}$ (mM)	34.21 (estimated)	38.6
V_a (μL)	11.8	7.1

Table 3-8 Bioavailability for instilled Timolol using different vehicles

Fluid	Bioavailability
below 4.4 cp Newtonian	1.16 %
10 cp Newtonian	1.16 %
40 cp Newtonian	1.18 %
70 cp Newtonian	1.19 %
100 cp Newtonian	1.20 %
0.2 % NaHA	1.20 %
0.3 % NaHA	1.21 %

Table 3-9 The predicted T_{app} and T_{max} for shearing

Amplitude (degree)	T_{app} (min)	T_{max} (min)
1	52.3	280.3
2	25.2	133.6
3	14.0	78.2
4	8.9	53.5
5	6.2	40.2

Table 3-10 The predicted T_{app} and T_{max} for squeezing

Amplitude (μm)	T_{app} (min)	T_{max} (min)
1	6.7	37.8
2	2.3	16.5
3	1.1	9.8
4	0.7	6.7
5	0.4	4.8

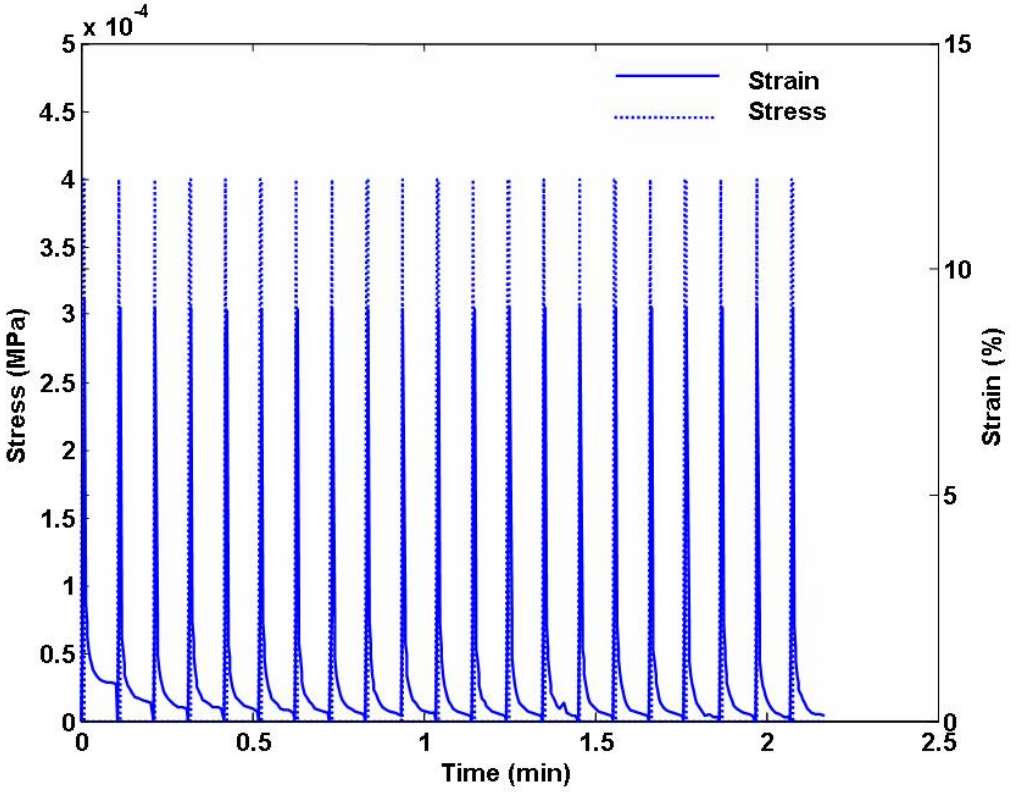

Figure 3-1 Stress and strain transients during loading-recovery cycles.

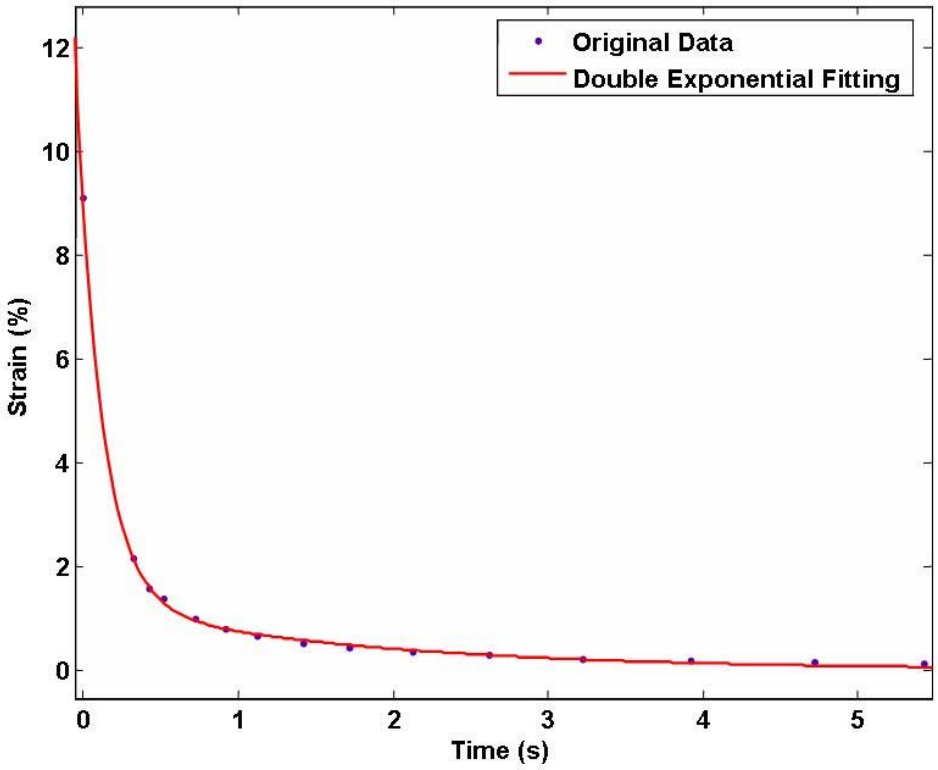

Figure 3-2 Sample data for one recovery cycle along with the best fit double-exponential curve.

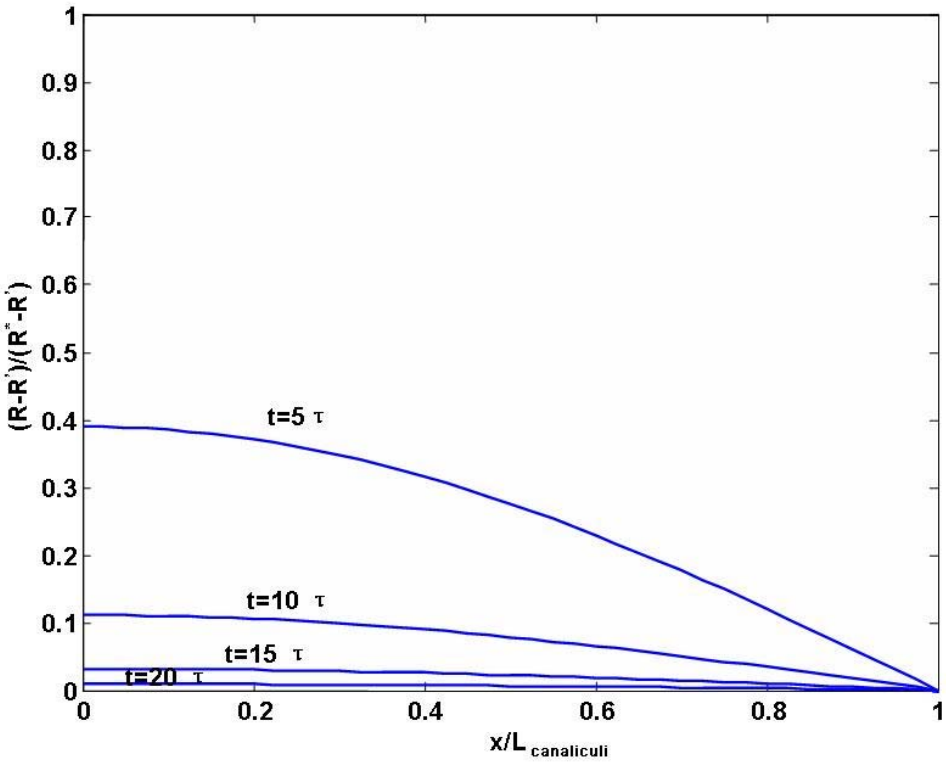

Figure 3-3 Radius-axial position profiles during the blink phase at four different times.

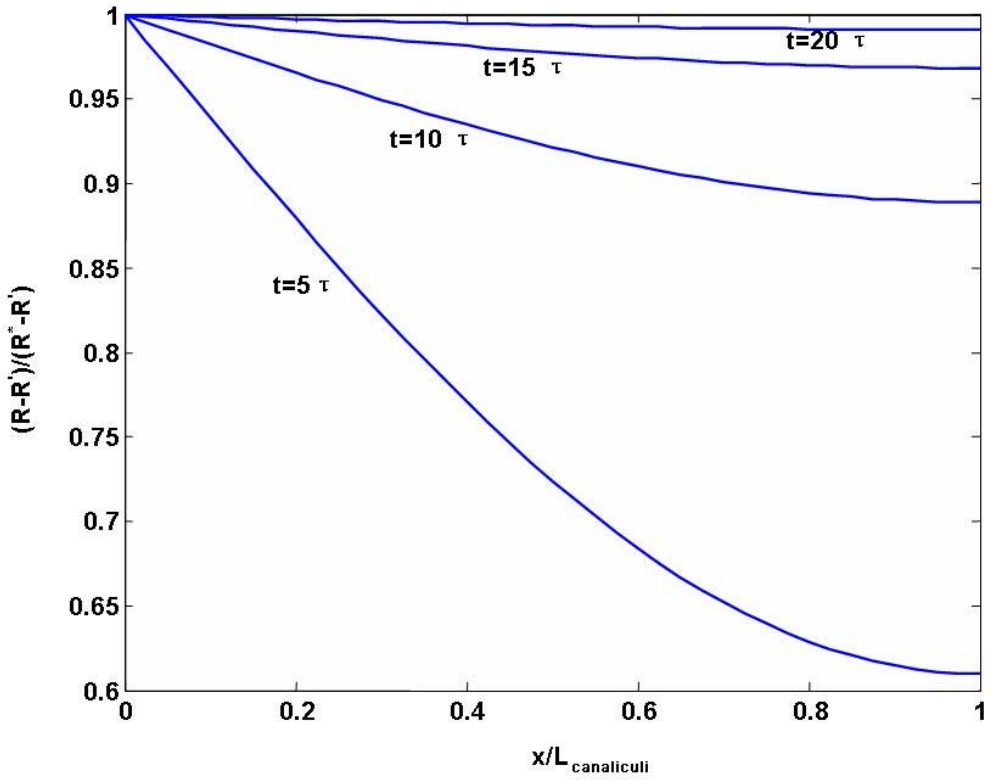

Figure 3-4 Radius-axial position profiles during the interblink phase at four different times.

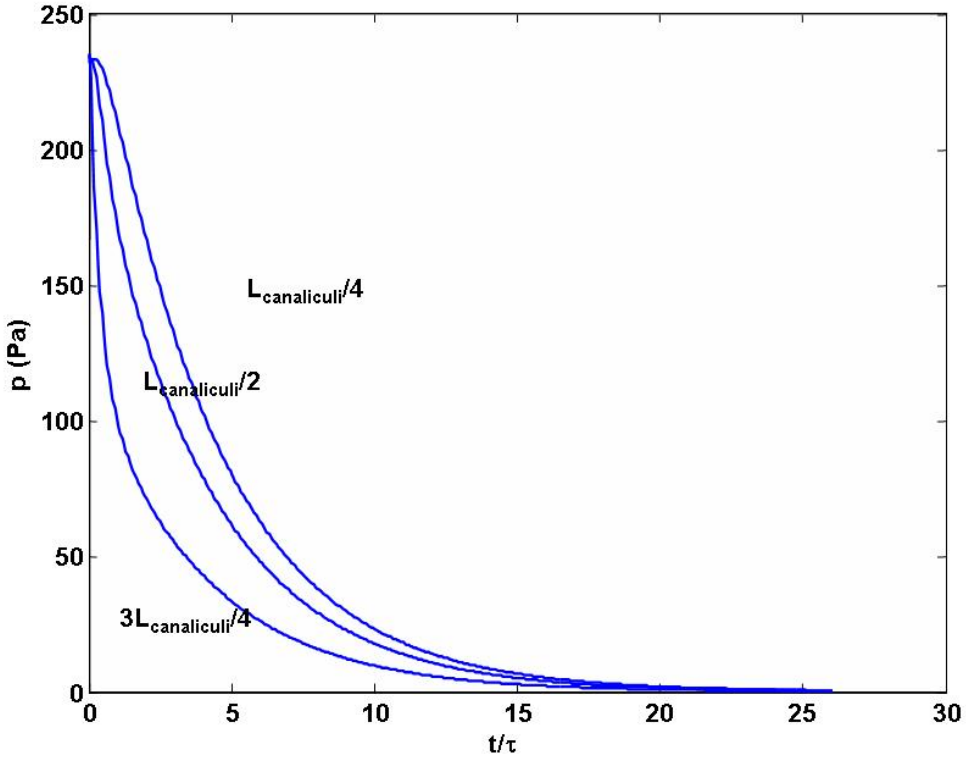

Figure 3-5 Pressure-time transients during the blink phase at three different location along the canaliculus

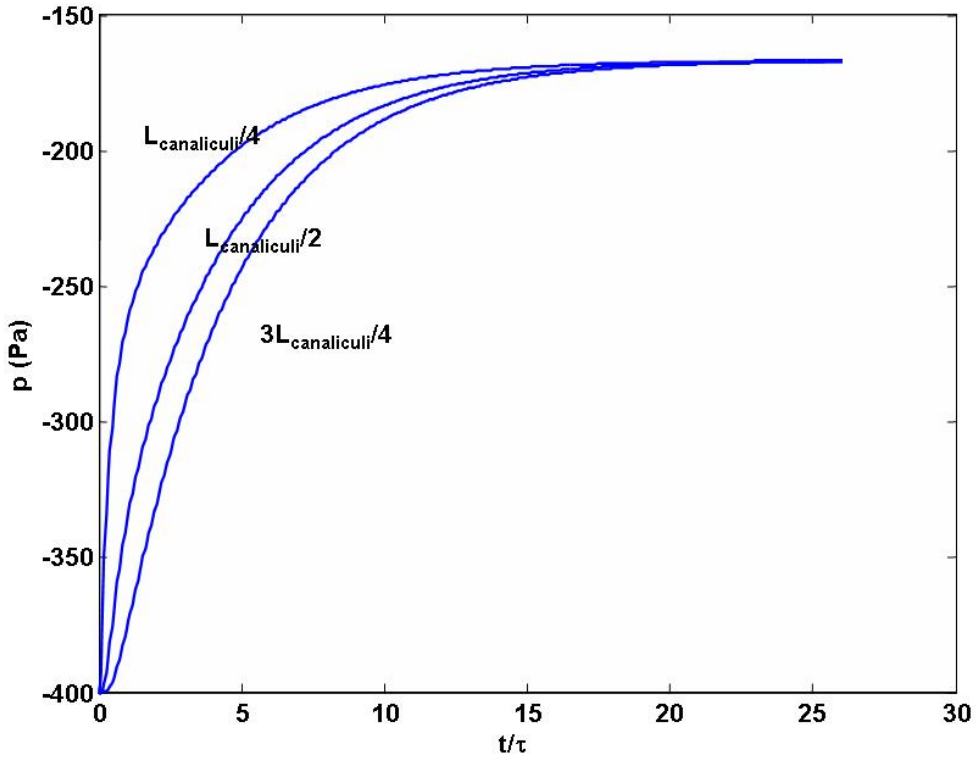

Figure 3-6 Pressure-time transients during the interblink phase at three different locations along the canaliculus.

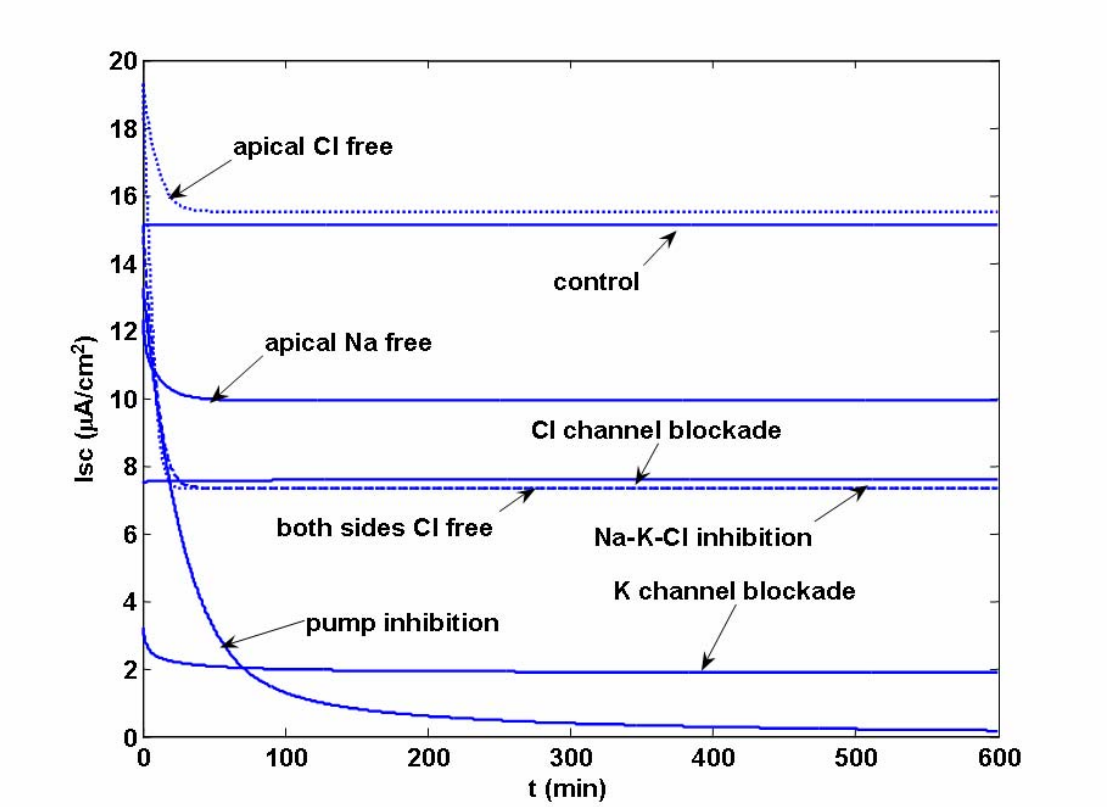

Figure 3-7 Time course of I_{SC} in Ussing-chamber experiments.

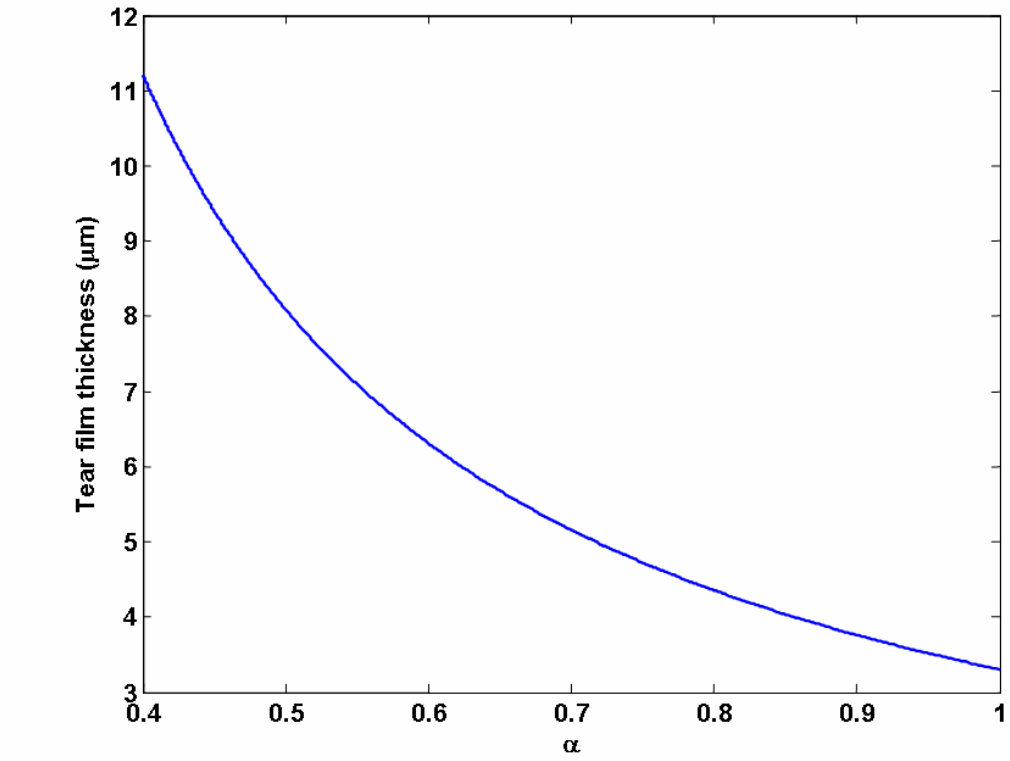

Figure 3-8 The effect of tear evaporation and absorption on tear film thickness.

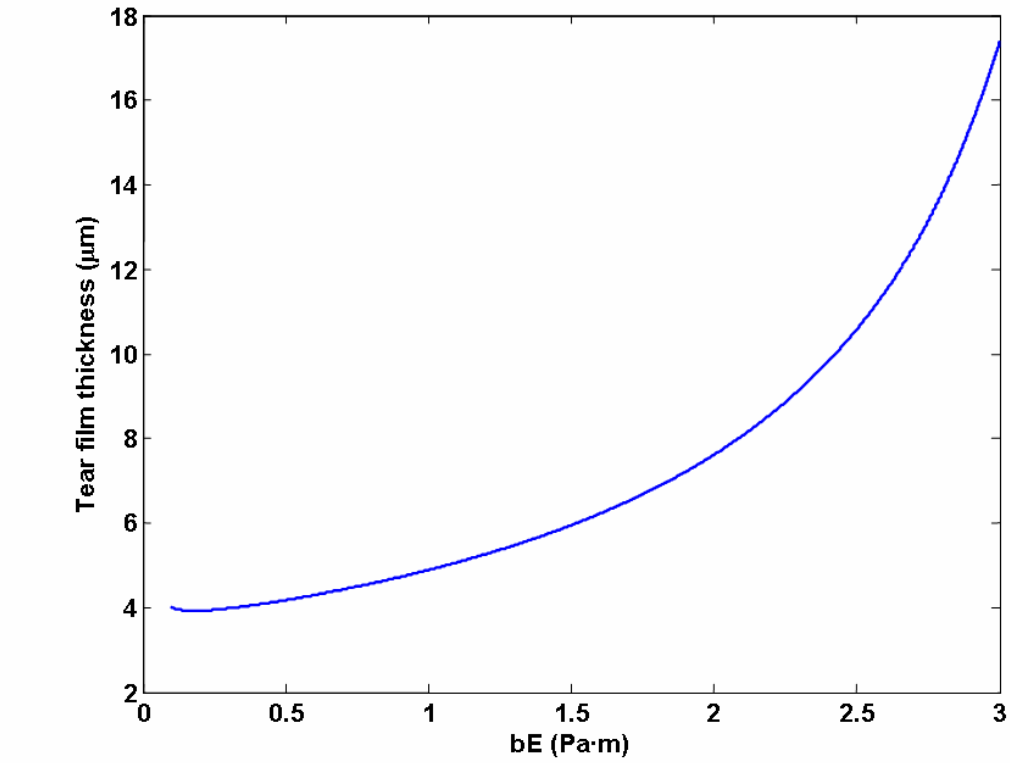

Figure 3-9 The effect of canaliculus properties on tear film thickness.

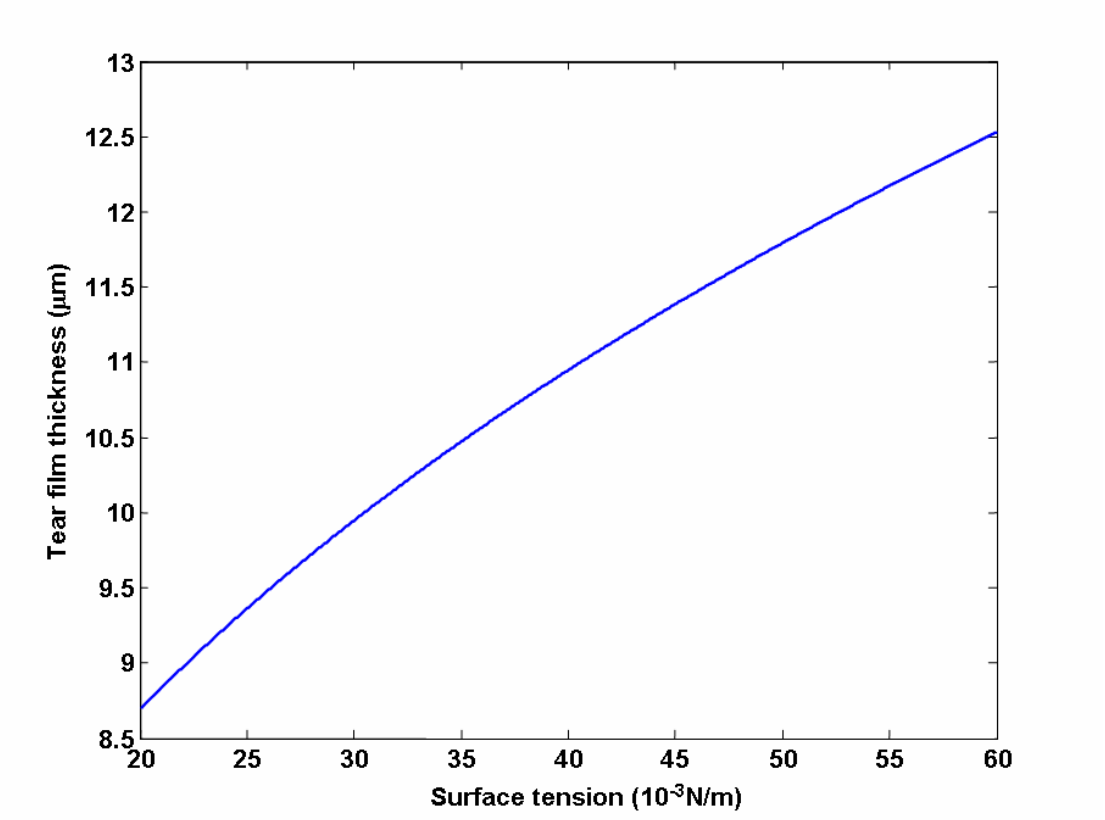

Figure 3-10 The effect of surface tension on tear film thickness.

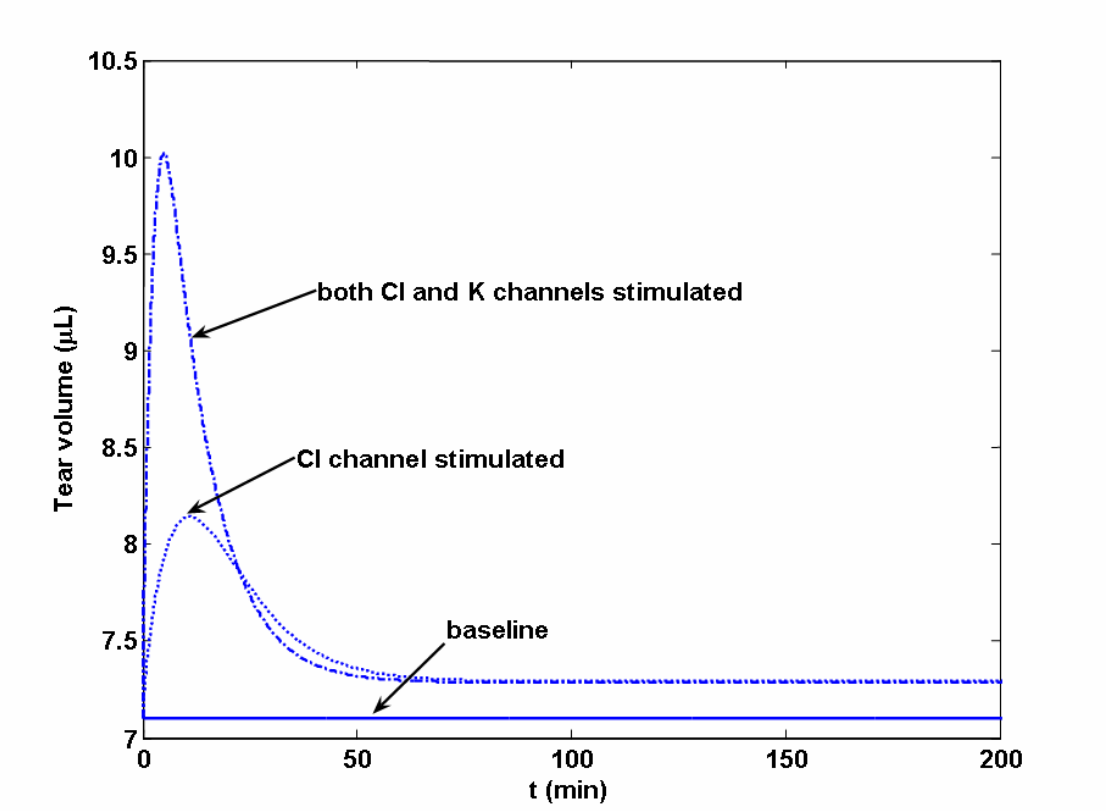

Figure 3-11 The effect of channel modulation on tear volume.

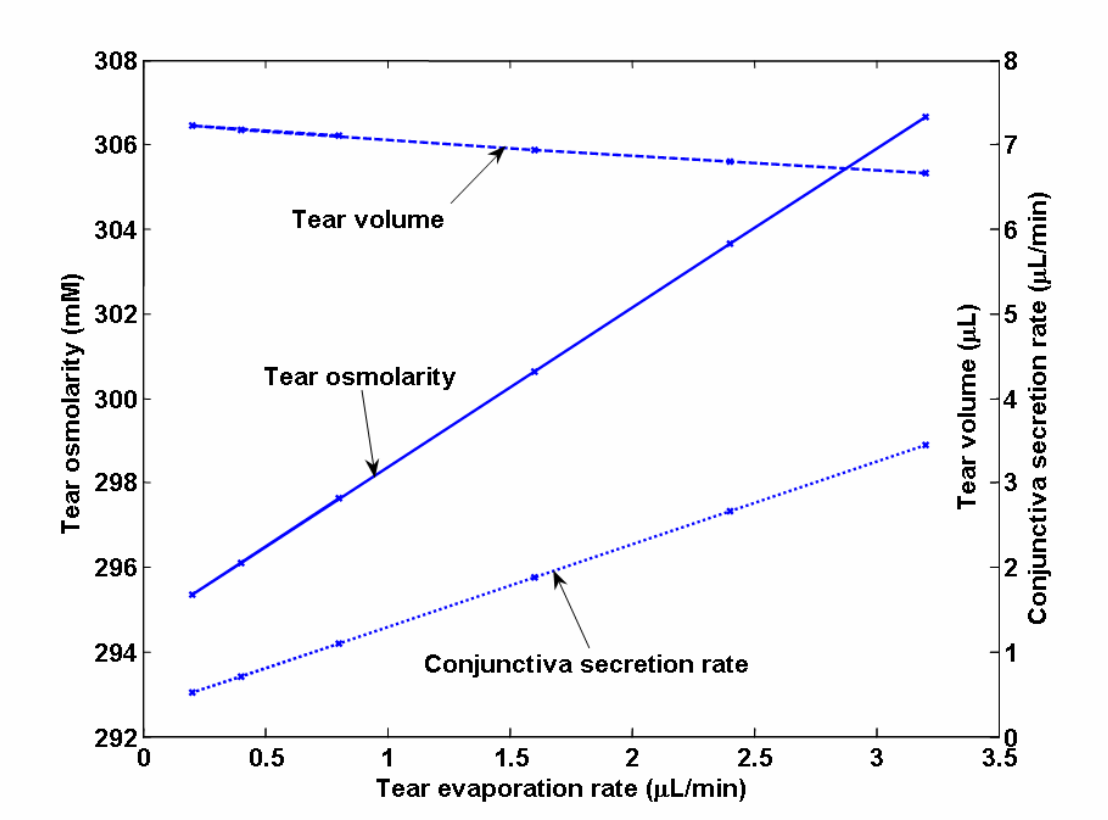

Figure 3-12 The effect of evaporation on tear volume, osmolarity and conjunctiva secretion rate.

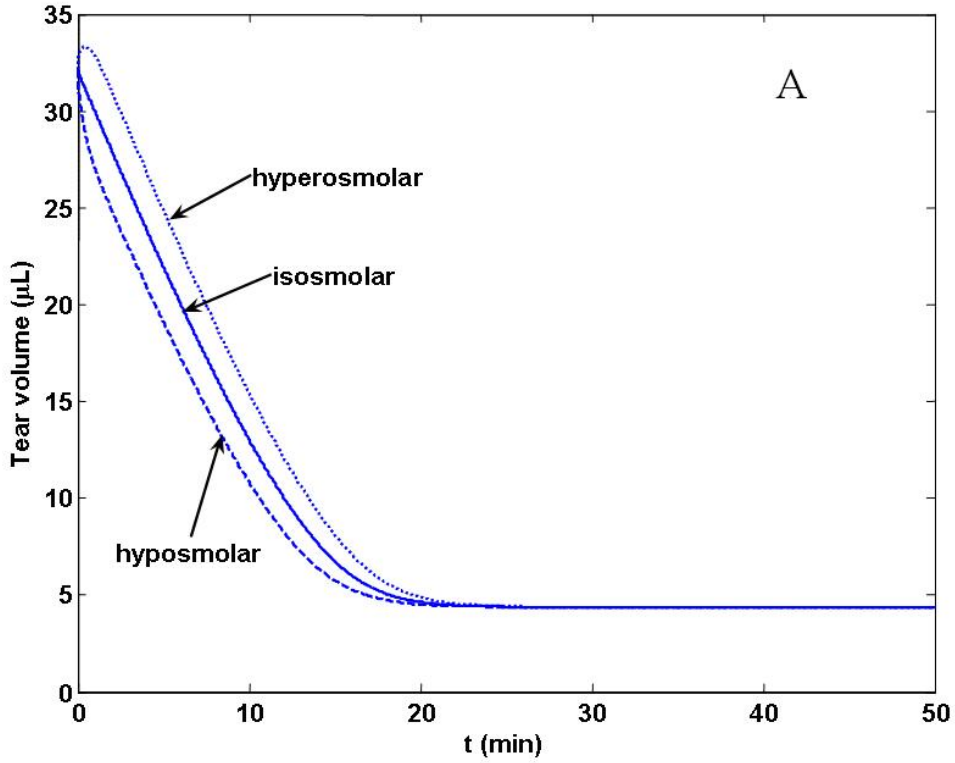
A
hyperosmolar
isosmolar
hyposmolar
Tear volume (µL)
t (min)
0
5
10
15
20
25
30
35
0
10
20
30
40
50

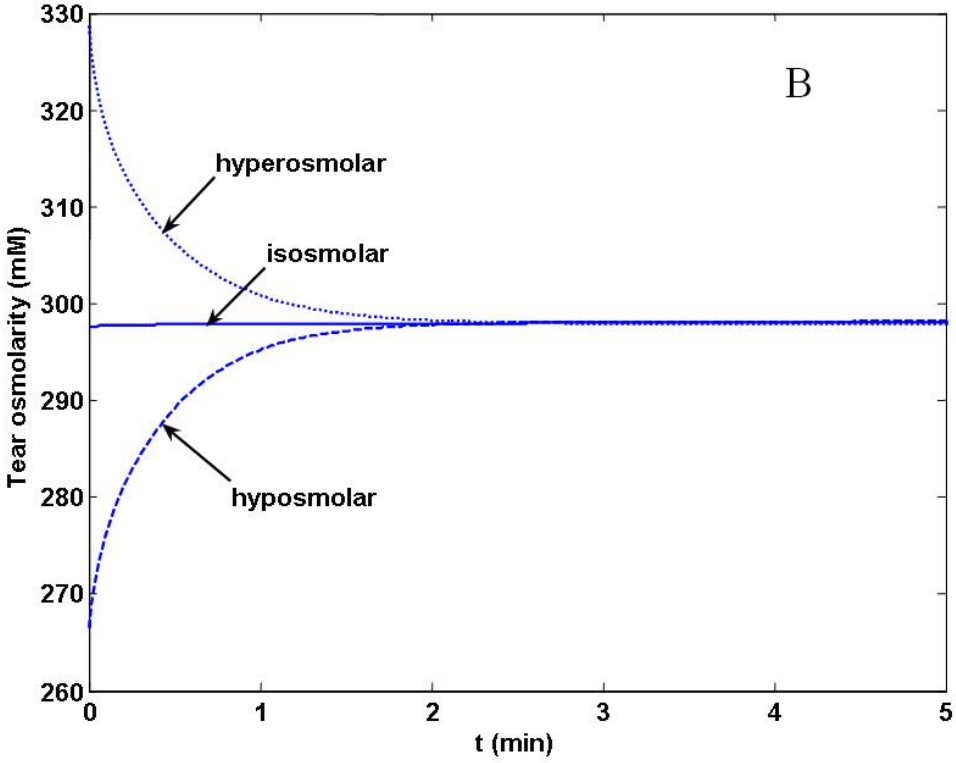
B
hyperosmolar
isosmolar
hyposmolar
Tear osmolarity (mM)
t (min)
260
270
280
290
300
310
320
330
0
1
2
3
4
5

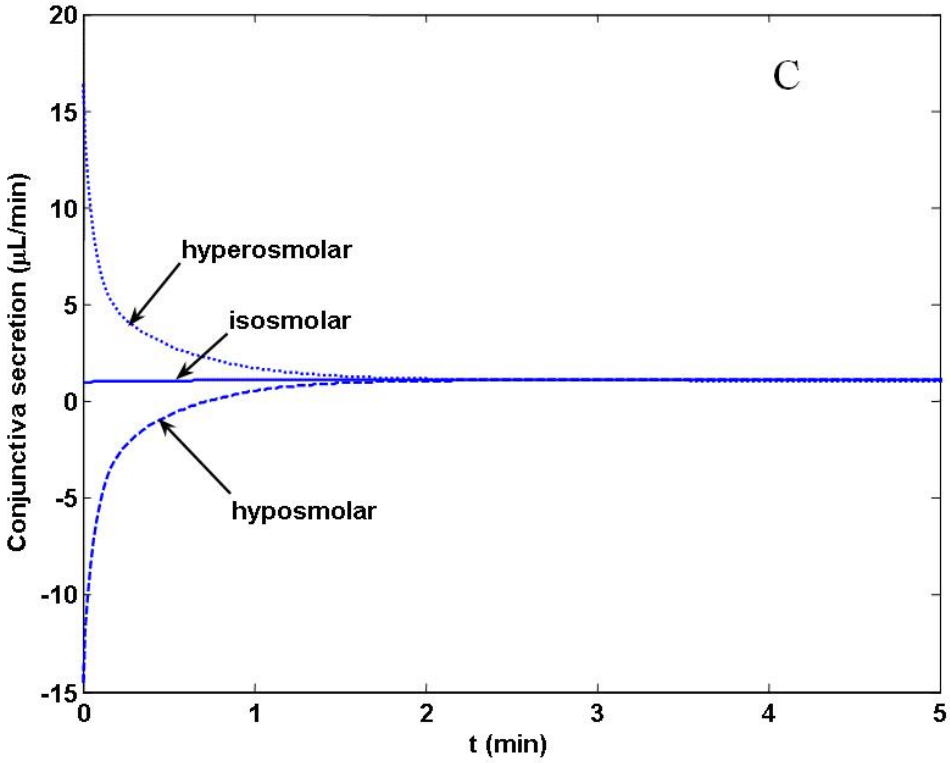

Figure 3-13 The effect of isosmolar and anisosmolar (osmolarity± 40 mM) fluid instillation on A) Tear volume. B) Tear osmolarity. C) Conjunctiva secretion rate.

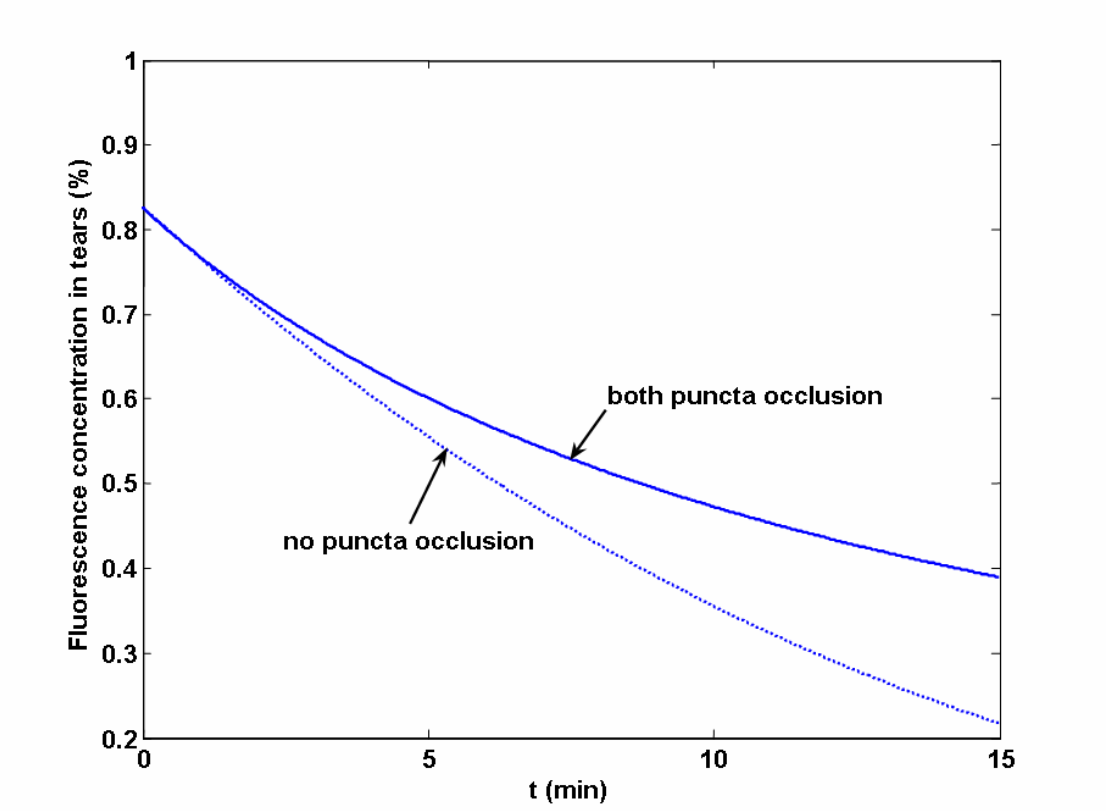

Figure 3-14 The effect of punctum occlusion on fluorescence clearance with different rates.

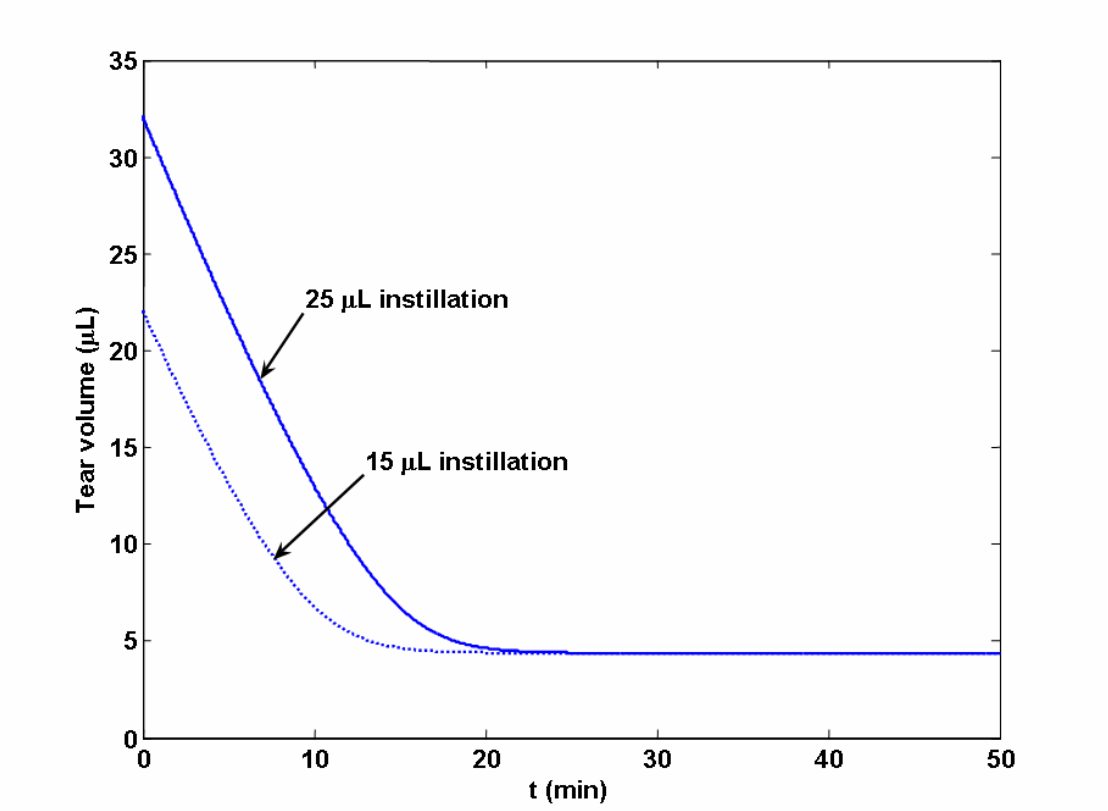

Figure 3-15 Clearance of instilled drops of isosmolar fluid with different volumes.

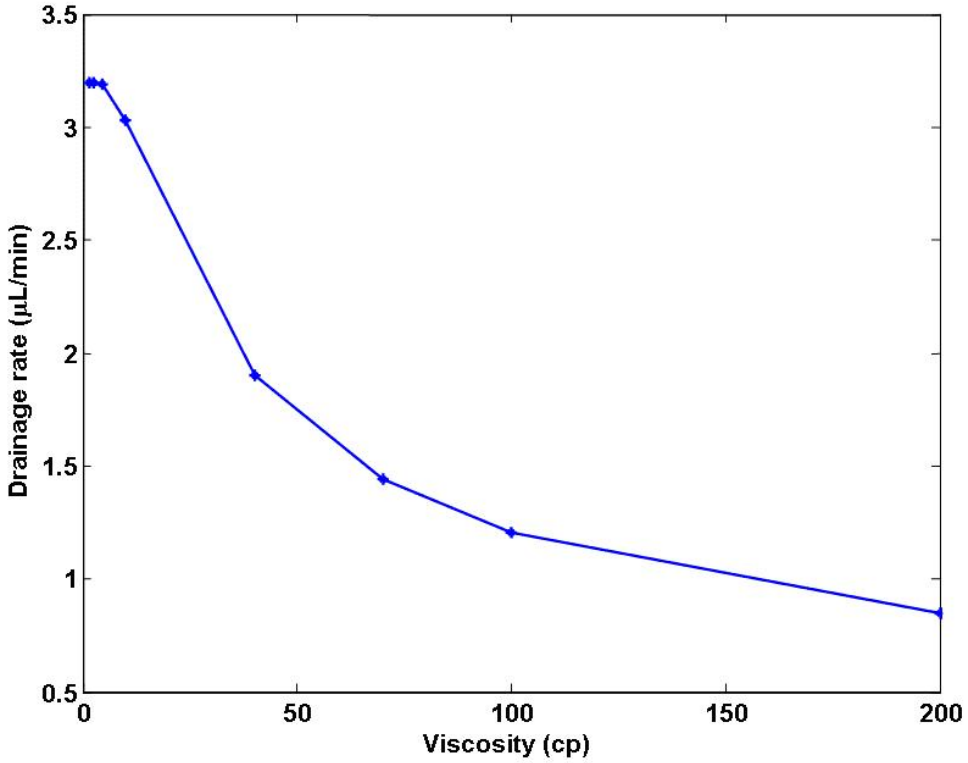

Figure 3-16 The effect of viscosity on the drainage rate through canaliculi for Newtonian fluids.

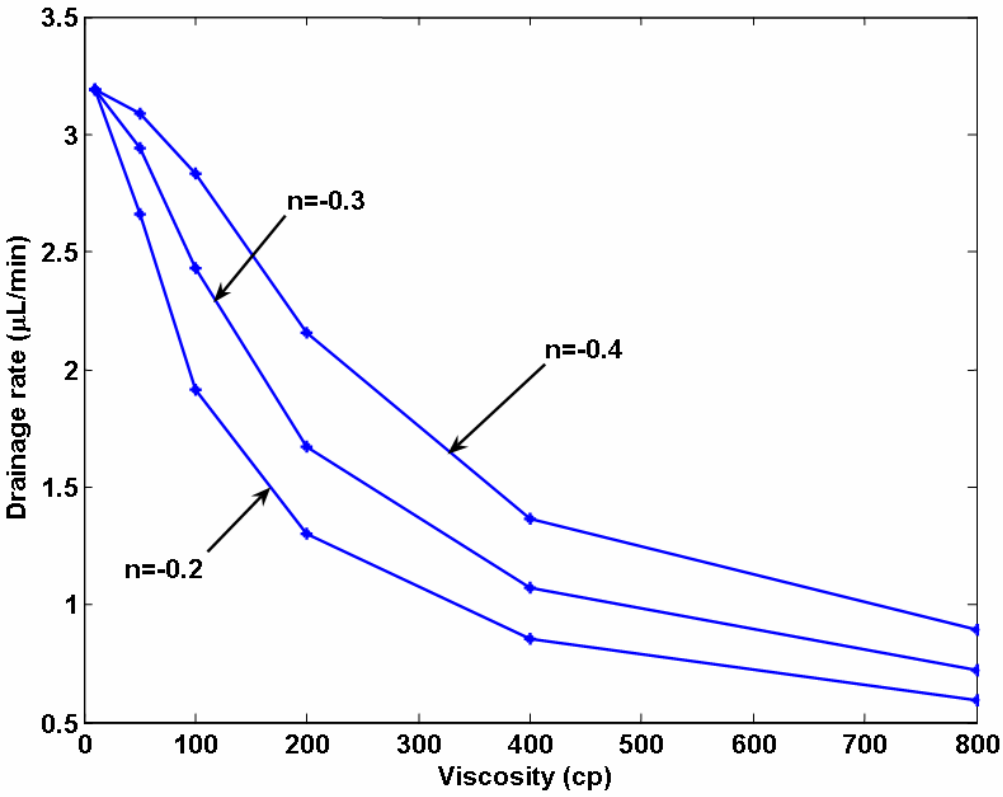

Figure 3-17 The effect of viscosity (μ_0) and the exponential parameter (n) on the drainage rate through canaliculi for power-law fluids.

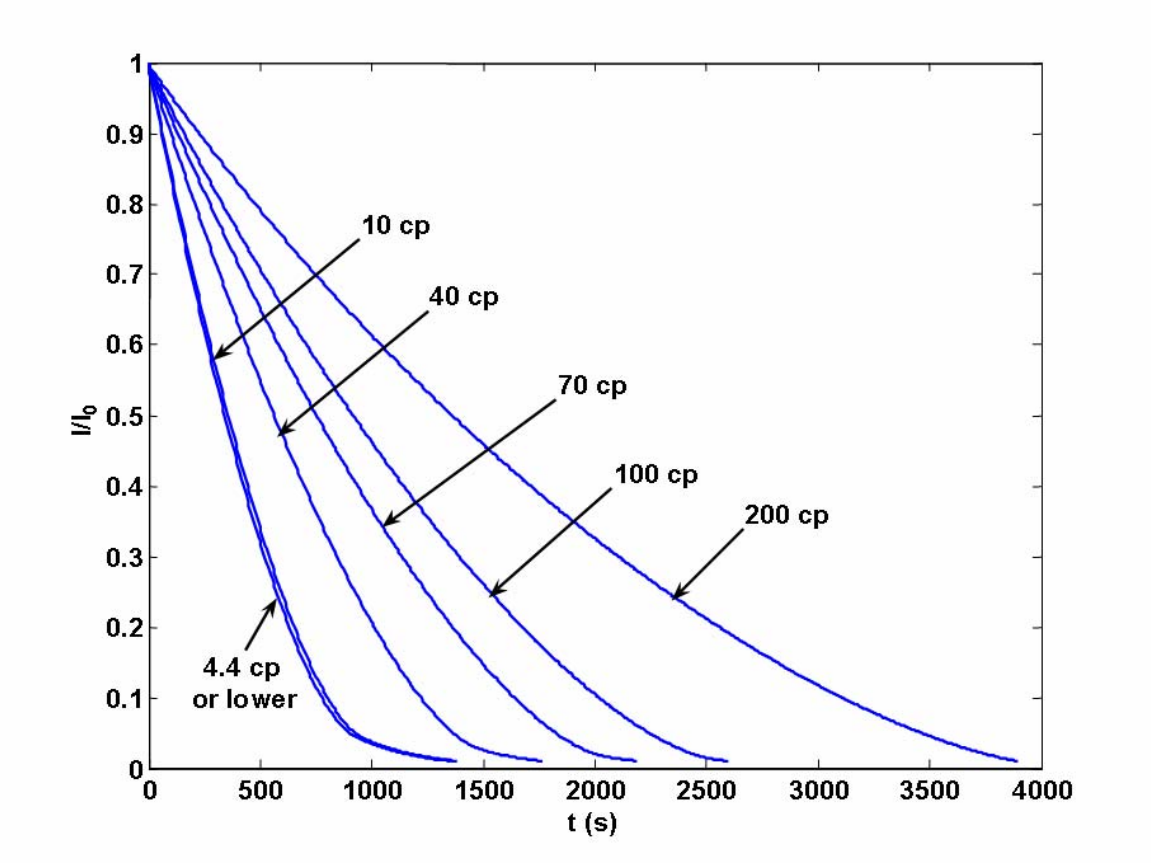

Figure 3-18 The transients of solute quantity (I) after the instillation Newtonian fluids with different viscosities.

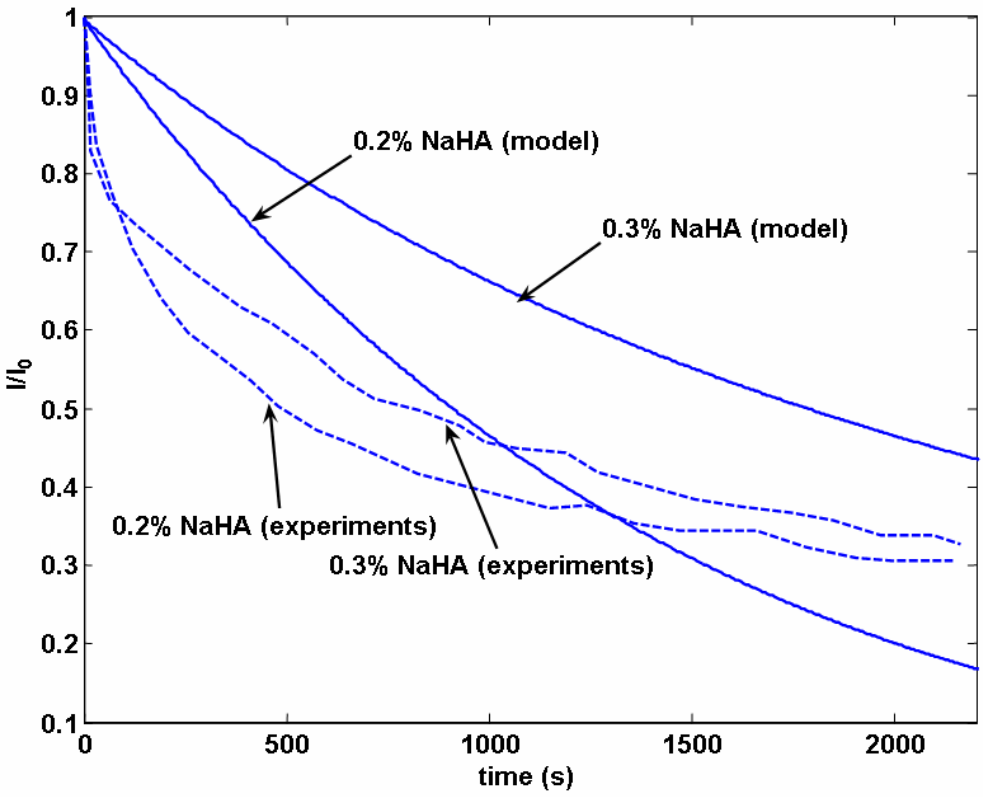

Figure 3-19 The transients of solute quantity (I) after the instillation 0.2% and 0.3% sodium hyaluronate.

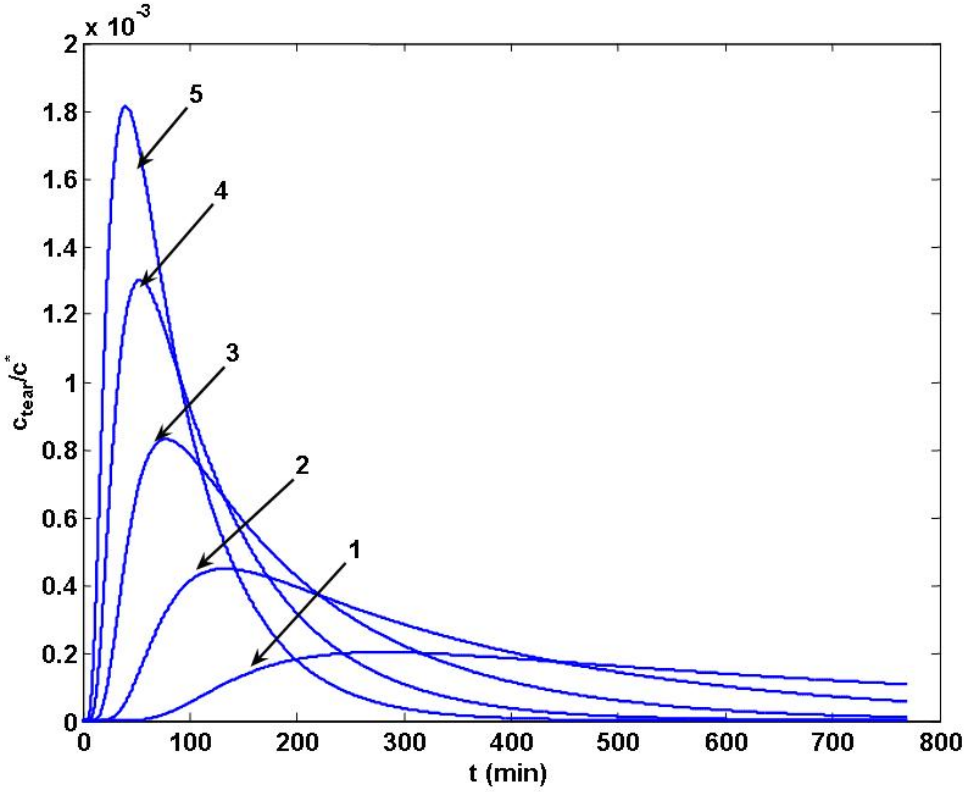

Figure 3-20 Concentration of fluorescence in the exposed tear film after instillation into the lower fornix for shearing amplitude of 1-5 degrees.

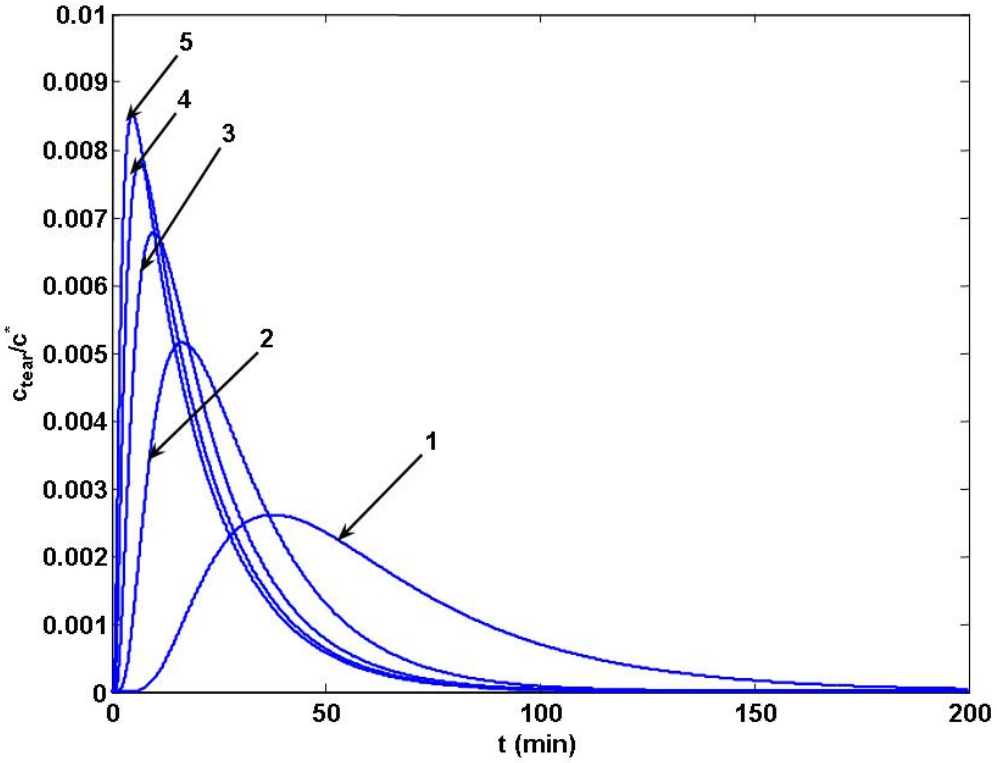

Figure 3-21 Concentration of fluorescence in the exposed tear film after instillation into the lower fornix for squeezing amplitude of 1-5 μm.

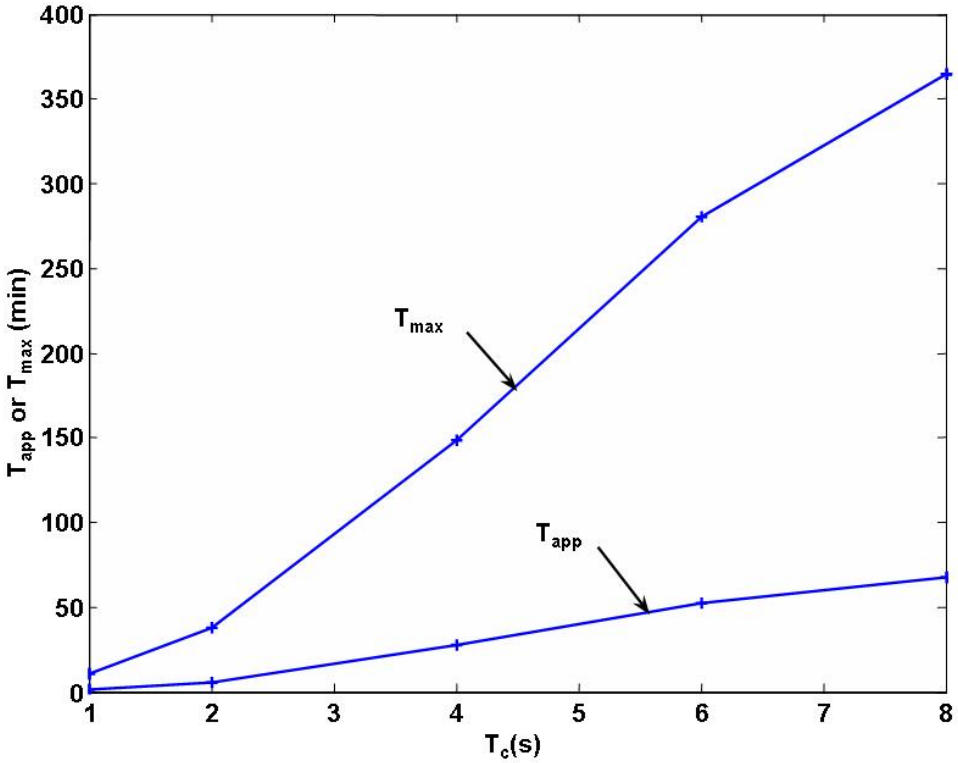

Figure 3-22 The predicted T_{app} and T_{max} for shearing for different blink cycle duration (T_c).

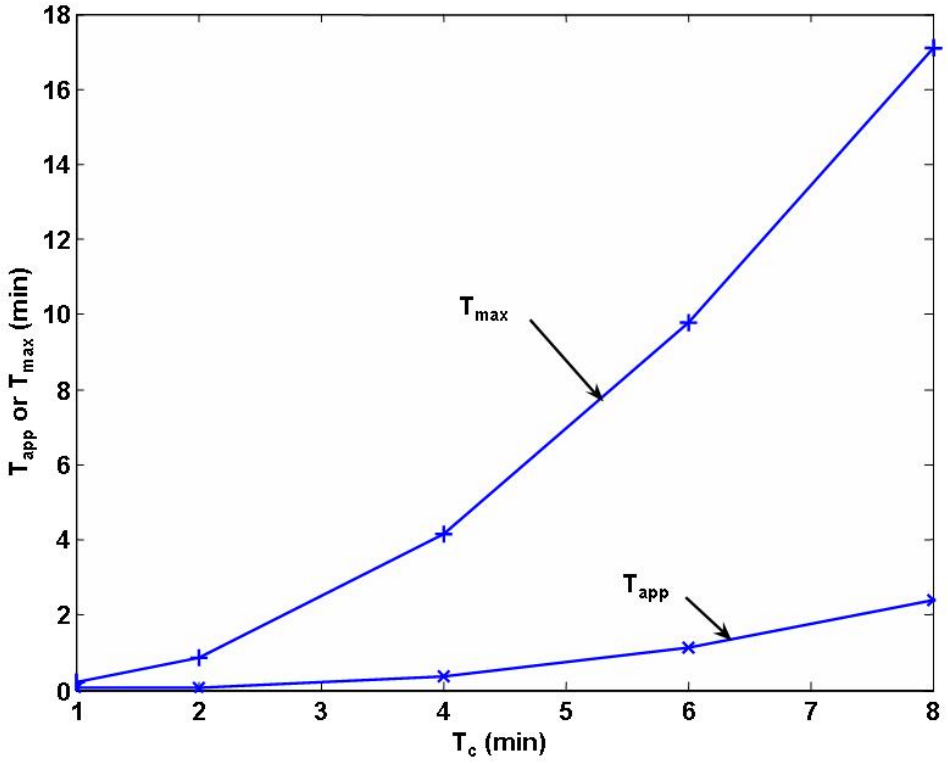

Figure 3-23 The predicted T_{app} and T_{max} for squeezing for different blink cycle duration (T_c).

CHAPTER 4
DISCUSSION

Mechanical Properties of Porcine Lacrimal Canaliculi

DMA has been routinely used to study the mechanical properties of non-biological materials,[90, 91, 92] and there have been reports of DMA measurement of bones,[93] but there are few reports on the application of DMA on soft tissues. Our study shows that DMA is a powerful tool for the mechanical measurement of soft tissues such as the lacrimal canaliculi, especially since these tests can be conducted under physiologically relevant conditions.

In the current study, compressive load was applied on the canaliculi that were cut open into a flat sheet, and the storage moduli, loss moduli and the stress-strain curve under repeated loading-recovery were measured. Results show that the magnitude of E' and E" are comparable and that they both depend significantly on frequency. The relevant frequencies differ significantly between the blink and the interblink phase ranging between 1 Hz and 25 Hz during each blinking cycle, and so the frequency dependence of the rheological properties must be taken into account while trying to understand any issue related to tear drainage. In particular, these results suggest that our previous tear drainage model can be improved by using a more complex constitutive equation for the lacrimal canaliculi, which include both the elastic and the damping properties of the tissue.

The current study did not find any significant differences in the rheological properties between the 6~9 months old and the >2 years old groups. However, we note that the typical lifespan of pigs is about 12~16 years,[94] and therefore the differences in ages between these two groups is not significant. Therefore, further studies are needed with more widely spaced age groups to determine the effect of age on rheological properties of the canaliculus.

It is noted that while the magnitude of loads were adjusted to simulate physiological situations, the loading conditions in the tests were still significantly different from those in vivo. The first major difference is that the canaliculus is a cylindrical tube and the stress is applied is mainly in the radial direction but the tests were conducted with flat sheets. In fact the major component of the stress in vivo is the hoop stress, which is absent in the in vitro experiments. It is perhaps most relevant to measure the viscoelastic response of the canaliculus in experiments in which the canaliculus filled with tears is submerged in a bath of tears, and is then subjected to pressure oscillations. Such experiments have been conducted with blood vessels[95] but because of the small length, low stiffness, and the complicated shape of the canaliculi, these experiments are extremely difficult to conduct. It is noted that the mechanical properties of an isotropic system will not depend on the direction of loading but a canaliculus is likely to be anisotropic. Furthermore, the properties of the canaliculi are likely to vary depending on the location, and also the magnitude of the applied force also varies with position. Anatomic studies show that the Horner's muscle applies contraction force on both the vertical and the horizontal parts of the canaliculi, and the force is largest for the vertical part and it decreases along the horizontal part towards the lacrimal sac.[96] Finally, in the current study porcine canaliculi were used rather than human canaliculi. The blinking rate of pig is about 30~36 blinks/minute,[97] which is similar to that in humans, but it is unlikely that the mechanical properties of the human canaliculus are the same as that of porcine canaliculus. Despite such limitations, it is instructive to compare the results of the measurements reported above with those reported in literature for the value of the modulus and for the time scale of pressure relaxation.

It has been shown that the parameter bE, which is the product of the canaliculus wall thickness and the Young's modulus, is the most important parameter to the model of canalicular

tear drainage. Due to the lack of data, in our previous tear drainage model we assumed the canaliculi to be linearly elastic and estimated bE to be about 2.75 Pa·m by equating the outflow of tears under normal condition with the tear production obtained in experiments. According to the current study, the product of the storage modulus and the sample thickness (in Pa·m) is 4.51±1.11 (1 Hz), 4.96±1.48 (10 Hz) and 7.51±2.67 (25 Hz) for the 6-9 months group, and 4.33±2.01 (1 Hz), 4.56±2.54 (10 Hz) and 7.11±4.45 (25 Hz) for the +2 years group. Therefore, the bE value estimated in our earlier model is comparable with the measured values of the corresponding parameter, bE', particularly considering the fact that the measurements correspond to porcine canaliculus. We note that the storage modulus of lacrimal canaliculi is much smaller than those of cornea and arteries, both of which are of the order of 10^6 Pa.[98,99]

The recovery of the canaliculus is directly related to the pressure changes inside the canaliculus which have been measured experimentally by Wilson and Merrill.[70] In Figure 4-1, we plot a typical strain transient during the recovery (interblink) period along with the measurements for pressure that were obtained by inserting a polyethylene tubing (inner diameter 0.27mm; outer diameter 0.6mm) 8 mm into the lower punctum.[70] In the same figure, we also plot the pressure profiles predicted by our tear drainage model. It is noted that in Figure 4-1, $t = 0$ is defined as the start of the interblink period, the solid line connecting the stars is an exponential fit to the strain data.

The time scale for the strain recovery in the current study is comparable to the time scale of pressure relaxation obtained by direct measurement (Figure 4-1), and it is much longer than the pressure relaxation time scale predicted by our previous model. The good agreement between the time required for pressure relaxation in in vivo experiments and that for the strain recovery in our measurements strongly suggests that the recovery of canaliculi during the

interblink period is controlled by the rheological properties of the tissue. In our previous tear drainage model, the tissue was assumed to be purely elastic which implies that any stress on the tissue will result in an instantaneous strain response. Therefore the rate of canaliculi recovery was controlled by the viscous resistance offered by the fluid (tears) as it flows from the tear film into the canaliculi to relieve the vacuum. However the measurements reported in this study show that the canaliculus is viscoelastic, and the time scale for the recovery is longer than the time scale for the tears to flow into the canaliculi. Accordingly the shape and the pressure changes in the canaliculi are controlled by the canaliculus rheology and not by the tear viscosity.

The good fitting of the strain recovery transient using the double exponential function suggests that there are two time scales for the strain recovery. The short time scale of about 0.1 to 0.2 second is corresponding to the physiological recovery of the canaliculi, as suggested by Figure 3-2 and the fact that the fitting parameter "a" accounts for almost all the strain recovery. There is a small portion of the strain recovery, which corresponds to the fitting parmeter "b" and the long time scale of about 2 second.

Validation of the Tear Drainage Model

The tear dynamics model is based on a number of assumptions that are stated in the method and result sections. Below we first discuss the validity of some of the main assumptions and then compare the model predictions with experimental data available in literature and finally discuss some of the model predictions.

Steady State Assumption

The tear film is reformed in each blink and it stays relatively stable during the interblink period.[100] However, during this period the tears are drained through the canaliculi and the film also deforms due to the effects of gravity. Thus, the tear film is never truly at a steady state. However, the tear flow rate under normal conditions is about 1~4μL/min[13] and the normal tear

volume is about 10μL, [2] and thus the tear turnover time of about 2.5~10 min is much larger than the interblink period of about 6 seconds. Therefore, the change of the volume of the preocular tears during the interblink is negligible compared with the total volume itself, and it is valid to assume a time independent R_m and set the left hand side of equation (11) to zero. This is in accordance with the observation by Yokoi et al. that the meniscus radius does not have significant variation during most of the interblink period unless the gaze direction is changed.[101]

Comparison of the Predicted Pressure Changes with Literature Results

Wilson and Merrill[70] inserted a polyethylene tubing (inner diameter 0.27mm; outer diameter 0.6mm) 8 mm into the lower punctum and connected the tube to a pressure transducer to measure the dynamic pressure in the canaliculi. According to their measurements, during voluntary blinks, the pressure in the canaliculi starts from an initial value of zero before a blink, and then goes through a rapid increase of about 3-4 mm Hg (about 400 to 533 Pa) in about 0.1~0.2 second after the blinking begins. The pressure then drops quickly to 3-4 mm Hg below zero (about -400 to -533 Pa) while the eyelids are opening in about 0.1~0.2 second, and then slowly returns to the initial value of zero during the interblink in another 0.5~0.6 second. [70] The pressure transients obtained from the model are similar to those in the studies of Wilson and Merrill, but they differ quantitatively. During the blink phase, the pressure in the canaliculi starts from an initial value of -167 Pa before a blink, and then goes through a rapid increase to about 233 Pa immediately after the blink begins. Subsequently, the pressure drops from about 233 Pa to zero in about 0.0010 to 0.0546 second, depending on the model parameters. The pressure then drops immediately to -400 upon the removal of p_0, and then slowly returns to -167 Pa during the interblink in another 0.0010 to 0.0546 second. The major difference between the pressure transients from the experiments and the model are the following:

(1) The model predicts that the time to attain steady state is the same for the blink and the interblink, but in the experiments the time taken for the pressure to stabilize in the interblink is about 3-5 times that during the blink. The discrepancy can be explained by noticing that in the experiments the outer diameter of the tube was larger than the canalicular diameter, and thus the lower canaliculus was not directly connected to the tear menisci. It was however connected indirectly through the upper canaliculus (Figure 1 of Wilson and Merrill[70]) . Consequently the length over which the tear fluid had to flow in the interblink was twice the length over which fluid has to flow during the blink. According to the model, the equilibration time scales as L^2, and thus doubling of length is expected to increase the time by a factor of 4. Additionally, in our model it is assumed that the lacrimal sac does not contribute to the driving of tear drainage, but recent research suggested that the role of the lacrimal sac in the tear drainage may be underestimated.[102] Thus the time scale in the pressure measurement may include the time for the expansion of the lacrimal sac as well as the expansion of the canaliculus.

(2) The time scale for equilibration during the blink is about 0.1 s in experiments but the equilibration time scale predicted by the model is about 0.0010 to 0.0546 second. The upper limit of the prediction is close to the experimental value but the lower limit is far below. There are a number of factors that may contribute to an under-prediction of the equilibration time. In the proposed model the pressure applied on the canaliculi is assumed to be uniform and constant. However, the actual pressure applied on canaliculi in the blink phase is neither uniform nor constant.[32] Also in the model we have assumed the canaliculus to be a straight pipe, and thus we have neglected the bend in the canaliculi. The presence of the bend causes additional resistance, and thus neglecting the bend is expected to contribute to a lower prediction of the equilibration time. Furthermore, the time for the pressure increase from 0 to the maximal pressure during the

blink phase (period 1) and for the pressure drop from 0 to the minimal pressure during the interblink phase (period 3) are neglected in the model as such pressure changes are assumed to be instantaneous. Period 1 and 3 last about 0.04 and 0.06 s, respectively, and thus inclusion of these periods will increase the prediction of the equilibration time by about 0.1s. Finally, we note that the presence of the tube in the canaliculus could have led to changes in the equilibration time because the tube offers extra resistance to deformation.

Comparison of the Predicted Drainage Rates with Literature Results

Rosengren[27] inserted a tube through the lower puncta into the canaliculi and obtained the flow rate through the canaliculi. This horizontal tube was connected with a vertical cylinder, the fluid level in which was at the same height as the puncta. A bubble was intentionally trapped in the horizontal tube to detect the direction and measure the magnitude of the fluid flow inside the tube during a blink and an interblink. (Figure 4 of Rosengren[27]) During a blink the fluid was expected to flow both into the tube and into the lacrimal sac. It was found that during the blink phase, the bubble moved quickly away from the punctum by about 0.5 mm, which corresponded to 0.29 mm^3 of fluid flow out of the punctum into the glass tube. Since the pressure at either side of the lower canaliculus (sac and the glass tube) is about zero for the blink phase, the total tears squeezed is about 0.58 mm^3 for the lower canaliculus. The squeezed tear volume per blink by single canaliculus predicted by our model with equation (29) can vary between 0.4001 mm^3 and 0.0100 mm^3 for bE between 0.649 Pa·m and 34.022 Pa·m. Again the model predictions for the lowest value of bE are consistent with experiments. Rosengren's experiments also showed that during the interblink phase, 0.87 mm^3 of fluid flows into the lower canaliculus, which is about three times as much as the amount of fluid squeezed out during the blink phase. However, according to the mathematical model developed in this study, the flow rates in the blink and the interblink should be equal. This difference between the model predictions and the experiments

can be resolved by noting that in Rosengren's experiments, the pressure at the entrance of the lower canaliculus is zero, i.e. atmospheric, and the pressure at the entrance of the upper canaliculus is $-\sigma/R_m$, since it is connected with the upper tear meniscus. Therefore the pressure difference between the entrances of the lower and upper canaliculus will drive flow into the lower canaliculus and out of the upper punctum. From a rough Poiseuille flow estimation, the fluid flow driven by such a pressure difference during the interblink phase may be of the order of a few microliters. Thus, this flow may be the cause of the difference between the flows in the blink and the interblink in Rosengren's experiments.

Sahlin et al. measured the tear drainage capacity with an overloaded tear film by the drop test and concluded the tear drainage could be as much as 1.11~4.03 mm^3 per blink for different voluntary blink frequencies and age groups.[103] Our model can be used to predict the tear drainage rates from an overloaded tear film by assuming that the radius of curvature of the tear menisci is close to infinity, which makes the pressure outside the puncta larger than that in normal conditions, and increases the tear drainage. Additionally, in an overloaded tear film, both the upper and the lower canaliculus are used for tear drainage. Thus, the volume squeezed per blink of an overloaded tear film is larger than that of a normal tear film. It is noted that in the experiments by Sahlin et al., the blink is voluntary and the frequency is about 30 and 60 blinks per minute, which is much higher than the normal blink frequency of 10 blinks per minute. The drainage rate is dependent on the duration of the blink cycle as suggested by equation (29) and therefore also dependent on the blink frequency. Thus, the volume drained per blink is a more appropriate choice for comparison with the model than the volume drained per minute.
The dependence of the tear drainage rate for both normal and overloaded tear films and the time scale for achieving steady states on the product bE is depicted in Figure 4-2. According to curve

1 in Figure 4-2, as bE increases from 0.649 to 34.022 Pa·m, the time to reach steady states of the blink phase and the interblink phase (τ_0) decreases from 0.0546 to 0.0010 s. According to curves 2 and 3, when bE increases from 0.649 to 34.022 Pa·m, the drainage rate decreases from 4.00 μL/min to 0.10 μL/min for the normal tear film and from 11.74 μL/min to 0.28 μL/min for the overloaded tear film. We note that for the same bE value, the drainage rate of the overloaded tear film is always larger than the drainage rate of the normal tear film. Specifically, if bE=0.649 Pa·m, the drainage rates from an overloaded tear film can be as large as 1.174 mm^3 per blink. The difference in drainage rate of a single canaliculus due to the overloaded tear film, as well as the participation of the upper canaliculus, explains the large drainage rate in the measurements by Sahlin et al.[103]

Relationship Between Tear Film Thickness and the Meniscus Radius of Curvature

In normal conditions the lower canaliculus is mainly responsible for the active tear drainage,[28] and thus the meniscus radius that is used to calculate the drainage should be that of the lower meniscus. However the meniscus radius that is used in equation (20) which relates the tear film thickness to the radius of curvature should be that of the upper meniscus because tears are deposited by the dragging action of the upper eyelid.[20] As shown by Creech et al.,[16] the radii of the upper and lower menisci may not be the same. According to their observation, for one specific subject the R_m for the upper meniscus is 60% smaller than that for the lower meniscus after instilling fluorescein dye[16]. In our model we have treated both of the menisci radii as equal and this will lead to some errors. We also note that the meniscus radius and lid velocity are not constants during the deposition of tear film,[20] and thus the deposited tear film thickness is not expected to be uniform, which is contrary to the assumptions of our model. Furthermore, the tear film thickness obtained by equation (20) is the thickness immediately after the upward

movement of the lid.[20] It has been verified that after the eyelid movement, further change of tear film thickness is possible due to the dragging of the aqueous tears by the lipid layer flow driven by the surface tension gradient,[104] which may cause the tear film thickness change that is not included in equation (20). The above assumptions may affect the quantitative model predictions. It is noted that the detailed behavior of the tear film deposition can easily be incorporated into the proposed model. However, these inclusions will make the model much more complex and thus have been avoided. Finally it is noted that King-Smith et al.[104] suggested that consideration of the extensibility of the lipid layer modifies the right-hand side of equation (20) by a constant factor of about 0.63. If this modification is applied to the current study, the predicted tear film thickness values will decrease and will also match the recent experimental measurements obtained by King-Smith et al.[105] and Wang et al.[106]

Validation of the Conjunctiva Transport Model by the Simulation of Ussing-chamber experiments

In the Ussing-chamber experiments, typically the time course of I_{SC} is measured after performing maneuvers such as changing the composition of the apical or the basolateral or both compartments, and adding compounds that preferentially block certain transport pathways. Below we first compare the magnitude of the change in I_{SC} and then the time scales for the changes in I_{SC} after such maneuvers.

The predicted value for control I_{SC} is within 10% of the experimentally measured value. Also the values of predicted I_{SC} after K channel blockade, Na-K pump blockade, and apical Na elimination are within 10% of the measured values. The predictions for other cases listed in Table 3-4 are within 30% of the measured values except the case corresponding to apical Cl elimination. In this case there are significant differences between the values reported in two different experimental studies, and one of the study reports a negligible increase in I_{SC}, which is

consistent with the prediction. The differences between the predictions and the measurements are about 40-50% for the net Na and Cl fluxes through the epithelium under both short-circuit and open circuit conditions (Table 3-6). Although there are quantitative difference between the predictions and the experimental values, such difference could partially be attributed to experimental errors, and uncertainties in the model parameters.

It can be shown by the model that the time scale for the conjunctival transport to equilibrate depends strongly on the cellular glucose consumption rate. In view of this strong dependency, it was decided to obtain r_{Glu}^0 by matching the predicted time scale for the changes in I_{SC} after blockade of Na-K-Cl cotransport with the experimentally measured value. Therefore, the good agreement shown in Table 3-5 for the Na-K-Cl inhibition case is expected. The predictions listed in Table 3-5 agree qualitatively in each case, but the quantitative agreement is poor for Cl channel blockade and K channel blockade. In all these cases, the predicted $t_{1/2}$ is smaller than the experimental $t_{1/2}$. One of the reasons for the discrepancy could be that it takes a finite period of time for the chemicals to be mixed in the compartments and then to be fully effective on the corresponding transport pathways; however, the concentrations change instantaneously in the simulations. It is also possible that when the transport pathways are modulated, the kinetics of cellular glucose consumption is changed. Since glucose consumption is essential to the prediction of time scale, such change in the consumption kinetics may cause changes in the predicted time scale. In addition, the time scale prediction may also be different if the epithelium is modeled as a multilayer of cells instead of a single layer. We note that as shown in Figure 3-7, the model predicts that maneuvers such as Cl, K channel blockade, pump inhibition and Cl free conditions lead to an instantaneous change of I_{SC} in the beginning, and a slower change after that, while in experiments the I_{SC} change has a single time scale. This could

also arise due to the instantaneous change in the kinetic parameters in the model compared to gradual changes in the experiments. For the simulation of Na-K-Cl cotransport inhibition, there is no instantaneous change of I_{SC} because Na-K-Cl cotransporter is electroneutral, and therefore its inhibition impacts I_{SC} only indirectly through the change in ion concentrations.

Application of the Tear Dynamics Model

The Effect of Surface Tension on the Tear Film Thickness

Figure 3-10 shows that lower surface tension will lead to thinner tear film, which is contradictory to the expectation that a smaller value of surface tension indicates a thicker lipid layer and is thus expected to correspond to smaller evaporative losses and thicker films. The reason for the discrepancy is that the evaporation rate is assumed constant when the surface tension is varied in Figure 3-10, and since larger surface tension values leads to smaller drainage rates, the film thickness increases. If the increase in evaporative losses due to an increase in surface tension is included in our model, a larger surface tension will presumably correspond to thinner films. Although the contradiction between Figure 3-10 and clinical observations show that the role of surface tension on tear film thickness can not be fully captured by the current model, it clarifies the role of surface tension on the drainage rate and also encourages further study on the effect of tear evaporation on the tear film thickness.

Comparison of Predicted Residence Time of Instilled Fluid and Solutes with Experiments

The experimental studies on tear and solute dynamics have focused on three classes of measurements. These studies used a variety of techniques to measure the dynamic tear volumes $V_{total}(t)$ or the solute concentration $c(t)$ or the total solute quantity in the tears, which is simply $c(t)V_{total}(t)$. Below we first describe the experiments reported in literature for each of these classes and then compare the results of our model with the experiments.

Overview of the residence time experiments

Dynamic tear volumes. Yokoi et al.[107] used a photographic system called video-meniscometer to follow the radius of curvature of tear menisci and therefore to obtain the dynamic change in tear volume. They observed the swelling of the tear meniscus after instillation and the subsequent shrinking due to drainage. They found that after instilling 15μL artificial tear consisting of 0.1%KCl and 0.4%NaCl, the radius of curvature of tear meniscus returned to the value which is not distinguishable from that before the instillation after about 5 minutes. Also with video-meniscometer, Ishibashi et al.[108] observed that after instilling 15μL of 0.5% aqueous timolol, the tear meniscus radius returned to the value which is not distinguishable from that before the instillation after about 10 minutes.

Total tracer amount. The quantity of tracer present in the tears can be measured without invasive sampling by measurement of fluorescence or radioactivity. Snibson et al.[109] divided the ocular region into five regions of interest and measured the dynamic radioactivity in each region of interest after instillation of solutions (sodium hyaluronate solutions and saline) that contained radioactive technetium-99m labeled diethylene-triamine-pentacetic acid (^{99m}Tc-DTPA). For the region of "ocular surface" (see Figure 2 of Snibson et al.[109]), after the instillation of 25μL aqueous fluid, the remaining radioactivity of labeled saline reached the steady state level within about 1000 seconds. Wilson et al.[110] studied the ocular residence time of a carbomer gel in humans using radiolabeled saline as control. The residence time of 25μL saline was about 900 seconds. Also with a similar technique, Meseguer et al[111] studied the ocular residence of pilocarpine eyedrops with and without viscosity enhancers. They found that 1 minute after the instillation of 25μL control saline without viscosity enhancers, the remaining radioactivity on the ocular surface is 23%; and 21 minutes after the instillation the remaining radioactivity is 12%. Additionally, the radioactivity is reduced to an undetectable value after about 6 minutes.

Meadows et al[112] used non-penetrating fluorescent tracers and a biomicroscope as a fluorometer to study the ocular residence time for solutions with different viscosities. In their study with the saline solution, a conservative estimate of the residence time of tracers after the instillation of 25 μL solution was reported to be about 15 minutes.

Tracer concentration in the tears. In contrast to the above non-sampling methods, the measurement of the solute concentration in the tears requires withdrawal of small tear samples at various instances in time. Scuderi et al[113] instilled one drop (~40μL) of 3mg/mL netilmicin and then withdrew 0.5μL samples at various times, which are analyzed with high performance liquid chromatography (HPLC). The netilmicin concentration returned to a value that was less than 5% of the initial concentration after about 80 minutes.

Comparison with experiments

The comparison between the model predictions and the reported experimental results is summarized in Table 4-1.[107,108,113,109,110,112] Table 4-1 shows that the predicted residence times are longer than the measured values for the cases of volume and tracer quantity measurements, and are shorter than the reported values for the concentration measurements. The overprediction for the case of volume and intensity can perhaps be attributed to the fact that in the model the rate of evaporation is assumed to be unaffected by fluid instillation. This assumption is contrary to the reports which show that weakening of the lipid layer, which may be caused by the instillation of extra fluids, could increase the evaporation rate by as much as 17 times.[110] If the amount of evaporation is increased, the model prediction for the residence times will become smaller. For example, if the rate of evaporation is 4 times the normal value at the instillation and decreases linearly with ocular fluid volume after that, the predicted time for remaining tracer

quantity to become 1% of the initial value after 25 μL instillation decreases from 1566 to 1426 seconds.

Contrary to the cases of the intensity and volume measurements, the predicted values for the concentration decay are smaller than those measured experimentally. The results in Table 4-1 show that the predicted concentration decay time is only about half of the experimental value obtained by the sampling method. A possible reason for this discrepancy could be the stimulated tearing caused by the invasive sampling of the tears, which is needed for the concentration measurement. Additionally, it was pointed out by the researchers that the drug used in their study is irritant and therefore it may cause more reflex tearing than the solutes used in the studies that measured the intensity decay. In fact it was reported that in experiments there was an 11-fold dilution after the instillation of drug,[113] while in the other studies such a dilution is not reported. The proposed model can be modified to include the effect of stimulated tearing by using larger tear secretion rate. It was verified that if the secretion rate in the model is increased by a factor of 3, the predicted concentration decay time matches that reported in the experiment.

In addition to quantitative discrepancies discussed above, there are a few other differences between the model results and the experiments based on the radioactivity measurements. The experiment by Meseguer et al. shows that after about 6 minutes following the instillation of saline, the residual activity reached a steady state of about 15% of the initial value.[111] Similar residual radioactivities are also obtained in other experiments using the same technique. In contrast, the model does not predict such residual radioactivity since no absorption of tracers is included. The residual activity may be due to permeation of the tracer into the ocular tissue. It is suggested that the cut-off molecular weight for corneal penetration is larger than 400 [114] and that for conjunctival penetration is larger than 20,000 .[115] Since the molecular weight of the

radioactive tracers is lower than these cut-off values, these tracers may penetrate the corneal and conjunctival epithelia. Another difference between the model and the experimental results is that the radioactivity studies show a bi-exponential decay with very fast decay rates within the first 1~2 minutes, which is not predicted by the model. The radioactivity experiments of Snibson et al.[109] have shown that the remaining radioactivity drops to 50% of the initial value within 1 minute, while the model prediction is about 7.0 minute. Furthermore, the time for the tracer quantity to decrease to 23% of the initial value is 1 min according to Mesegure et al.[111] while the model prediction is about 12.5 min. The fast clearance during the first 1~2 minutes can be explained by noticing the dynamic changes in different regions in the experiments of Snibson et al.[109] The decay time in the radioactivity experiments cited above is for the "ocular surface" region, which excludes the area near the medial canthus. (Figure 2 of Snibson et al.[109]) Therefore, it is possible that the initial fast decay of tracer quantity for the "ocular surface" described in the radioactivity studies is mainly caused by the movement of tracers to the medial canthus area instead of the drainage through the canaliculi. This explanation is supported by Figure 3-13a of Snibson et al.,[109] which shows that the radioactivity in the "medial canthus & lacrimal sac" area undergoes fast increase almost at the same time during which the fast clearance in "ocular surface" area occurs, suggesting the possibility of movement of tracers from the latter area to the former area.

Values of Ocular Bioavailability and the Effect of Drop Size on Ocular Bioavailability

The model predicts that for a 40 μl drop of timolol, the ocular bioavailability, which is defined as the fraction of the instilled drug that enters the cornea is 1.27%. This model prediction is in agreement with the results quoted in the literature.[80] Also, the model predicts that the ocular bioavailability decreases on reduction in the permeabilities. The model results

shown in Table 4-2 also demonstrate that the ocular bioavailability is expected to be relatively independent of the drop volume. This is in direct contrast with the experiments of Patton[116] on rabbits using pilocarpine nitrite which showed that when the instilled volume decreases from 25 μL to 5 μL, the ocular bioavailability increases by 160%. This discrepancy could be partially due to the larger spillage for larger drops. Furthermore, increase in drop size is expected to lead to an increase in the conjunctival area for absorption of drug and a larger area will lead to a larger flux into the conjunctiva and thus reduce the ocular bioavailability. In fact, if the effective surface area of the conjunctiva is decreased to a value of 1/3 of its total surface area, the predicted ocular bioavailability for a 5 μL drop of timolol solution increases from 1.3% to 3.4%. The dependence of bioavailability on other parameters will be discussed later.

The Effect of Ion Channel Modulation

A ten fold increase in Cl channel permeability leads to a large transient increase in the tear volume and the conjunctival secretion rate followed by a gradual decrease. Both tear volume and conjunctival secretion reach steady states in about 50 minutes at values that are only 2.7% and 1.8% higher, respectively than the control. The initial rapid increase in tear volume after Cl channel stimulation could be attributed to the instantaneous increase in the Cl flux that leads to an increase in the paracellular current, and which in turn causes an increased electro-osmosis driven water secretion. The increased Cl secretion reduces the cellular Cl concentration, and therefore the increased permeability is more or less balanced by the decreased Cl concentration difference. As a result, at the steady state, changes in permeability cause small differences in tear volumes and conjunctival secretion. When the K channel is stimulated in addition to the Cl channel, the channel associated K flux out of the cell increases, and this leads to an increase in the Na-K pump turnover rate. As the pump is the primary driving force for the electric current in the system, the paracellular current from the basolateral side to the apical side increases, leading

to higher elecro-osmosis driven water secretion. Thus the system settles at a higher tear volume than that in the case of only Cl channel stimulation. We note that some experimental studies show a much larger increase in water secretion than the predicted increase,[15,24] and this suggests that some of the ion and water transport mechanisms are not accurately taken into account in the current model.

The Effect of Evaporation

As shown in Figure 3-12, an increase in the evaporation rate reduces the tear volume and increases the tear osmolarity, and both of these factors could potentially lead to dry eye symptoms. Interestingly, the increase in osmolarity leads to an increased secretion from the conjunctiva, which partially cancels the effect of the increased evaporation, leading to only a weak dependence of tear volumes on evaporation rates. Specifically, if the tear evaporation rate is increased to 4 times its normal value, the model predicts that the steady state tear osmolarity increases by about 9.0 mM, which is slightly larger than the reported increase in osmolarity from 304.4 mM to 310 mM in dry eye sufferers.[83] However, some other researchers have measured a much larger difference in osmolarities between normal subjects and dry eye patients.[87] This suggests that in addition to increased evaporation due to deterioration in the lipid layer, there may be other mechanisms that increase the osmolarity in dry eye patients such as an increase in the osmolarity of the secreted tears. Our simulation shows that if the osmolarity of the lacrimal gland secretion increases, the system equilibrates at a larger tear osmolarity, a larger osmotic secretion from the conjunctiva, and consequently a larger tear volume. These results suggest that the increased osmolarity in dry eye patients results from a combination of the above mentioned factors.

The Effect of Osmolarity in Dry Eye Medications

Recently, it has been reported that there are only minor differences in effectiveness of hypoosmolar and isosmolar solutions for dry eye treatment.[87] In this study it was argued that the difference between the effects of hypoosmolar and isosmolar solutions is minor because the reduction in tear osmolarity after the application of drops lasts only briefly. Also, studies by Candia et al. show that both hyperosmolar and hypoosmolar instillation decreases the diffusional water permeability of conjunctiva epithelium,[117] and our model suggests that if these permeabilities are reduced, water secretion from conjunctiva decreases, which offsets the addition of fluid. This could further reduce the efficacy of hypoosmolar instillations.

Our simulations predict that changes in osmolarity in tear film caused by instillation of 25 μl of hyptertonic (+40 mM by adding NaCl) and hypoosmolar (-40 mM by subtracting NaCl) vanish after only about 3 minutes (Figure 3-13B). Our model also predicts that the dynamic tear volumes for the case of hyperosmolar solution are only about 10% higher than those for the hypoosmolar solutions, and these differences vanish in about 25 min (Figure 3-13A). Thus the model predictions are in agreement with the studies cited above. However as stated above, there are some other studies in the literature that claim that the hypoosmolar solutions are more effective as dry eye treatments. One possible reason could be that the transient lowering of tear osmolarity by hypoosmolar solutions aids the epithelial cells in recovering from inflammations that are common in dry eye patients. Furthermore, in most studies with hypoosmolar solutions, sodium hyaluronate solutions were used instead of aqueous solutions, and this difference could enhance the effect of the hypoosmolar solution on epithelial cell recovery because of an increase in the residence time. It is noted that the current model does not include the regulation of water transport as a function of cell volume and other parameters such as osmolarity. It is observed that

the water permeability of cell membrane is subject to volume regulation.[118] It is also reported that aquaporin-3 exists on the basolateral membrane of the conjunctival epithelium, and these may play a role in facilitating the transcellular water transport, and in regulating the paracellular water transport.[47] Therefore, the neglect of the water transport regulation may make the model less accurate for conditions involving large changes in cell volume or osmolarity.

The Effect of Punctum Occlusion and Moisture Chambers

In the case where both puncta are occluded, the model predicts that the tear volume increases monotonically (Figure 3-14), and is expected to lead to overflow. While there are some reports of tear overflow due to insertion of punctum plugs, a monotonic increase of tear volume predicted by the model is not commonly observed in clinical practice. The reason could be that the sensation of ocular surface decreases after punctum occlusion, which leads to decreased lacrimal gland secretion[88]. As shown in Figure 3-14, when the lacrimal gland secretion rate is decreased, the rate of increase of tear volume after punctum occlusion becomes slower. It is also possible that the punctum plugs do not completely block the tear flow, partly because the canaliculi deforms to a larger radius on punctum plug insertion.[119] For the fluorescence clearance after punctum occlusion, the predicted fluorophore concentrations at 15 min after instillation are 0.39% and 0.22%, for the occlusion of both puncta and normal drainage without punctum occlusion, respectively, which agree at least qualitatively with the measured mean values of 0.49% and 0.28%, respectively.[88] The measured values after punctum occlusion are larger than the prediction partly because punctum occlusion leads to reduced lacrimal secretion,[88] which slows down the decrease in fluorophore concentration, and this effect is not included in the current model. We note that in the simulation, it is assumed that the fluorophores does not penetrate into the ocular surface. If the fluorescence penetration is included, it will affect the

measurement of fluorescence clearance, but whether it will lead to overestimation or underestimation of the remaining fluorescence is not clear.

Implication on Basic Tear Physiology

In addition to predicting the effects of various physical and physiological parameters and conditions on tear dynamics, our model can also help in resolving some outstanding issues related to mechanisms of tear dynamics. Two such issues are discussed below.

Can conjunctiva secretion account for all the normal tear secretion?

Since the fluid secretion rate of the conjunctival epithelium can be 1~2 μL/min, which is about the same as the estimated tear turnover rate, it has been speculated that under normal conditions the secretion from the conjunctiva accounts for all the tear fluid production.[15] In the model, if the rate of lacrimal gland secretion is set to zero, the system reaches a steady state with essentially zero drainage through the canaliculi, which is not realistic. This implies that without the supplement of electrolytes from lacrimal glands, the electrolyte secretion by the conjunctiva is insufficient to balance the electrolyte loss through canalicular drainage. Therefore, the model suggests that under normal conditions where conjunctival secretion accounts for a large portion of tear fluid production, the secretion from the lacrimal glands are still necessary.

Water transport mechanism

There are controversies regarding the mechanism of water transport through epithelia.[25] The current model includes both electro-osmosis and osmotic flows to account for the water transport in the epithelium. The electro-osmosis mechanism was included because Ussing-chamber experiments show a net water secretion from the basolateral side to the apical side even in the absence of osmolarity gradient.[15] There is however a possibility that the transport of water occurs through other routes such as through a cotransporter or through water channels aquaporins. The electro-osmosis mechanism is shown to be valid in corneal endothelium[25] and a

model of electro-osmosis has also been developed for a general leaky epithelium.[120] However, it is not yet proven that the same assumption applies to the conjunctival water transport. To test whether a combination of osmotic flow and electro-osmosis correctly account for all transport routes for water, we simulated the Ussing-chamber experiments related to water transport with our model, and below we compare the results with experiments. Simulations show that if the apical glucose concentration is increased by 20 mM, the fluid secretion increases. This is contradictory to the experiments, which report a 77% decrease in fluid secretion.[24] In fact, it has been reported that the permeability of the paracellular Na-Glucose cotransporter increases with an increase in glucose concentration,[121] and if this fact is included in the model, the predicted secretion rate will increase further. This contradiction suggests that there may be other mechanisms responsible for the water transport in conjunctiva such as the cotransport of water by the Na-Glucose cotransporter[122] or through aquaporins. Once these mechanisms are experimentally determined, these can be included in the conjunctiva transport model developed in this study.

Effect of Viscosity on Tear Drainage and Ocular Residence Time

Drainage Rates

There are three important time scales relevant to the drainage process; blink time t_b (~0.04 s), interblink time t_{ib} (~6 s) and the time scale for the canaliculus radius to achieve steady state τ_0. Based on the relative magnitude of τ_0 with respect to t_b and t_{ib}, there are three different scenarios for the tear drainage. When the viscosity is less than 4.4 cp, $\tau_0 < t_b$ and $\tau_0 < t_{ib}$ and so the canaliculus radius can reach steady state during both the blink phase and the interblink phase. In this case, the canaliculus radius is uniform at the end of both the blink and the interblink phase, and $V_{interblink}$ and V_{blink} can be calculated from the steady state radii, and changing viscosity

within this range will not change the drainage rate $q_{drainage}$. When the viscosity is larger than 4.4 cp but smaller than 654 cp, $t_b < \tau_0 < t_{ib}$, and so the canaliculus radius cannot reach steady state during the blink phase but still can reach steady state during the interblink phase. In this case the canaliculus radius can still reach the same steady state and be uniform at the end of the interblink phase, but the canaliculus radius is not uniform at the end of the blink phase and V_{blink} need to be calculated by determining the position dependent radius at the end of the blink and then using equation (28). Increasing viscosity within this range will decrease the drainage rate, and this range is applicable to most of the high viscosity Newtonian fluids that are used for ocular instillation. When the viscosity is larger than 645 cp, $\tau_0 > t_{ib} > t_b$, and the canaliculus radius cannot reach steady state during either both the blink phase and the interblink phase. However at this high viscosity the shearing to the ocular surface is likely to be high and may cause irritation. Therefore Newtonian fluids with viscosities higher than 645 cp are not likely to be used for ocular instillation and are not considered in this study.

Since drainage rates through the canaliculi are not typically measured, it is not possible to compare the predictions with experiments. It is noted that the data shown in Figure 3-16 has three distinct regions. In the first region ($\mu < 4.4$ cp), there is no effect of viscosity on drainage rates. In the second region ($4.4 < \mu < 100$ cp), the viscosity has the maximum impact on the drainage. In the last region ($\mu > 100$ cp), the effect of viscosity on drainage rates becomes small. These trends qualitatively agree with observations noted in literature. Also, the data in Figure 3-16 suggests that it may be best to use eye drops with a viscosity of about 100 cp to increase the retention time, and yet not cause damage to ocular epithelia due to excessive shear during blinking.

The trends shown in Figure 3-17 for shear-thinning non Newtonian fluids are similar to those for Newtonian fluids. When the value of μ_0 is below 400 cp, the viscosity parameter μ_0 has a relatively large impact on the drainage, and when μ_0 is higher than 400 cp the impact on drainage becomes small. The trends for the three typical n values are similar, with larger n yielding smaller drainage rates at the same μ_0. The data in Figure 3-17 suggests that the best range of μ_0 for non-Newtonian eye drops should be below 400 cp. However, it has been reported that some polymers in such non-Newtonian eye drops have the ability to bind to the mucous ocular surface and thus increase the residence time of such eye drops. The binding effect is not included in the current study due to the insufficient information about the binding isotherms of such polymers, and for polymers with binding ability the actual drainage rate should be lower than that predicted by this model. Also from Figure 3-17 it seems that a larger n value is beneficial for lowering drainage rates. However, solutions with larger n values will likely cause excessive shear during blinking.

Comparison of Residence Time for Newtonian or Non-Newtonian Fluids

The transients of solute quantity predicted by our model can be compared with the experimental studies in which a tracer-laden fluid is instilled and the transients of the tracer amount are measured.[109, 123, 124, 125] These experimental studies measured the transients of tracer quantity in different regions on the ocular surface, and generally a fast decrease in tracer quantity was observed immediately after the instillation. In some studies the precorneal area was measured, and in some other studies the "ocular surface" was measured, which is defined as the whole ocular surface excluding the medial canthus area. As discussed earlier, the data from these studies could suggest that such fast decrease in tracer quantity may simply due to the mixing of the instilled fluids on the ocular surface, which takes only a few blinks for low viscosity fluids,

instead of the drainage through canaliculi. In the model presented above the fluids on the whole ocular surface is considered, which includes the "ocular surface" defined in the above studies and the medial canthus area. As the tracer mixing on the whole ocular surface will not affect the total tracer quantity in the same region, the transients plotted in Figure 3-18 earlier are not expected to show a immediate decrease in tracer quantity. Additionally, in the model presented above we have neglected transport of tracers through the ocular epithelia and also binding to the ocular surface. Such possibility is supported by the fact that the radioactivity measurements typically level off at finite values rather than going to zero, which would be expected in the absence of permeation and/or binding. Since these two factors may bring substantial difference in the tracer quantity prediction, the tracer quantity transients predicted by the above model are rescaled in order to compare with the experimental studies that only measured part of the whole ocular surface, such as the precorneal or the "ocular surface" area that excludes the medial canthus region. It has been shown that instilled fluids are mixed with tears within a few blinks. Therefore it is assumed that after the instillation of the fluids, they are well-mixed on the whole ocular surface immediately. If the tracer quantity I decreases from I_0 to $I_0^{'}$ immediately due to the initial mixing, and the amount of tracers absorbed or binded to the ocular surface at the end of the measurements is I_r, the predicted tracer quantity can be rescaled using the following equation.

$$I^{'} = I(I_0^{'} - I_r) + I_r \tag{52}$$

Equation (52) is applicable only when the instillation of fluids with lower viscosities so that the mixing time is negligible compared to the drainage through canaliculi. The transient profiles can also be used to determine the residence time, which is defined as the time for I to decrease to within 0.01 I_0 to the end value. In the model calculation and the experimental studies mentioned below, the volume of the instilled fluids is 25 μL.

The results for I(t) for viscosities of 5 cp and 8 cp Figure 4-4 can be compared with the experimental study by Snibson et al. using radioactive tracers ($^{99}Tc^{m}$),[123] in which the viscosities of two kinds of Newtonian fluids, 1.4% PVA and 0.3% HPMC were measured to be about 5 cp and 8 cp, respectively. The experimentally measured $I'(t)/I_0$ are also plotted in Figure 4-4 as dashed lines, with $I_0^{'}=0.6I_0$ and $I_r=0.131I_0$ according to the data by Snibson et al.. The theoretical profiles are in reasonable agreement with the experiments, with a slower decrease in the first 300 seconds. The residence times for fluids with viscosities of 5 and 8 cp are 1344 s and 1362 s, respectively, and these are in reasonable agreement with the residence time of about 1900 s for both solutions calculated from the experimental data, which is taken as the time for the solute quantity reaches within 1% of the final value. Greaves et al. measured the precorneal residence of 0.3% HPMC, which is Newtonian and has a viscosity of 6.649 cp.[124] The solute quantity transients predicted by the current study after rescaling using equation (52) is plotted in Figure 4-5 in solid line, together with the experimental data by Greaves el al. in dashed line. The residence time predicted by the model is about 1362 s, but the residence time from the experimental data is only about 550 s.

For non-Newtonian fluids, the model predictions can be compared to experiments for 0.2% NaHA, 0.3% NaHA conducted by Snibson et al.[109] The experiments showed that the clearance of NaHA was slower than that of the control saline solution, and that 0.3% NaHA was cleared more slowly than 0.2% NaHA. The predicted transient profiles for these two cases are plotted in solid lines Figure 3-19, together with the experimental data shown in dash lines. It is noted that in this case since the viscosity is much higher than that of tears, the initial mixing of tracers is not likely to be instantaneous, as supported by the lack of sudden drop of tracer quantity in the experimental data. Also from the experimental data presented for both NaHA solutions, it is

difficult to judge whether the tracer quantity transient had reached steady state at the end of the measurement. Therefore the rescaling in equation (52) is not applicable, and the predicted transients for NaHA solutions are plotted directly without rescaling. The predicted residence times for the two solutions are 4884 s and 26580 s. It is noted that in the experimental study lasted only 2000s after the instillation and it is not possible to determine the residence time from the data because the profiles had not leveled off by 2000 s. Therefore it is not possible to compare the residence time predictions with experiments.

The model predictions are in reasonable agreement with the experiments for the two Newtonian fluids 1.4% PVA and 0.3% HPMC and the non-Newtonian NaHA and CMC solutions. There are several possible causes for the discrepancies between experiments and model predictions. First, the rescaling in equation (52) assumes the tracers are well-mixed instantaneously after instillation, while it is expected that such mixing is viscosity-dependent. The rescaling can be improved if quantitative information of the dependence of mixing on viscosity is available. Also a more realistic description of tracer permeation and binding would require permeability and binding isotherm measurements for these tracers, which if available can be included in the current model. Another possible source of discrepancy between the experiments and the model is the assumption of the linear changes in viscosity of the fluid due to tear turn over. After the solutions are instilled onto the ocular surface, they are subject to dilution because of tear refreshing and such dilution is expected to decrease the viscosity of the solution, and change in viscosity is often not linear to the polymer concentration. This issue could also be more accurately in the model if the relationship between polymer concentration and solution viscosity is known for the solution of interest. It is also noted that this issue will cause only a small difference for solutions with starting viscosities of 10 cp or less. It is also

noted that the current model assumes that the surface tension of tears (~43×10^{-3}N/m) is not changed after the instillation of extra fluids, which may not be good assumption particularly if the tracers are surface active. Finally, there are several assumptions involved in developing the tear drainage model, which are discussed earlier, and these could cause additional errors in model predictions

Besides the experimental studies mentioned in the above comparison, there are also other studies on the effect of viscosity on the residence time of instilled fluids. However, they are not used to compare with the model predictions because some of them used rabbits as subjects in stead of human, and the others lack either the clear definition of the area being measured or the viscosity data of the exact solution used for instillation. It is known that rabbits have a much lower blinking rate than human. The drainage of instilled fluids through canaliculi is driven by blinking, and thus instilled fluids are expected to be cleared differently from rabbit eyes. Although the effect of viscosity on the residence time showed a similar qualitative trend to that of human, the rabbit studies were not used in the comparison because the current model is based on the tear drainage physiology of human. There can be considerable difference for the transients of tracer quantity in different regions on the ocular surface, and therefore it is inappropriate to compare the residence time without a clear definition of the area of interest.

The Effect of Viscosity on Bioavailability

It has been shown that increasing the viscosity of eye drops will increase the ocular uptake/bioavailability of the drug. Podder et al. showed that by using eye drops with viscosity-enhancing polymers the ocular absorption could be increased two-fold for rabbits.[126] Although the current model predicts that the timolol bioavailability increases for higher viscosity, the increase is much smaller. One of the reasons for the small increase is that the bioavailability depends not only on the viscosity of the eye drops but also on the permeabilities of cornea and

conjunctiva to the drugs. In an extreme case where punctal pulgs are applied and the drainage through the canaliculi is completely blocked, the bioavailability will be

$$\beta = \frac{K_{cornea} S_{cornea}}{K_{cornea} S_{cornea} + K_{conj} S_{conj}} \tag{53}$$

and according to the parameter values in Table 2-1, b would be 1.34%, which is the maximal bioavailability achievable for this drug. The time scale for drug absorption into the conjunctiva can be estimated by $\tau_{absorption}=V/(K_{conj}S_{conj})$, and for this study it is about 35 s, which is much smaller than the time scale of the drainage through canaliculi (~1000 s). This suggests that the systemic absorption predicted by the model is mainly due to the conjunctival absorption. Since in the current model any change in viscosity only affects the drainage through canaliculi, significant change in bioavailability is not expected, which agrees with the theoretical study by Keister et al.[127] It is noted that the permeability data in Table 2-1 is only for Timolol and were measured on rabbits. Based on the above estimation of $\tau_{absorption}$, viscosity is expected to have a larger impact on bioavailability if the permeability of a drug through conjunctiva is higher. Additionally, it has been suggested that some polymers that are used as viscosity enhancers can bind to the ocular surface. Increased binding will potentially increase bioavailability, but such effect was not included in the calculation of bioavailability due to the insufficient information on the binding isotherms of such polymers on the ocular surface. Furthermore, it has been suggested that at least part of the drug that is absorbed by the conjunctiva can reach the intraocular space instead of the systemic circulation. Therefore the current prediction of bioavailability may be an underestimation and it could be improved if more information about the mechanisms of conjunctiva absorption is available.

Drainage of Tears

In our previous study of the tear drainage model, tears are assumed to be Newtonian and a constant viscosity of 1.5 cp is used. However tears are in fact non-Newtonian as shown the fitting in Table 2-3, possibly due to the presence of mucin other large molecules. The current study shows that any variance of viscosity below 10 cp leads to indistinguishable changes in the drainage rate through canaliculi, as evident from Figure 3-18. Therefore the above assumption for the tear drainage model is valid, and similar assumption can be used for any fluids with viscosity varying below 10 cp.

Tear Mixing Under the Lower Eyelid

Comparison with Experiments

In the experimental study by Macdonald and Maurice,[55] the mean values of the appearance time and the time for maximal concentration of fluorescence after applying less than 0.2 μl of solution at the bottom of the lower cul-de-sac are 3.8 min and 8.0 min, respectively. In the current study, the predicted values of T_{app} and T_{max} vary significantly depending on the magnitude of lid and eyeball motion. The measured values are within the range of theoretical predictions, and the significant variations in the predictions are consistent with the large variations reported in the experiments (0.5-9 min for T_{app} and 2-17 min for T_{max}). The reasonable match between the model prediction and the observations in experiments supports the contention of Macdonald and Maurice that the mixing under the lid could be driven mainly by the combination of periodic "convective movement" and diffusion. The closer match between the T_{app} and T_{max} predicted from squeezing than those from shearing suggests that under normal conditions, the squeezing motion may play a more important role in the tear mixing in the lower fornix.

While the model predicts time scales comparable to experimental measurements, there are still several possible causes for discrepancies between the model and the experiment. Firstly, the model is based on a 2D geometry which implies that it does not explicitly include the nasal-temporal motion. The potential contribution from the nasal-temporal motion to tear mixing is discussed later. The 2D model essentially assumes that the concentration is uniform in the third (nasal-temporal) direction. This assumption is certainly inaccurate, particularly at short times after the drop instillation. It is noted that the weak dependence of the T_{app} and T_{max} on the value of η^* is encouraging because it suggest that some inaccuracies in the initial conditions do not lead to significant variations in the concentration profiles. A 2D geometry has been used successfully to model ophthalmic problems such as tear mixing behind a contact lens and ophthalmic drug delivery by contact lenses.[128, 129] Thus, while we expect the use of 2D geometry to introduce quantitative errors, it still preserves the important mechanisms and so the predictions of the model are expected to be in reasonable agreement with experiments. Secondly, in the model it is assumed that once the dye reaches the exposed tear film, it instantly mixes within the exposed tear film due to the refreshing of tears and the blinking of the upper eyelid, and thus in the model the concentration in the exposed tear film is uniform. However, after the fluorescence reaches the exposed tear film from under the lower lid, it is likely that the distribution of the dye is not uniform. Since in the experiment the fluorescence was measured in a small region on the cornea surface, the well-mixed assumption in the model may contribute to the discrepancies. To estimate whether the assumption leads to an overestimate or underestimate of T_{max}, more information is needed about the mixing in the exposed tear film, which is not within the scope of the current study. Furthermore, the current study only includes the shearing and squeezing motion of the lower eyelid and the globe, and there might be other modes of motion also

contributing to the tear mixing in this region, such as horizontal shearing, which will be discussed later, and the torsional eye movements.[52] Additionally, in the current study the tears are assumed to be Newtonian fluid, while in fact tears are shown to be shear-thinning fluid. The effect of the non-Newtonian property of the fluid on mixing requires a more complex model. It is also noted that there are discrepancies in the literature regarding the values of $T_{shearing}$,[130] and different values of $T_{shearing}$ will lead to different predicted values of T_{app} and T_{max}. Finally, in the case of forceful, voluntary blinking, which often happens in experimental settings, the time periods for lid/globe movements and the blinking will be different,[131] and this case is not included in the current study.

Horizontal Shearing

In addition to the shearing and squeezing motion described by the model, it is reported that during blinking the globe moves in the nasal direction for about 1˚ and then moves back in the temporal direction. It is also observed that the lower eyelid moves in the horizontal direction during blinking.[59] This horizontal motion of both the globe and the lid may also contribute to the tear mixing in this region. This horizontal shearing could lead to a rapid spreading of the solute towards the canthus, and when the dye reaches the medial canthus region in the conjunctiva sac, the geometrical constraint could force the dye to be transported upward and reach the exposed tear film. If the amplitude of the horizontal shearing is 3 μm, as suggested by Macdonald and Maurice, it can be estimated that the dispersion coefficient D^* is 3.56×10^{-7} m^2/s, which corresponds to a time scale of about 17 min for the horizontal dispersion of the fluorescent dye. Since such time scale is comparable to the experimental values and those predicted in the previous sections for shearing and squeezing, the horizontal shearing may also play a considerable role in the tear mixing in this region. Such mechanism is supported by the tendency

of the dye appearance near the inner canthus region observed by Macdonald and Maurice.[55] However, the mechanism of the dye appearance due to horizontal shearing is more complex, and the kinematics of the torsional eye movements is not clear. Therefore more information is needed before these motions can be included in the model.

Implications on the Mathematical Model of Tear Dynamics

In the mathematical modeling of tear dynamics, an important assumption is that the solutes in tears are well-mixed, i.e. the concentration of a solute is uniform in the tear film. The current study and the observations by Macdonald and Maurice[55] suggest that the tears under the lower eyelids are not well-mixed, and the typical mixing time is several minutes. However, it is noted that the current study only includes the cyclic motions of the eyelid and the globe when the gaze position of the subjects is fixed at some certain angles, which corresponds to the conditions in the experiments. However, under normal conditions the gaze position is not fixed but is likely to vary from time to time, and the shearing motion might be larger than that in the experimental condition and in the model. Additionally, under normal conditions there will also be more irregular, saccadic movements of the globe and the lids[130] in addition to the periodic shearing and squeezing motion modeled in this study. The amplitude of such movement could be well above 1~5˚ and the frequency of such movement can also be higher than the normal blink frequency. It has been shown that with increased amplitude and frequency, the mixing time for instilled solutes can be reduced to below 1 minute. Because in the previous tear dynamics studies, the time scale of interest is a few minutes, the assumption of well-mixed tears is perhaps valid.

Implication of Tear Mixing for Drug Application

As tear mixing under the lower lids is slower than that in other regions of the eyes, it has been suggested that the residence time of ophthalmic drugs can be increased by instillation in the lower fornix.[132] However this proposal is invalidated by some experimental observations.[55] As

discussed above, in normal conditions the mixing time of tears under the lower lids could be below 1 min due to the changes in gaze positions and saccadic lid/globe movements. Therefore, the current study resolves the apparent contradiction between the studies that show a limited mixing beneath the lower lid and those which show no appreciable increase in residence time/bioavailability of drugs delivered in the lower fornix. However, if drugs are delivered using methods other than drops, such as ocular inserts into the lower fornix, the dispersion of drugs in the lower fornix could be important. If the dispersion is the rate-limiting step for drug transport, the model can be incorporated into a pharmacokinetic model for systems such as ocular inserts.

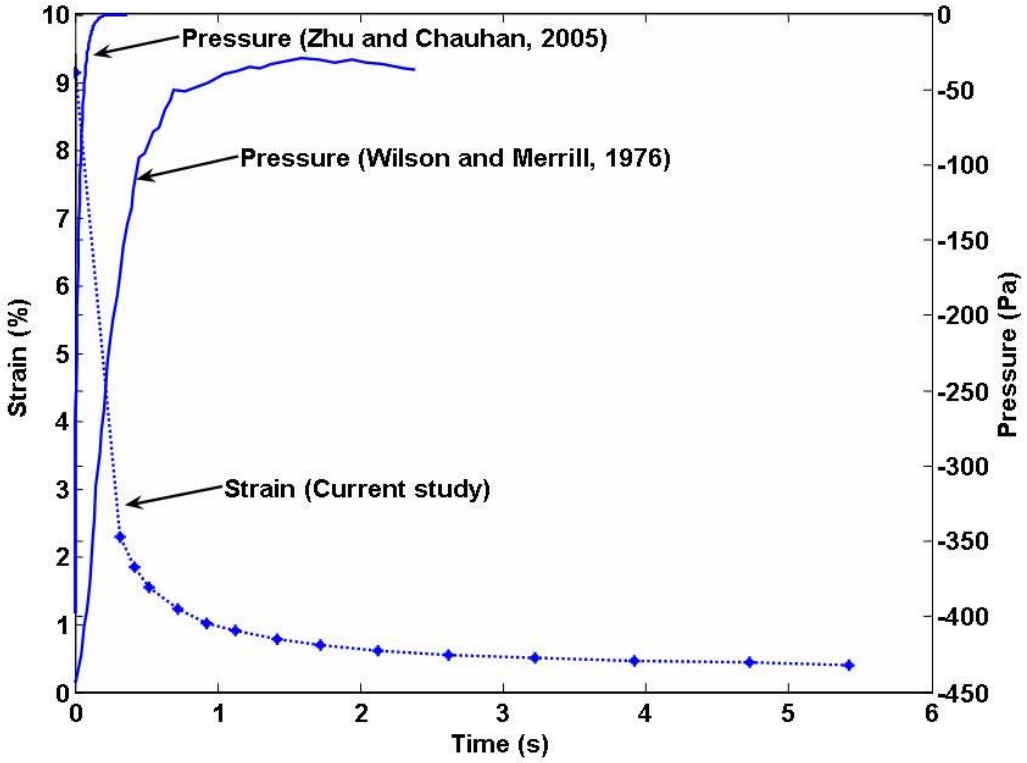

Figure 4-1 Pressure and strain transients obtained by previous experiment and model, and the current study

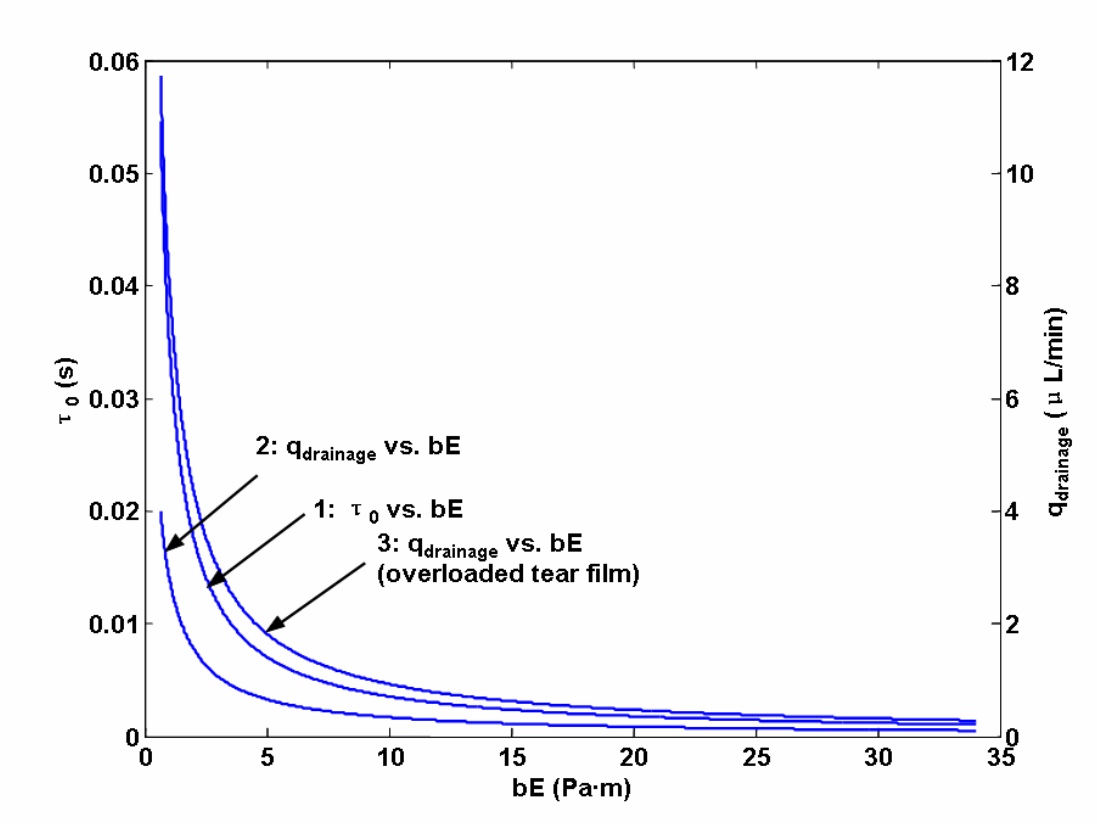

Figure 4-2 Dependence of time scale and tear drainage rate on bE

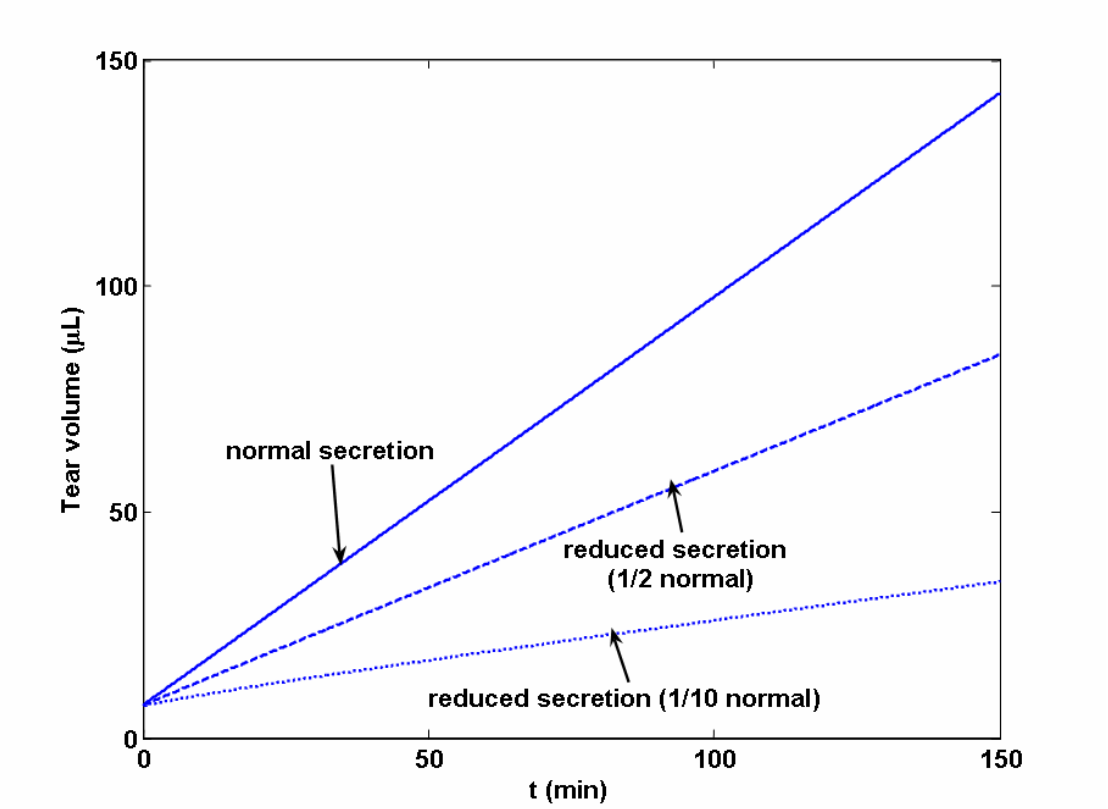

Figure 4-3 Effect of punctum occlusion on tear volume

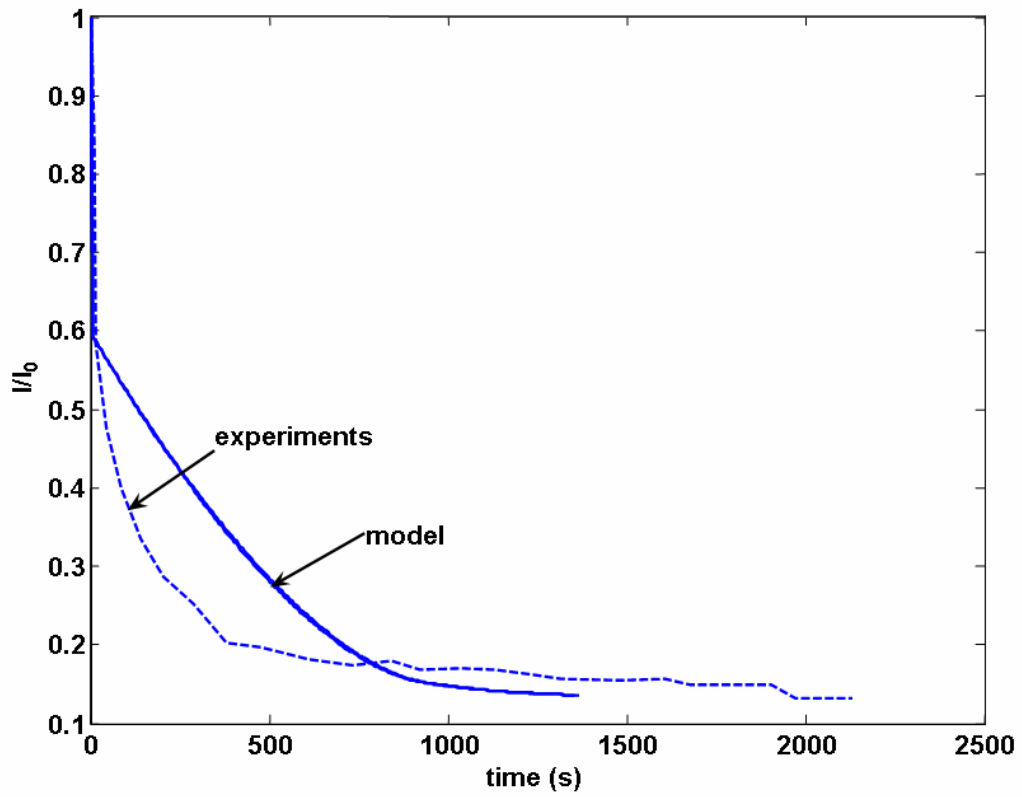

Figure 4-4 Comparison of the predicted and experimental transients of ocular surface solute quantity for 0.3% HPMC and 1.4% PVA

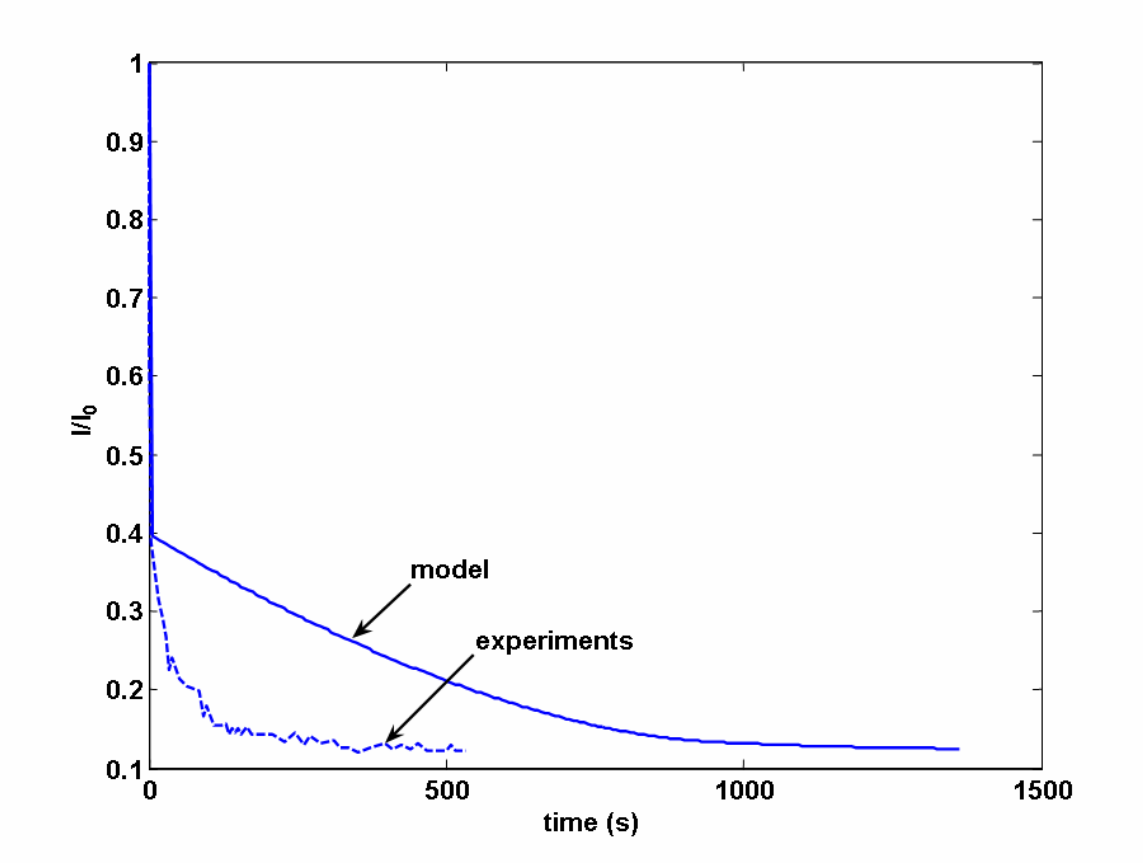

Figure 4-5 Comparison of the predicted and experimental transients of precorneal solute quantity for 0.3% HPMC

Table 4-1 Decays of tear volume, concentration and solute quantity after instillation.

	Experiment	Model
Volume decay (15μL instillation)	300 s [107] >600 s [108]	1115 s
Concentration decay (~40μL instillation)	4800 s [113]	2401 s
Quantity decay (25μL instillation)	~1000 s [109] >900 s [110] ~900 s [112]	1454 s

Table 4-2 Predicted ocular bioavailability for different drop volumes

	β (timolol)	β (small K)
5 μL	1.28%	0.92%
15 μL	1.28%	0.89%
25 μL	1.27%	0.88%
40 μL	1.27%	0.86%

CHAPTER 5
CONCLUSIONS

A better understanding of tear dynamics could be useful in a wide variety of areas related to ocular drug kinetics, contact lens fitting, and treatment of diseases such as dry eyes. This study combines models for individual contributors to the tear flows in the eyes into a comprehensive tear dynamics model. In addition a mathematical model also developed for the tear mixing under lower eyelids. The tear dynamics model can compute both the steady and the transient compositions, volume, and potential of tears and the conjunctival cells and also the canalicular drainage rate, and fluxes of water and ions and solutes across the conjunctiva. A majority of the model predictions are shown to be at least in qualitative agreement with experiments, and for predictions that do not agree with experiments, possible sources of discrepancies have been discussed. The model can be further improved by including more accurate values of parameters and by including other transport pathways. Additionally, the mechanical properties of the lacrimal canlaliculi, which are responsible for tear drainage, have not been reported in the literatures. Therefore in this study we also report the mechanical properties of porcine canaliculus that were measured in compression mode while submerged in fluid by using a dynamic mechanical analyzer (DMA).

The model presented in this study can help develop a better understanding of the effect of various physiological parameters on issues related to tear dynamics. Additionally, this model can be useful in understanding the causes of reduced tear volumes or increased osmolarity in dry eye patients, and furthermore, the model can help in preliminary evaluation of the effectiveness of various dry eye treatments. The tear dynamics model can also help relate different experiments that focus on the same issue such as the experiments that measure either the volume decay or the tracer concentration decay or fluorescence/radioactivity decay after instillation of

fluid in the eyes. Finally this model can help the experimentalists in identifying the critical parameters and assumptions, and designing the most useful experiments.

It is noted that this model presents a basic framework for tear dynamics, and it could be further improved by including several issues that may be important to tear dynamics such as corneal transport, effect of proteins, neural regulation and other feedback mechanisms, permeability regulation, lipid dynamics, tear film deposition and breakup, mixing in the eye, etc. This model could also easily be adapted to include presence of a contact lens or a drug eluding device or nanoparticles in the tear film. While this model is expected to be useful, it is not intended to serve as a replacement for experiments. It is expected to serve as a tool to enhance the mechanistic understanding of tear dynamics, to design and understand experiments in a quantitative manner, and serve as a guide in design of various protocols for the treatment of dry eyes and the delivery of ophthalmic drugs.

APPENDIX A
DERIVATION OF EQUATIONS FOR TEAR DRAINAGE

Pressure-Radius Relationship

The radius of the canaliculus R is less than the undeformed radius R_0. The deformation of the canaliculus leads to a hoop strain of $\frac{\Delta R}{R_0}$ ($\Delta R \equiv R - R_0$) and a concomitant hoop stress, which equals $E\frac{\Delta R}{R_0}$. Neglecting the axial variations, the radial force balance on the canaliculi gives.[133]

$$-2RL(p_o - p) = 2bL\left(E\frac{R - R_0}{R_0}\right) \qquad \text{(A1)}$$

Determination of R_b and R_{ib}

If the time scale to attain steady state is shorter than the duration of the interblink and the blink, canalicular radius will reach the steady state values in each cycle. If the steady state pressure is known, the steady state radius can be calculated from equation (A1). At the steady state of the blink phase, the pressure outside the canaliculus wall is p_0 and the pressure inside is the pressure at the sac end of the canaliculus (p_{sac}). By equation (A1), the radius at the steady state of a blink (R_b) can be expressed with equation (4) in the main text.

At the steady state of an interblink phase, the pressure outside the canaliculus wall is zero as the canaliculus is not squeezed, and the pressure inside is equal to the pressure in the meniscus outside the puncta, which is given by $-\sigma/R_m$. By equation (A1), the radius at the steady state of an interblink (R_{ib}) can be expressed with equation (5) in the main text.

Derivation of the Equation for the Drainage of Newtonian Fluids

The mass balance of fluid in a differential section of the canaliculus lying between axial locations x and x + dx is[133]

$$\frac{\partial(\pi R^2)}{\partial t} = -\frac{\partial q}{\partial x} \tag{A2}$$

The Reynolds number (Re), which is the ratio between inertial terms and viscous terms in the fluid mechanics equation, determines whether the flow is inertia dominated or viscosity dominated. According to the above definition, $\mathrm{Re} = \frac{\rho u R|\Delta R|}{\mu L} \sim \frac{\rho R|\Delta R|}{\mu t}$, where $|\Delta R|$ is the magnitude of change in radius during the blink or the interblink phase. In normal conditions, the time scale for blinking is about 10^{-1}s.[70] During the blink cycle the radius changes between R_b and R_{ib}; $|\Delta R|$ is thus taken to be R_{ib}-R_b and with the value of parameters given in the main text, $|\Delta R|$ is at most $0.1R_0$. According to the above estimation, Re is about 10^{-2}, which means the viscous term is much larger than the inertial term in normal conditions. Thus the inertial terms in the fluid flow equation can be neglected and the flow is locally like a Poiseuille flow. The flow rate for Poiseuille flow in a cylindrical pipe is[133]

$$q_p = -\frac{\partial p}{\partial x}\frac{\pi R^4}{8\mu} \tag{A3}$$

where q_p is the Poiseuille flow rate, R is the pipe radius, μ is the fluid viscosity and $\frac{\partial p}{\partial x}$ is the pressure gradient driving the flow. Also, the Re stays small for the entire range of bE used in this study. By substituting q in equation (A2) with q_p given by equation (A3) and substituting p with the pressure given by equation (A1), the following equation of R as a function of x and t is obtained:

$$\frac{\partial}{\partial x}\left(\frac{\partial\left(p_0+\frac{bE}{R_0}\frac{R-R_0}{R}\right)}{\partial x}\frac{\pi R^4}{8\mu}\right)=\frac{\partial\left(\pi R^2\right)}{\partial t} \tag{A4}$$

As stated above $|\Delta R|$ is small in comparison to R_0, and thus equation (A4) can be linearized as equation (1) in the main text.

Derivation of the Equation for the Drainage of Non-Newtonian Fluids

The flow rate q through a cylindrical pipe of power-law fluids that obeys Equation (34) can be written as

$$q=\pi R^2\left(-\frac{1}{2\mu_0}\frac{\partial p}{\partial x}\right)^{\frac{1}{n}}\left(\frac{n}{3n+1}\right)R^{\frac{n+1}{n}} \tag{A5}$$

Equation (35) can be obtained by combing equations (A5) and (A2) and some algebraic manipulation.

APPENDIX B
RELATIONSHIP BETWEEN THE MENISCUS CURVATURE AND TOTAL OCULAR FLUID VOLUME

The thickness of the exposed tear film is determined by the balance between the viscous drag force and the capillary suction force on the tear film, and the tear film thickness can be expressed by equation (20). Therefore, the volume of the exposed precorneal tear film can be expressed as

$$V_{exposed} = 2.12R_m\left(\frac{\mu U}{\sigma}\right)^{\frac{2}{3}} A_{exposed} \quad \text{(A6)}$$

where $A_{exposed}$ is the palpebral aperture area. The tear volume in the menisci can be calculated after assuming that the radii of curvature of the upper and the lower menisci are the same and uniform along the eyelids. Because the height and radius of curvature values of tear meniscus are comparable,[134] we approximate the geometry of the tear meniscus cross-sectional area to be the geometry shown in Figure A1 Therefore the cross section area of tear meniscus is (R_m^2-$\pi R_m^2/4$), and the tear volume in the meniscus ($V_{meniscus}$) is approximated by

$$V_{meniscus} = (R_m^2 - \frac{1}{4}\pi R_m^2)L_{lid} \quad \text{(A7)}$$

where $V_{meniscus}$ is the tear volume in the lacrimal menisci, and L_{lid} is the perimeter of the lid margin. Finally, the tear volume in the conjunctival sac can be estimated by assuming the thickness of the unexposed tear film that fills the conjunctival sac to be the same as the exposed tear film thickness.[2] As the total area of the unexposed and exposed tear film is estimated to be about half of the surface area of the globe,[2] the sum of V_{sac} and $V_{exposed}$ can be expressed as

$$V_{exposed} + V_{sac} = 2.12R_m\left(\frac{\mu U}{\sigma}\right)^{\frac{2}{3}}\left(\frac{1}{2}\times 4\pi R^2_{globe}\right) \quad \text{(A8)}$$

where R_{globe} is the globe radius, after approximating the geometry of the globe to be a perfect

sphere. From equations (A6) and (A7), the total tear volume can be estimated as a function of the radius of curvature of tear meniscus, equation (21) in the main text.

It should be noted that in the derivation of the above equation, the shape of the assumed cross-sectional of the tear menisci (Figure A1) is not completely accurate because the meniscus is assumed to be tangential to the lid. In fact it has been observed that near the lid surface, the meniscus shape could be convex. This discrepancy may affect the estimation of the meniscus cross-sectional area and in turn the total tear volume. The calculated area of the tear menisci based on the geometry shown in Figure A1 and for the normal value for R_m listed in Table 2-1, is about 0.03 mm^2 which is smaller than the value of 0.05 mm^2 obtained by Mishita et al.[2] However it is noted that Mishita et al[2] instilled 1 μL of fluorescein solution prior to the observation, and based on the eyelid perimeter listed in Table 2-1, this volume corresponds to an increase in cross section of about 0.02 mm^2, which is very close to the difference between the computer area based on Figure A1 and the measured value. Therefore, we conclude that even though the geometry shown in Figure A1 is not precise, it serves as a reasonable approximation to predict the menisci area and the tear volume.

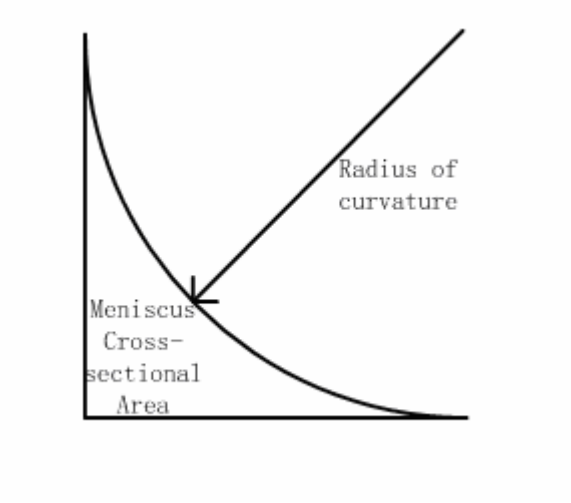

Figure A-1 Simplified meniscus cross-sectional area geometry

APPENDIX C
DERIVATIONS IN THE CONJUNCTIVA TRANSPORT MODEL

Flux Equations

The flow of ions through the ion channels and the paracellular pathway driven by both the concentration gradients and the electric potential difference is modeled by the constant field equation.[135]

$$J_{ion,12} = \frac{P_{ion} z F V_{12}}{RT} \left[\frac{C_{ion,1} - C_{ion,2} \exp\left(\frac{-zV_{12}F}{RT} \right)}{1 - \exp\left(\frac{-zV_{12}F}{RT} \right)} \right] \tag{A9}$$

where $J_{ion,12}$ is the flow rate of ions from compartment 1 to compartment 2, P_{ion} is the permeability of the ions through the channel or the paracellular pathway, z and F are the ion valence and the Faraday's constant, R is the universal gas constant, T is temperature, V_{12} is the potential difference between compartment 1 and compartment 2, and $C_{ion,1}$, $C_{ion,2}$ are the concentrations of the ion in compartment 1 and 2, respectively. This equation is used for the apical Cl channel, basolateral K channel and the paracellular pathway of Na, K and Cl. The temperature is set to be 310 K and the ion permeabilities are either calculated from experimental data (see below), as in the case of Cl channel and K channel, or adopted from literature, as in the case of paracellular ion transport.

Alternatively, when the solute is passively driven by only concentration gradient, the following equation is used:

$$J_{solute,12} = P_{solute} \left(C_{solute,1} - C_{solute,2} \right) \tag{A10}$$

where $J_{solute,12}$ is the flow rate of the solute from compartment 1 to 2, P_{solute} is the permeability of the solute, and $C_{solute,1}$, $C_{solute,2}$ are the solute concentrations in compartment 1 and 2, respectively. Equation (A10) is applicable for the paracellular glucose transport, and the

paracellular ion transport in the short-circuit case, where there are no potential difference between compartment 1 and 2 as a driving-force for ion flow. It is noted that for the case of short-circuit experiments, i.e., $V_{12}= 0$, Equation (A9) reduces correctly to equation (A10). The permeabilities for these cases are adopted from literature.

The kinetics of Na-K pump and the Na-K-Cl cotransporter are described using Michaelis-Menten model.

$$J_{pump} = J_{pump,\max}\left(\frac{C_{Na,c}}{C_{Na,c}+K_{pump,Na}}\right)^3\left(\frac{C_{K,b}}{C_{K,b}+K_{pump,K}}\right)^2\left(-5\times10^{-3}V_{cb}+1.25\right)$$

(A11)

$$J_{Na-K-Cl} = J_{Na-K-Cl,\max}\left(\frac{C_{Na,b}}{C_{Na,b}+K_{Na,Na-K-Cl}}\frac{C_{K,b}}{C_{K,b}+K_{K,Na-K-Cl}}\frac{C_{Cl,b}}{C_{Cl,b}+K_{Cl,1,Na-K-Cl}}\frac{C_{Cl,b}}{C_{Cl,b}+K_{Cl,2,Na-K-Cl}}\right.$$
$$\left.-\frac{C_{Na,c}}{C_{Na,c}+K_{Na,Na-K-Cl}}\frac{C_{K,c}}{C_{K,c}+K_{K,Na-K-Cl}}\frac{C_{Cl,c}}{C_{Cl,c}+K_{Cl,1,Na-K-Cl}}\frac{C_{Cl,c}}{C_{Cl,c}+K_{Cl,2,Na-K-Cl}}\right)$$

(A12) In equation (A11), J_{pump} and $J_{pump,max}$ are the turnover rate and the maximal turnover rate of the pump. Since this transport is not electroneutral, the above equation includes a potential dependent term[68]. In equation (A12), $J_{Na\text{-}K\text{-}Cl}$ and $J_{Na\text{-}K\text{-}Cl,max}$ are the turnover rate and the maximal turnover rate of the cotransporter. The K's are the Michaelis constants. The values of the maximal turnover rate and the Michaelis constants are adopted form the literature.

The kinetic equation of Na-Glucose cotransporter is based on the study by Eskandari et al. on the rabbit intestinal Na-Glucose cotransporter that was cloned in *Xenopus laevis* oocytes.[136] From a six-state transport model which assumes an ordered binding of Na and glucose and a stoichiometry ratio of 2:1 between Na and glucose, the turnover rate of the cotransporter can be expressed as a function of the concentrations of sodium and glucose in the apical and cellular compartments and the potential difference between the two compartments.

$$J_{Na-Glu} = C_T \left(\frac{\varepsilon C_{Na,a}^2 C_{Glu,a} + \phi C_{Na,a}^2 + \gamma}{\alpha + \beta C_{Glu,a} + \chi C_{Na,a}^2 + C_{Na,a}^2 C_{Glu,a}} \right) \quad \text{(A13)}$$

where C_T is a constant representing the density of the cotransporter and can be obtained from the experimental data of $J_{Na\text{-}Glu}$, and ε, ϕ, γ, α, β and χ are functions of $C_{Na,c}$, $C_{Glu,c}$ and the potential difference, and contain kinetic constants directly adopted from the literatures.[136] The same equation as (A13) was earlier developed by Parent et al.[137], but Eskandari et al.[136] used additional data from experiments done in the reverse mode, i.e. the turnover of the cotransporters from inside to outside the cells. Both of these studies obtained kinetic parameters for equation (A13) by fitting the experimental data to the equation. To confirm which parameters are more accurate, we simulated the Na-K pump inhibition in Ussing-chamber experiments by using kinetic parameters from both of these studies. Of these two sets of parameters only the ones obtained by Eskandari et al.[136] correctly predict the decrease in turnover rate of Na-Glucose contransporters after pump inhibition.[35,36] The reason for such decrease is that the inhibition of the pump leads to decreased Na gradient across the apical membrane. The dependence of the cotransporter turnover rate on intracellular Na concentration is weak for the parameters obtained by Parent et al.,[137] and therefore the change in cellular Na concentration due to Na-K pump inhibition cannot lead to detectable difference in Na-Glucose cotransport turnover rate. The above comparison shows that the conjunctiva transport model can be also used to compare and evaluate different kinetic models for a specific transport pathway.

The flux of water is assumed to be the sum of two parts: one part driven by electro-osmosis through the paracellular pathway, and the other part, osmotic flow, driven passively by osmosis difference through both the transcellular and paracellular pathways. The first part can be described as: [25]

$$J_w = v_w r_{eo} F \sum z_{ion} J_{ion,paracellular} \quad \text{(A14)}$$

where v_w is the partial molar volume of water, $J_{ion,paracellular}$ is the paracellular ion flux, z_{ion} is the valance of the ions and F is the Faraday's constant, and r_{eo} is a constant denoting the coupling ratio between the water flow driven by electro-osmosis and the paracellular current. This coupling ratio is estimated to be 0.0073 C^{-1}mol. from the experimental data for water transport in the absence of transepithelial osmosis difference.[15] The paracellular current is first calculated using the model under open-circuit condition with the apical and basolateral concentrations used in the experiment and cellular composition given in Table 2-1, and then the coupling ratio is calculated so that the resulting paracellular water transport rate is the same as the fluid secretion rate measured in the experiment. The water transport driven by osmosis difference is described by:

$$J_{w,1-2} = P_{w,1-2} v_w \left(Osm_2 - Osm_1 \right) \quad \text{(A15)}$$

where $J_{w,1-2}$ is the water flux from compartment 1 to compartment 2, $P_{w,1-2}$ is the water permeability of the barrier between compartments 1 and 2, v_w is the partial molar volume of water, and Osm_1, Osm_2 are the osmolarities in compartments 1 and 2, respectively. It is assumed that the osmotic flow exists for both the transcellular and the paracellular pathways. The water permeabilities are adopted from measurements on rat reported in literature.[47] It is noted that the value used as the paracellular water permeability is actually that of the whole tissue, which may be an overestimation. But it can be shown by simulation that such an overestimation is not likely to introduce significant error in this study.

Kinetic Parameters

Of the required parameters in the above kinetic equations for transport pathways, some are available in literature, as listed in Table 2-1 in the main text. On the other hand, the parameters

listed in Table 2-2 need to be obtained by fitting experimental data. Briefly, according to the Ussing-chamber experiments,[36,37] apical Cl channel accounts for 60% of the total short-circuit current (I_{SC}) of 14.4 $\mu A/cm^2$ at the steady state. Therefore the flux of Cl through the apical Cl channel must be $0.6I_{SC}/F$, where F is the Faraday's constant. Using this flux and the apical and the basolateral compositions used in Shi and Candia's experimental study[37] and the cellular concentrations in Table 2-1 (measured values) in equation (A9), we compute the permeability of the Cl channel ($P_{Cl,channel}$), which is listed in Table 2-2. Based on the mechanisms shown in Figure 2-2, if Cl channel accounts for 60% of the I_{SC}, the Na-Glucose cotransporter should account for remaining 40%. Therefore, the flux of Na through the Na-Glucose cotransporter can be obtained as $0.4I_{SC}/F$, and the parameter C_T can be calculated from equation (A13) by using the same apical, basolateral and cellular compositions as used above to determine $P_{Cl,channel}$. Using stoichiometrical relations that can be obtained from Figure 2-2, the steady state fluxes through the basolateral K channel, the Na-K pump and the Na-K-Cl cotransporters can be calculated. Using a similar approach as described above for the Cl channel and Na-Glucose cotransporters, the K channel permeability ($P_{K,channel}$), the maximal turnover rate of Na-K pump ($J_{pump,max}$) and the maximal turnover rate of the Na-K-Cl cotransporters ($J_{Na\text{-}K\text{-}Cl,max}$) can be obtained from their respective kinetic equations, which are (A9), (A12) and (A13), respectively. When using Equation (A12) to calculate $J_{pump,max}$, the transcellular potential difference is assumed to be -50 mV, with the extracellular compartment as reference, which is based on a typical value for cornea cells.[25] The same apical, basolateral and cellular compositions are used in these calculations as used above in the estimation of $P_{Cl,channel}$.

APPENDIX D
DERIVATION OF THE TAYLOR DISPERSION COEFFICIENT D^*

Below we derive D* for the shearing motion as an example. The 2D mass balance of the instilled solutes can be described by equation (42) Three time scales are involved in this problem, the time scale of blinking ($1/\omega$), the time scale of diffusion in x direction (L^2/D) and the time scale of diffusion in y direction (h_0^2/D), where ω is the angular velocity of blinking, L is the characteristic length in x direction and h is the characteristic length in y direction. For the current problem, the period of the blink cycles is assumed to be 6 s and therefore ω is about 1.05 rad/s, h is about several microns and L is about several millimeters. It can be shown that the first two time scales are comparable for this problem ($\omega h^2/D \sim 1$), and they are both much shorter than the time scale for diffusion in x direction. By using a multiple time scale analysis, the solute concentration can be treated as a function of positions ($\eta \equiv \frac{x}{L}$ and $\xi \equiv \frac{y}{h_0}$), a short time scale (τ_{short}) represented by ωt, and a long time scale (τ_{long}) represented by Dt/L^2, i.e.

$$c = c\left(\eta, \xi, \omega t, \frac{Dt}{L^2}\right).$$

As described in equation (38), the velocity of the tears in the lower fornix for the shearing scenario should be

$$u(t,\xi) = \Delta_0 \omega f'(\omega t)\xi \tag{A16}$$

in which $\xi = y/h_0$ and h_0 is the normal thickness of the tear film.

This periodic function can be written in Fourier series form

$$u(t,\xi) = \Delta_0 \omega \xi \sum_{\substack{n=-\infty \\ n\neq 0}}^{n=+\infty} d_n e^{i\omega\omega n} \tag{A17}$$

where i is the imaginary unit, d_n is the Fourier series coefficients and can be obtained by

$$d_n = \frac{1}{T}\int_t^{t+T} u(t,\xi)e^{-i\omega\omega n}dt \tag{A18}$$

Equation (A17) can be substituted into Equation (A15) and in this case the velocity in y direction is zero. The dimensionless form of the resulting equation is

$$\Omega\frac{\partial c}{\partial \tau_s} + \varepsilon^2\frac{\partial c}{\partial \tau_1} + \varepsilon\frac{d_0\omega h}{D}\xi\sum_{\substack{n=-\infty \\ n\neq 0}}^{n=+\infty} d_n e^{i\omega\omega n}\frac{\partial c}{\partial \eta} = \varepsilon^2\frac{\partial^2 c}{\partial \eta^2} + \frac{\partial^2 c}{\partial \xi^2} \tag{A19}$$

where $\Omega=\omega h^2_0/D$ is the ration between the time scale of blinking and the time scale of the diffusion in y direction, and it can be shown that these two time scales are comparable. It can also be shown that $d_0\omega h/D\sim 1$. Because $\varepsilon\equiv h_0/L<<1$, the concentration can be expanded in ε as the following

$$c = c_0 + c_1\varepsilon + c_2\varepsilon^2 + \ldots \tag{A20}$$

After substituting Equation (A20) into (A19), the resulting equation can be analyzed at different order of ε.

ε^0

$$\Omega\frac{\partial c_0}{\partial \tau_s} = \frac{\partial^2 c_0}{\partial \xi^2} \tag{A21}$$

with $\frac{\partial c_0}{\partial \xi} = 0$ at ξ=0,1

This suggests that c_0 does not depend on either τ_{short} or ξ.

ε^1

$$\Omega\frac{\partial c_1}{\partial \tau_s} + \frac{d_0\omega h}{D}\sum_{\substack{n=-\infty \\ n\neq 0}}^{n=+\infty} d_n e^{i\omega\omega n}\xi\frac{\partial c_0}{\partial \eta} = \frac{\partial^2 c_1}{\partial \xi^2} \tag{A22}$$

with $\frac{\partial c_1}{\partial \xi} = 0$ at ξ=0,1

Assuming $c_1 = \frac{d_0 \omega h}{D} \sum_{\substack{m=-\infty \\ m\neq 0}}^{m=+\infty} c_{1,m}(\xi) e^{i\omega\omega m} \frac{\partial c_0}{\partial \eta}$, Equation (A22) becomes

$$\Omega \sum_{\substack{m=-\infty \\ m\neq 0}}^{m=+\infty} c_{1,m}(\xi) \frac{\partial e^{im\tau_s}}{\partial \tau_s} + \sum_{\substack{n=-\infty \\ n\neq 0}}^{n=+\infty} d_n e^{i\omega\omega n\xi} = \sum_{\substack{n=-\infty \\ n\neq 0}}^{n=+\infty} \frac{\partial^2 c_{1,m}}{\partial \xi^2} e^{i\omega\omega m} \tag{A23}$$

with $\frac{\partial c_{1,m}}{\partial \xi} = 0$ at ξ=0,1

ε^2

$$\Omega \frac{\partial c_2}{\partial \tau_s} + \frac{\partial c_0}{\partial \tau_1} + \frac{d_0 \omega h}{D} \xi \sum_{\substack{n=-\infty \\ n\neq 0}}^{n=+\infty} d_n e^{i\omega\omega n} \frac{\partial c_1}{\partial \eta} = \frac{\partial^2 c_0}{\partial \eta^2} + \frac{\partial^2 c_2}{\partial \xi} \tag{A24}$$

After integration from 0~2π with respect to τs and from 0~1 with respect to ξ and some algebra, Equation (A24) becomes Equation (43), with c_{sac} approximated by the leading order concentration c_0 and with D^* defined as

$$\frac{D^*}{D} = 1 - \frac{\left(\frac{d_0 \omega h}{D}\right)^2}{2\pi} \int_0^1 \int_0^{2\pi} \sum_{n=1}^{n=+\infty} \xi d_n c_{1,-n}(\xi) d\tau_s d\xi \tag{A25}$$

After solving for $c_{1,-n}(\xi)$ from Equation (A23) and the corresponding boundary conditions and substituting the result into Equation (A25), the expression for D^* for the shearing scenario can be obtained.

$$\frac{D^*}{D} = 1 + \sum_{n=1}^{\infty} \frac{4 d_n d_{-n}}{n^2} \frac{\Delta_0^2 N^2}{2h^2} \left[1 - \frac{(\sinh\kappa_n + \sin\kappa_n)}{\kappa_n (\cosh\kappa_n + \cos\kappa_n)} \right] \tag{A26}$$

which is Equation (44). Using a similar approach, the dispersion coefficient for the squeezing case in Equation (46) can also be obtained.

LIST OF REFERENCES

1 Johnson ME, Murphy PJ, Changes in the tear film and ocular surface from dry eye syndrome. *Prog Retin Eye Res.* 2004 Jul;23(4):449-74.

2 Mishima S, Gasset A, Klyce SD Jr, Baum JL, Determination of tear volume and tear flow. *Invest Ophthalmol.* 1966 Jun;5(3):264-76.

3 Holly FJ, Tear film physiology. *Am J Optom Physiol Opt.* 1980 Apr;57(4):252-7.

4 Holly, F. J., and Lemp, M. A., Tear Physiology and Dry Eyes, *Survey of Opthalmology*. 1977 Sep-Oct;22(2):69-87.

5 Lemp, M. A., Dohlman, C. H., and Holly, F. J., Corneal Desiccation Despite Normal Tear Volume. *Annals of Opthalmology.* 1970; 2, 258-261.

6 Dohlman, C. H., Friend, J., Kalevar, V., Yadoga, D., and Balazs, E. The glycoprotein (mucus)content of tears from normals and dry eye patients. *Experimental Eye Research.* 1976 Apr;22(4):359-65..

7 Holly, F. J., and Lemp, M. A. Wettability and wetting of corneal epithelium. *Exp Eye Res.* 1971 Mar;11(2):239-50.

8 Sharma, A. and Ruckenstein, E., Mechanism of Tear Film Rupture and Formation of Dry Spots on Cornea. *J. Colloid Interface Sci.* 1985; 106, 12-27.

9 Tseng SC, Tsubota K, Important concepts for treating ocular surface and tear disorders. *Am J Ophthalmol.* 1997 Dec;124(6):825-35.

10 Maurice DM, The dynamics and drainage of tears. *Int Ophthalmol Clin.* 1973 Spring;13(1):103-16.

11 Paulsen F, The human nasolacrimal ducts. *Adv Anat Embryol Cell Biol*. 2003;170:III-XI, 1-106.

12 Craig J. Structure and function of the preocular tear film. In Korb D, Craig J, Doughty M, Guillon JP, Tomlinson A, Smith G, editors. *The tear film: structure, function and clinical examination.* Oxford, Boston: Butterworth-Heinemann, 2002;37-39

13 Eter N, Gobbels M. A new technique for tear film fluorophotometry. *Br J Ophthalmol*. 2002;86:616-9.

14 Tsubota K. Tear dynamics and dry eye. *Prog Retin Eye Res.* 1998 Oct;17(4):565-96

15 Li Y, Kuang K, Yerxa B, Wen Q, Rosskothen H, Fischbarg J. Rabbit conjunctival epithelium transports fluid, and P2Y2(2) receptor agonists stimulate Cl(-) and fluid secretion. *Am J Physiol Cell Physiol.* 2001 Aug;281(2):C595-602.

16 Creech JL, Do LT, Fatt I, Radke CJ. In vivo tear-film thickness determination and implications for tear-film stability. *Curr Eye Res.* 1998 Nov;17(11):1058-66.

17 Hodges RR, Dartt DA. Regulatory pathways in lacrimal gland epithelium. *Int Rev Cytol.* 2003;231:129-96.

18 Candia OA. Electrolyte and fluid transport across corneal, conjunctival and lens epithelia. *Exp Eye Res.* 2004 Mar;78(3):527-35.

19 Pavlidis M, Stupp T, Grenzebach U, Busse H, Thanos S. Ultrasonic visualization of the effect of blinking on the lacrimal pump mechanism. *Graefes Arch Clin Exp Ophthalmol.* 2005 Mar;243(3):228-34

20 Wong H, Fatt I I, Radke CJ. Deposition and Thinning of the Human Tear Film. *J Colloid Interface Sci.* 1996 Dec 1;184(1):44-51.

21 Levin MH, Kim JK, Hu J, Verkman AS. Potential difference measurements of ocular surface Na+ absorption analyzed using an electrokinetic model. *Invest Ophthalmol Vis Sci.* 2006 Jan;47(1):306-16.

22 Zhu H, Chauhan A. A mathematical model for tear drainage through the canaliculi. *Curr Eye Res.* 2005 Aug;30(8):621-30.

23 Doane MG. Blinking and the mechanics of the lacrimal drainage system. *Ophthalmology.* 1981 Aug;88(8):844-51.

24 Shiue MH, Kulkarni AA, Gukasyan HJ, Swisher JB, Kim KJ, Lee VH. Pharmacological modulation of fluid secretion in the pigmented rabbit conjunctiva. *Life Sci.* 2000;66(7):PL105-11.

25 Fischbarg J, Diecke FP. A mathematical model of electrolyte and fluid transport across corneal endothelium. *J Membr Bio*l. 2005 Jan;203(1):41-56.

26 Jones LT. Epiphora. II. Its relation to the anatomic structures and surgery of the medial canthal region. *Am J Ophthalmol*. 1957;43:203-12.

27 Rosengren B. On lacrimal drainage. Ophthalmologica. 1972;164:409-21.

28 Nagashima K, Kido R. Relative roles of upper and lower lacrimal canaliculi in normal tear drainage. *Jpn J Ophthalmol*. 1984;28:259-62

29 Rossomondo RM, Carlton WH, Trueblood JH, Thomas RP. A new method of evaluating lacrimal drainage. *Arch Ophthalmol*. 1972;88:523-5.

30 Jones LT. Anatomy of the tear system. *Int Ophthalmol Clin.* 1973;13:3-22.

31 Kominami R, Yasutaka S, Taniguchi Y, Shinohara H. Anatomy and histology of the lacrimal fluid drainage system. *Okajimas Folia Anat Jpn.* 2000;77:155-60.

32 Shinohara H, Kominami R, Yasutaka S, Taniguchi Y. The anatomy of the lacrimal portion of the orbicularis oculi muscle (tensor tarsi or Horner's muscle). *Okajimas Folia Anat Jpn.* 2001;77:225-32.

33 Pedrosa-Domellof F, Holmgren Y, Lucas CA, Hoh JF, Thornell LE. Human extraocular muscles: unique pattern of myosin heavy chain expression during myotube formation. *Invest Ophthalmol Vis Sci*. 2000; 41: 1608-16

34 Wasicky R, Ziya-Ghazvini F, Blumer R, Lukas JR, Mayr R. Muscle fiber types of human extraocular muscles: a histochemical and immunohistochemical study. *Invest Ophthalmol Vis Sci.* 2000;41:980-90.

35 Nichols BA. Conjunctiva. *Microsc Res Tech.* 1996 Mar 1;33(4):296-319.

36 Kompella UB, Kim KJ, Lee VH. Active chloride transport in the pigmented rabbit conjunctiva. *Curr Eye Res.* 1993 Dec;12(12):1041-8.

37 Shi XP, Candia OA. Active sodium and chloride transport across the isolated rabbit conjunctiva. *Curr Eye Res.* 1995 Oct;14(10):927-35.

38 Hosoya K, Kompella UB, Kim KJ, Lee VH. Contribution of Na(+)-glucose cotransport to the short-circuit current in the pigmented rabbit conjunctiva. *Curr Eye Res.* 1996 Apr;15(4):447-51.

39 Horibe Y, Hosoya K, Kim KJ, Lee VH. Kinetic evidence for Na(+)-glucose co-transport in the pigmented rabbit conjunctiva. *Curr Eye Res.* 1997 Oct;16(10):1050-5.

40 Kompella UB, Kim KJ, Shiue MH, Lee VH. Cyclic AMP modulation of active ion transport in the pigmented rabbit conjunctiva. *J Ocul Pharmacol Ther*. 1996 Fall;12(3):281-7.

41 Turner HC, Alvarez LJ, Candia OA. Cyclic AMP-dependent stimulation of basolateral K(+)conductance in the rabbit conjunctival epithelium. *Exp Eye Res.* 2000 Mar;70(3):295-305.

42 Shiue MH, Kim KJ, Lee VH. Modulation of chloride secretion across the pigmented rabbit conjunctiva. *Exp Eye Res.* 1998 Mar;66(3):275-82.

43 Shiue MH, Gukasyan HJ, Kim KJ, Loo DD, Lee VH. Characterization of cyclic AMP-regulated chloride conductance in the pigmented rabbit conjunctival epithelial cells. *Can J Physiol Pharmacol.* 2002 Jun;80(6):533-40.

44 Hosoya K, Ueda H, Kim KJ, Lee VH. Nucleotide stimulation of Cl(-) secretion in the pigmented rabbit conjunctiva. *J Pharmacol Exp Ther.* 1999 Oct;291(1):53-9.

45 Turner HC, Alvarez LJ, Bildin VN, Candia OA. Immunolocalization of Na-K-ATPase, Na-K-Cl and Na-glucose cotransporters in the conjunctival epithelium. *Curr Eye Res.* 2000 Nov;21(5):843-50.

46 Turner HC, Alvarez LJ, Candia OA. Identification and localization of acid-base transporters in the conjunctival epithelium. *Exp Eye Res.* 2001 May;72(5):519-31.

47 Levin MH, Verkman AS. Aquaporin-dependent water permeation at the mouse ocular surface: in vivo microfluorimetric measurements in cornea and conjunctiva. *Invest Ophthalmol Vis Sci.* 2004 Dec;45(12):4423-32.

48 Levin MH, Verkman AS. CFTR-regulated chloride transport at the ocular surface in living mice measured by potential differences. *Invest Ophthalmol Vis Sci.* 2005 Apr;46(4):1428-34.

49 Zaki I, Fitzgerald P, Hardy JG, Wilson CG. comparison of the effect of viscosity on the precorneal residence of solutions in rabbit and man. *J Pharm Pharmacol*. 1986 Jun;38(6):463-6.

50 Wilson CG. Topical drug delivery in the eye. *Exp Eye Res.* 2004 Mar;78(3):737-43.

51 Choi SH, Park KS, Sung MW, Kim KH. Dynamic and quantitative evaluation of eyelid motion using image analysis. *Med Biol Eng Comput.* 2003 Mar;41(2):146-50.

52 Evinger C, Manning KA, Sibony PA. Eyelid movements. Mechanisms and normal data. *Invest Ophthalmol Vis Sci.* 1991 Feb;32(2):387-400.

53 Guitton D, Simard R, Codere F. Upper eyelid movements measured with a search coil during blinks and vertical saccades. *Invest Ophthalmol Vis Sci*. 1991 Dec;32(13):3298-305.

54 Gittins J, Martin K, Sheldrick JH. A line imaging system for measurement of eyelid movements. *Physiol Meas.* 1995 Nov;16(4):303-11.

55 Macdonald EA, Maurice DM. The kinetics of tear fluid under the lower lid. *Exp Eye Res.* 1991 Oct;53(4):421-5.

56 Riggs LA, Kelly JP, Manning KA, Moore RK. Blink-related eye movements. *Invest Ophthalmol Vis Sci*. 1987 Feb;28(2):334-42.

57 Macdonald EA, Maurice DM. Loss of fluorescein across the conjunctiva. *Exp Eye Res.* 1991 Oct;53(4):427-30.

58 Maurice DM. Mixing of the tear film under the eyelids. *Adv Exp Med Biol.* 1994;350:263-6.

59 Doane MG. Interactions of eyelids and tears in corneal wetting and the dynamics of the normal human eyeblink. *Am J Ophthalmol.* 1980 Apr;89(4):507-16.

60 Bour L, Ongerboer de Visser B, Aramideh M, Speelman J. Origin of eye and eyelid movements during blinking. *Mov Disord.* 2002;17 Suppl 2:S30-2.

61 Paulsen FP, Thale AB, Hallmann UJ, Schaudig U, Tillmann BN. The cavernous body of the human efferent tear ducts: function in tear outflow mechanism. *Invest Ophthalmol Vis Sci.* 2000;41:965-70.

62 National Institute of Health, (free resource) http://rsb.info.nih.gov/ij/, Last accessed: Jun 29, 2007

63 Kompella UB, Kim KJ, Shiue MH, Lee VH. Possible existence of Na(+)-coupled amino acid transport in the pigmented rabbit conjunctiva. *Life Sci.* 1995;57(15):1427-31.

64 Hosoya K, Horibe Y, Kim KJ, Lee VH. Na(+)-dependent L-arginine transport in the pigmented rabbit conjunctiva. *Exp Eye Res.* 1997 Oct;65(4):547-53.

65 Das BN, Sengupta S, Das BK, Goswami NR. Tear glucose estimation--an alternative to blood glucose estimation. *J Indian Med Assoc.* 1995 Apr;93(4):127-8.

66 Magnani M, Stocchi V, Serafini N, Piatti E, Dacha M, Fornaini G. Pig red blood cell hexokinase: regulatory characteristics and possible physiological role. *Arch Biochem Biophys.* 1983 Oct 1;226(1):377-87.

67 Zurawski CA, McCarey BE, Schmidt FH. Glucose consumption in cultured corneal cells. *Curr Eye Res.* 1989 Apr;8(4):349-55.

68 Novotny JA, Jakobsson E. Computational studies of ion-water flux coupling in the airway epithelium. I. Construction of model. *Am J Physiol.* 1996 Jun;270(6 Pt 1):C1751-63.

69 Pandit JC, Nagyova B, Bron AJ, Tiffany JM. Physical properties of stimulated and unstimulated tears. *Exp Eye Res.* 1999;68:247-53

70 Wilson G, Merrill R. The lacrimal drainage system: pressure changes in the canaliculus. *Am J Optom Physiol Opt*. 1976;53:55-9.

71 Endo Y, Torii R, Yamazaki F, Sagawa S, Yamauchi K, Tsutsui Y, Morikawa T, Shiraki K. Water drinking causes a biphasic change in blood composition in humans. *Pflugers Arch*. 2001 Jun;442(3):362-8.

72 Mircheff AK. Lacrimal fluid and electrolyte secretion: a review. *Curr Eye Res.* 1989 Jun;8(6):607-17.

73 Candia OA, Shi XP, Alvarez LJ. Reduction in water permeability of the rabbit conjunctival epithelium by hypotonicity. *Exp Eye Res.* 1998 May;66(5):615-24.

74 Crambert G, Hasler U, Beggah AT, Yu C, Modyanov NN, Horisberger JD, Lelievre L, Geering K. Transport and pharmacological properties of nine different human Na, K-ATPase isozymes. *J Biol Chem.* 2000 Jan 21;275(3):1976-86.

75 Miyamoto H, Ikehara T, Yamaguchi H, Hosokawa K, Yonezu T, Masuya T. Kinetic mechanism of Na+, K+, Cl--cotransport as studied by Rb+ influx into HeLa cells: effects of extracellular monovalent ions. *J Membr Biol.* 1986;92(2):135-50.

76 Watsky MA, Jablonski MM, Edelhauser HF. Comparison of conjunctival and corneal surface areas in rabbit and human. *Curr Eye Res.* 1988 May;7(5):483-6.

77 Hirayama BA, Lostao MP, Panayotova-Heiermann M, Loo DD, Turk E, Wright EM. Kinetic and specificity differences between rat, human, and rabbit Na+ -glucose cotransporters (SGLT-1). *Am J Physiol*. 1996 Jun;270(6 Pt 1):G919-26.

78 Nagashima K, Kido R. Relative roles of upper and lower lacrimal canaliculi in normal tear drainage. *Jpn J Ophthalmol.* 1984;28:259-62

79 Murgatroyd H, Craig JP, Sloan B. Determination of relative contribution of the superior and inferior canaliculi to the lacrimal drainage system in health using the drop test. *Clin Experiment Ophthalmol.* 2004 Aug;32(4):404-10.

80 Urtti A, Salminen L. Minimizing systemic absorption of topically administered ophthalmic drugs. *Surv Ophthalmol.* 1993 May-Jun;37(6):435-56.

81 Prausnitz MR, Noonan JS. Permeability of cornea, sclera, and conjunctiva: a literature analysis for drug delivery to the eye. *J Pharm Sci.* 1998 Dec;87(12):1479-88.

82 Doughty MJ, Blades K, Button NF, Wilson G. Further analysis of the size and shape of cells obtained by impression cytology from the exposed portion of the human bulbar conjunctiva. *Ophthalmic Physiol Opt.* 2000 Sep;20(5):391-400.

83 Gilbard JP. Human tear film electrolyte concentrations in health and dry-eye disease. *Int Ophthalmol Clin.* 1994 Winter;34(1):27-36.

84 Iwata S. Chemical composition of the aqueous phase. *Int Ophthalmol Clin.* 1973 Spring;13(1):29-46.

85 Maurice DM. Electrical potential and ion transport across the conjunctiva. *Exp Eye Res.* 1973 May 10;15(5):527-32.

86 Mishima S, Maurice DM. The oily layer of the tear film and evaporation from the corneal surface. *Exp Eye Res.* 1961 Sep;1:39-45.

87 Papa V, Aragona P, Russo S, Di Bella A, Russo P, Milazzo G. Comparison of hypotonic and isotonic solutions containing sodium hyaluronate on the symptomatic treatment of dry eye patients. *Ophthalmologica.* 2001 Mar-Apr;215(2):124-7.

88 Yen MT, Pflugfelder SC, Feuer WJ. The effect of punctum occlusion on tear production, tear clearance, and ocular surface sensation in normal subjects. *Am J Ophthalmol*. 2001 Mar;131(3):314-23.

89 Zhu H, Chauhan A. A mathematical model for ocular tear and solute balance. *Curr Eye Res.* 2005 Oct;30(10):841-54.

90 Menard KP., 1999. *Dynamic Mechanical Analysis: A Practical Introduction*. Boca Raton: CRC Press LLC

91 Jones DS., 1999. Dynamic mechanical analysis of polymeric systems of pharmaceutical and biomedical significance. *International Journal of Pharmaceutics* 179: 167-178

92 Schlesing W, Buhk M, Osterhold M., 2004. Dynamic mechanical analysis in coatings industry. *Progress in Organic Coatings* 49: 197-208

93 Yamashita J, Furman BR, Rawls HR, Wang X, Agrawal CM., 2001. The use of dynamic mechanical analysis to assess the viscoelastic properties of human cortical bone. *J Biomed Mater Res.* 58(1):47-53.

94 Crisp E., 1865. The growth and maturity of animals. *Veterinary review and stockowners journal.*

95 Blondel W, Didelon J, Maurice G, Carteaux JP, Wang X, Stoltz JF., 2001. Investigation of 3-D mechanical properties of blood vessels using a new in vitro tests system: Results on sheep common carotid arteries. *Ieee Transactions on Biomedical Engineering,* 48(4):442-451.

96 Shinohara H, Kominami R, Yasutaka S, Taniguchi Y., 2001. The anatomy of the lacrimal portion of the orbicularis oculi muscle (tensor tarsi or Horner's muscle). *Okajimas Folia Anat Jpn.77*:225-32.

97 Stevens JR, Livermore A., 1978. Eye Blinking And Rapid Eye-Movement - Pulsed Photic Stimulation Of Brain. *Experimental Neurology.*60(3):541-556.

98 Wang H, Prendiville PL, McDonnell PJ, Chang WV., 1996. An ultrasonic technique for the measurement of the elastic moduli of human cornea. *J Biomech.* 9(12):1633-6.

99 Shadwick RE., 1999. Mechanical design in arteries. *J Exp Biol.* Dec;202(Pt 23):3305-13.

100 Doane MG. Blinking and the mechanics of the lacrimal drainage system. *Ophthalmology.* 1981 Aug;88(8):844-51.

101 Yokoi N, Bron A, Tiffany J, Brown N, Hsuan J, Fowler C. Reflective meniscometry: a non-invasive method to measure tear meniscus curvature. *Br J Ophthalmol.* 1999 Jan;83(1):92-7.

102 Thale A, Paulsen F, Rochels R, Tillmann B. Functional anatomy of the human efferent tear ducts: a new theory of tear outflow mechanism. *Graefes Arch Clin Exp Ophthalmol.* 1998;236:674-8.

103 Sahlin S, Laurell CG, Chen E, Philipson B. Lacrimal drainage capacity, age and blink rate. *Orbit.* 1998;17:155-159.

104 King-Smith et al., The thickness of the tear film. *Curr Eye Res.* 2004, 29(4-5):357-68

105 King-Smith PE, Fink BA, Fogt N, Nichols KK, Hill RM, Wilson GS. The thickness of the human precorneal tear film: evidence from reflection spectra. *Invest Ophthalmol Vis Sci.* 2000 Oct;41(11):3348-59.

106 Wang J, Fonn D, Simpson TL, Jones L. Precorneal and pre- and postlens tear film thickness measured indirectly with optical coherence tomography. *Invest Ophthalmol Vis Sci.* 2003 Jun;44(6):2524-8.

107 Yokoi N, Komuro A. Non-invasive methods of assessing the tear film. *Exp Eye Res.* 2004 Mar;78(3):399-407.

108 Ishibashi T, Yokoi N, Bron AJ, Tiffany JM, Komuro A, Kinoshita S. Retention of reversibly thermo-gelling timolol on the human ocular surface studied by video meniscometry. *Curr Eye Res.* 2003 Aug;27(2):117-22.

109 Snibson GR, Greaves JL, Soper ND, Prydal JI, Wilson CG, Bron AJ. Precorneal residence times of sodium hyaluronate solutions studied by quantitative gamma scintigraphy. *Eye.* 1990;4 (Pt 4):594-602.

110 Wilson CG, Zhu YP, Frier M, Rao LS, Gilchrist P, Perkins AC. Ocular contact time of a carbomer gel (GelTears) in humans. *Br J Ophthalmol.* 1998 Oct;82(10):1131-4.

111 Meseguer G, Buri P, Plazonnet B, Rozier A, Gurny R. Gamma scintigraphic comparison of eyedrops containing pilocarpine in healthy volunteers. *J Ocul Pharmacol Ther.* 1996 Winter;12(4):481-8.

112 Meadows DL, Paugh JR, Joshi A, Mordaunt J. A novel method to evaluate residence time in humans using a nonpenetrating fluorescent tracer. *Invest Ophthalmol Vis Sci.* 2002 Apr;43(4):1032-9.

113 Scuderi AC, De Lazzari A, Miano F, Zola P. Residence time of netilmicin in tears. *Cornea.* 2002 Jan;21(1):48-50.

114 LiawJ, Robinson JR: The effect of molecular weight on corneal transport and the related influence of penetration enhancers. *Pharm Res* 8: S152, 1991

115 Huang AJ, Tseng SC, Kenyon KR. Paracellular permeability of corneal and conjunctival epithelia. *Invest Ophthalmol Vis Sci.* 1989 Apr;30(4):684-9.

116 Patton TF. Pharmacokinetic evidence for improved ophthalmic drug delivery by reduction of instilled volume. *J Pharm Sci.* 1977 Jul;66(7):1058-9.

117 Candia OA, Alvarez LJ, Zamudio AC. Regulation of water permeability in rabbit conjunctival epithelium by anisotonic conditions. *Am J Physiol Cell Physiol.* 2006 Apr;290(4):C1168-78.

118 Lange K. Regulation of cell volume via microvillar ion channels. *J Cell Physiol.* 2000 Oct;185(1):21-35.

119 Gelatt KN, MacKay EO, Widenhouse C, Widenhouse TS, Stopek JB. Effect of lacrimal punctum occlusion on tear production and tear fluorescein dilution in normal dogs. *Vet Ophthalmol*. 2006 Jan-Feb;9(1):23-7.

120 Rubashkin A, Iserovich P, Hernandez JA, Fischbarg J. Epithelial Fluid Transport: Protruding Macromolecules and Space Charges Can Bring about Electro-Osmotic Coupling at the Tight Junctions. *J Membr Biol.* 2006 Jan;208(3):251-63. Epub 2006 Apr 20.

121 Turner JR. Show me the pathway! Regulation of paracellular permeability by Na(+)-glucose cotransport. *Adv Drug Deliv Rev.* 2000 Jun 30;41(3):265-81.

122 Loo DD, Zeuthen T, Chandy G, Wright EM. Cotransport of water by the Na+ /glucose cotransporter. *Proc Natl Acad Sci U S A.* 1996 Nov 12;93(23):13367-70.

123 Snibson GR, Greaves JL, Soper ND, Tiffany JM, Wilson CG, Bron AJ. Ocular surface residence times of artificial tear solutions. *Cornea.* 1992 Jul;11(4):288-93.

124 Greaves JL, Wilson CG, Birmingham AT. Assessment of the precorneal residence of an ophthalmic ointment in healthy subjects. *Br J Clin Pharmacol.* 1993 Feb;35(2):188-92.

125 Paugh JR, Chatelier RC, Huff JW. Ocular residence time of carboxymethylcellulose solutions. *Adv Exp Med Biol.* 1998;438:761-7.

126 Podder SK, Moy KC, Lee VH. Improving the safety of topically applied timolol in the pigmented rabbit through manipulation of formulation composition. *Exp Eye Res.* 1992 May;54(5):747-57.

127 Keister JC, Cooper ER, Missel PJ, Lang JC, Hager DF. Limits on optimizing ocular drug delivery. *J Pharm Sci.* 1991 Jan;80(1):50-3.

128 Creech JL, Chauhan A, Radke CJ. Dispersive mixing in the posterior tear film under a soft contact lens. *Industrial & Engineering Chemistry Research.* 40 (14): 3015-3026 JUL 11 2001

129 Li CC, Chauhan A. Modeling ophthalmic drug delivery by soaked contact lenses. *Industrial & Engineering Chemistry Research.* 2006 May;45 (10): 3718-3734.

130 Rottach KG, Das VE, Wohlgemuth W, Zivotofsky AZ, Leigh RJ. Properties of horizontal saccades accompanied by blinks. *J Neurophysiol*. 1998 Jun;79(6):2895-902.

131 Collewijn H, van der Steen J, Steinman RM. Human eye movements associated with blinks and prolonged eyelid closure. *J Neurophysiol.* 1985 Jul;54(1):11-27.

132 Fraunfelder FT. Extraocular fluid dynamics: how best to apply topical ocular medication. *Trans Am Ophthalmol Soc.* 1976;74:457-87.

133 Y.C. Fung. *Biodynamics, Circulation.* New York: Springer-Verlag New York Inc, 1984. 82-85, 91-94, 370-373

134 Oguz H, Yokoi N, Kinoshita S. The height and radius of the tear meniscus and methods for examining these parameters. *Cornea.* 2000 Jul;19(4):497-500.

135 James Keener, James Sneyd. *Mathematical Physiology* New York: Springer-Verlag, 1998

136 Eskandari S, Wright EM, Loo DD. Kinetics of the reverse mode of the Na/glucose cotransporter. *J Membr Biol.* 2005 Mar;204(1):23-32.

137 Parent L, Supplisson S, Loo DD, Wright EM. Electrogenic properties of the cloned Na+ /glucose cotransporter: II. A transport model under nonrapid equilibrium conditions. *J Membr Biol.* 1992 Jan;125(1):63-79. Erratum in: *J Membr Biol* 1992 Nov;130(2):203

BIOGRAPHICAL SKETCH

Heng Zhu was born to Quanshou Zhu and Yimei Zhang on May 19, 1980 in Suzhou, China. He grew up in Beijing, China and graduated from Beijing No. 5 High School in 1998. He was then admitted to Tsinahua University, China and obtained his bachelor's degree in chemical engineering in 2002. After that he joined Dr. Anuj Chauhan's group in the University of Florida to pursue his PhD in chemical engineering. His research focuses on the dynamics of tears and other fluids on the ocular surface, and its implications on ocular ailments and ophthalmic drug delivery.